Dream of Karma Yogi

UNIVERSITY OF ALBERTA

TRANSIENT HEAT TRANSFER THROUGH THIN FIBROUS LAYERS

BY

RAUL MUNOZ ANGUIANO ©

A thesis submitted to the Faculty of Graduate Studies and Research in partial fulfillment of the requirements for the degree of

MASTER OF SCIENCE

DEPARTMENT OF MECHANICAL ENGINEERING

EDMONTON, ALBERTA

SPRING 2006

Your file Votre référence
ISBN: 0-494-13856-4
Our file Notre référence
ISBN: 0-494-13856-4

ABSTRACT

This investigation focused on the experimental evaluation of transient heat transfer through thin fibrous layers. The study utilized a vertical heated air jet impinging on a flat surface with uncontrolled temperature made of skin simulant. Efforts were directed to understanding heat transfer as a function of time and location. It was found that the heat transfer profile across the plate depended on nozzle-to-plate separation. In addition, the performance of three commonly used fire resistant / flame retardant fabrics was analyzed. Fabrics were tested in contact and 6mm away from the plate. In all cases, Nomex® IIIA consistently allowed higher rates of heat transfer. Indura® and Kevlar®/PBI performed comparably during contact testing, but varied significantly as they were located away from the skin simulant.

ACKNOWLEDGEMENTS

I would like to gratefully acknowledge the enthusiastic supervision of Mr. Mark Ackerman during this work. Without his unconditional help and encouragement, this project would have never been done. Your support has really made an impact in both my personal and professional life.

I would also like to express my gratitude to Dr. Doug Dale for his motivation and invaluable technical input to this thesis. Thank you for your time, commitment and support.

Thanks to Dr. Brian Fleck for his supervision and friendship. Also, to all my colleagues, administrative and technical staff from the Department of Mechanical Engineering, your support was key to the completion of this work.

Finally, I would like to give my special thanks to Luis, whose patient love enabled me to complete this work.

TABLE OF CONTENTS

APPENDICES

LIST OF TABLES

LIST OF FIGURES

CHAPTER 4 RESULTS AND DISCUSSIONS

CHAPTER 1: INTRODUCTION

Every year, many people are injured in Canada and the United States as a result of industrial accidents involving high heat flux exposures. To minimize or prevent burns, workers wear thermal protective clothing. Consequently, extensive research has been conducted to better understand the mechanisms involved in heat transfer through thin fibrous layers and to improve upon protective clothing design and performance.

The present work is part of a larger series of ongoing projects carried out by the Department of Mechanical Engineering and the Department of Human Ecology at the University of Alberta. These projects aim to further knowledge in the area of protective clothing and test protocols used in the evaluation of materials, clothing and protective equipment. Despite the existence of numerous tests for evaluating fire resistant / flame retardant clothing, there are still many questions about their transient heat transfer response. This investigation focuses on the experimental evaluation of transient heat transfer through thin fibrous layers from an impinging heated air jet. The experiments mimic some of the standard flame tests, substituting the flame with a warm air jet and utilizing a multi-sensor square flat plate as the impingement surface. The goal is to broaden the understanding of the spatial heat transfer distribution that takes place during standard flame testing.

This chapter is an introduction intended to outline the scope and specific objectives of this project. Subsequent chapters provide a theoretical background, the methodology followed during experimentation, analysis of the obtained results and conclusions.

1.1 Motivation

A considerable amount of research in the area of air jets impinging on flat surfaces has been performed. However, no model or experimentation was found that provided results on transient heat transfer of impinging air jets through thin fibrous layers. Even some of the studies that dealt with transient heat transfer of impinging jets did not focus on the local heat transfer characteristics. Furthermore, the effects of having thin fibrous materials laid in contact and at a space away from the impinging surface have never been looked at using air jets. The main advantage of utilizing a warm air jet is to focus on heat transfer through conduction and convection only.

1.2 Objectives

The experimental work has 3 specific objectives:

1. To study heat transfer from a vertical warm jet of air (simulating a flame) impinging on a horizontal surface. Rates of heat transfer will be obtained as a function of time and location.

2. To study the performance of thin fibrous materials located in two positions relative to the horizontal surface – in contact and spaced away (air gap).

3. To compare the energy transfer across the air gap with a solid bottom boundary (shim stock) to that across an air gap with a porous bottom boundary (fabrics).

1.3 Experimental Work

The main objective for the testing was to gather heat transfer data from a vertical warm jet of air (from a round nozzle) impinging on a horizontal surface. The horizontal surface was a square flat plate made of colerceran material. It had 16 copper-constantan thermocouples mounted on its surface so that local heat transfer information could be obtained at various locations. This allowed the gathering of a heat transfer profile across the flat surface. Information was gathered for 10 different nozzle-to-plate separations. Three types of fire resistant / fire retardant (FR) fabrics were tested. The temperature and velocity of jet were kept constant.

1.4 Scope

This project was a parametric study that centred on the following experimental variables and constants:

Constants

- Experimental set-up – including nozzle diameter and flat plate (flat surface).
- Air jet temperature.
- Air jet velocity (Re).

Variables

- 10 nozzle-to-plate separations: 1 to 10 nozzle diameters.

  3 types of fire resistant / flame retardant fabrics: Indura® (339)* Nomex® IIIA (208)* and Kevlar®/PBI (208)* - where a star (*) denotes fabric mass in g/m^2.
- 2 locations of fire resistant / flame retardant fabrics: in contact and 6 mm away from flat surface.

- Shim stock located 6 mm away from the flat surface.

CHAPTER 2: LITERATURE REVIEW

This chapter is a review of published work related to the present study. The first section of this chapter explains the concept of high heat flux exposures, thermal injury in human skin, thermal protective clothing and methods for testing single layer fabrics. The second section is an outline of work completed by other authors on jets and flames impinging on flat surfaces. The chapter concludes with a justification of the present work with regards to linking and filling research gaps in those areas of study.

2.1 High Heat Flux Exposures

The main motivation for studying transient heat transfer through thin fibrous layers is to simulate accidental high heat flux exposures. This section intends to put the present study into context by introducing the concept of high heat flux exposures, thermal protective clothing and standard methods for testing protective clothing. One of the risks employees encounter in the oil, gas and petrochemical industries fieldwork is exposure to accidents involving high heat flux flames (usually flash fires or fireballs). These can result from the accidental release of combustible gas in environments where fuel and air become mixed in adequate concentrations to burn if ignited. The result is a rapidly moving flame front, which is characterized by high heat flux[1] for relatively short periods of time, typically less than 5 seconds [1]. Workers need to wear clothing that allows them suitable protection against skin

[1] Range of approximately 50-150 kW/m^2

damage in case they are ever exposed to this kind of accident. Because of the nature of their jobs, such protection needs to be achieved without compromising comfort and mobility at the work site. It is for this reason that workers often wear single layer coveralls made of FR materials. There are many commercially available FR fabrics in the market today. To evaluate their behaviour under different conditions, a wide range of standard tests has been developed (see section 2.1.2). The purpose of these tests is to compare FR materials under a set of known, controlled conditions in order to differentiate performance among FR materials.

2.1.1 Thermal Injury

The burning of human skin occurs as a complex heat transfer between a hot medium (by conduction, convection, radiation or a combination of) and the surface of the skin. The rate of heating depends upon the temperature and the heat capacity of the source as well as the heat capacity and thermal conductivity of the skin layers [2] – thermal properties of human skin is further studied in Chapter 3 (Table 3.1). Figure 2.1 shows the constituent layers of human skin with their approximate thickness.

Human skin consists of three layers: epidermis, dermis and hypodermis (also called subcutaneous fatty and muscle tissue). The epidermis is the most outer layer and contains both living and dead cells. Its thickness is approximately 75 to 100 μm, except in the human palms and soles where it is 400 to 600 μm. It lacks blood vessels and has few nerve endings. The bottom layer of the epidermis is called the *basal* layer where cells continually divide and move up through the epidermis to replace the

dead cells that fall off the skin surface. The middle layer is called the dermis. It is much thicker that the epidermis, usually 2000 μm thick but in some areas of the body it can be as thick as 4000 μm. This layer contains blood vessels, nerves, lymph vessels, hair follicles and sweat glands. The next layer is called the hypodermis, also known as subcutaneous layer, which consists of fat followed by muscle. The thickness of fat varies from almost none in certain areas to 1.5 to 2.0 cm in others. Furthermore, this thickness varies from individual to individual due to anatomical differences (i.e. underweight vs. overweight people). These differences can be very large and can play a role in determining the degree of injury in a severe burn [3]. Of particular interest is the interface between the epidermis and the dermis, or basal layer. It is there where blisters start forming and second-degree burns arise. If the temperature of the basal layer is sufficiently high (≥44°C) and maintained long enough, permanent skin damage will occur.

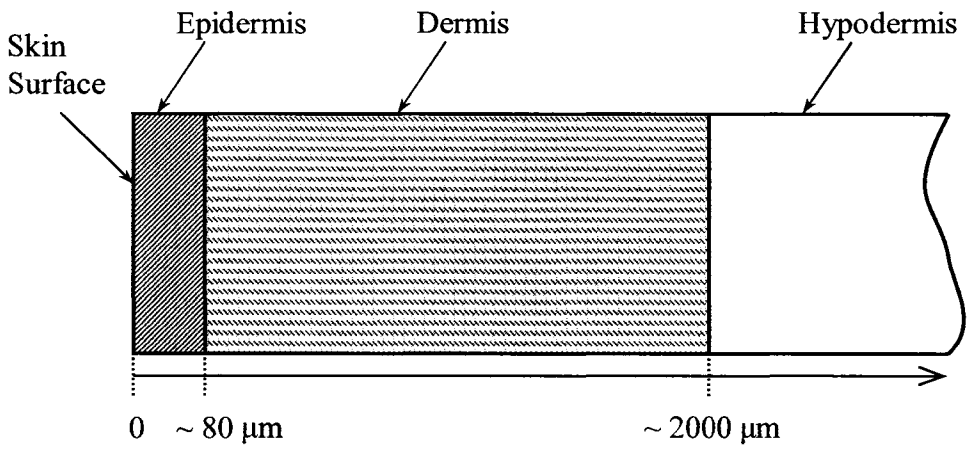

Figure 2.1 Cross section of human tissue. Units in micrometers (μm) – Source [2]

2.1.1.1 Skin Burn Classification

Burns are most commonly classified as first, second and third degree burns depending on the depth of skin damage resulting from the burn. Some classification systems include fourth and higher degrees to categorize the most severe burns. More detailed information can be found elsewhere [3, 4 and 5].

First-degree burns affect only the epidermis. The surface of the skin becomes reddish and painful, but no blisters occur. Sunburns are usually examples of this type of burns. No long-term effects or permanent damage is caused by first-degree burns and healing happens relatively quickly. Second-degree burns involve the epidermis and part of the dermis. The damaged area appears red, blistered and may be swollen and painful. This type of burn is subdivided into superficial and deep depending on the damage caused to the dermis. Superficial second-degree burns involve little damage to the dermis so that healing can proceed without significant medical attention. Deep second-degree burns, though, involve serious damage to the dermis, in which case medical attention is required for the healing process. Third-degree burns completely destroy the epidermis, the dermis and part of the subcutaneous tissue. The burn site appears white or charred and possibly leathery. There is no sensation in the area since the nerve endings are destroyed. Usually, there is little to no possibility for regeneration.

2.1.1.2 Stoll Second Degree Burn Criterion

Stoll [4] has carried out many investigations in the field of skin burns and skin damage as related to FR fabrics. Some of her early work included the experimental

determination of the time it takes to produce second-degree burns in human skin. In those experiments, blackened human forearms were exposed to various thermal irradiances from a 1000 W projection lamp. The lamp was attached to a variable resistor so as to produce a wide range of heat fluxes. The subjects were exposed to one heat flux at a time until they expressed unbearable pain and/or until blistering occurred.

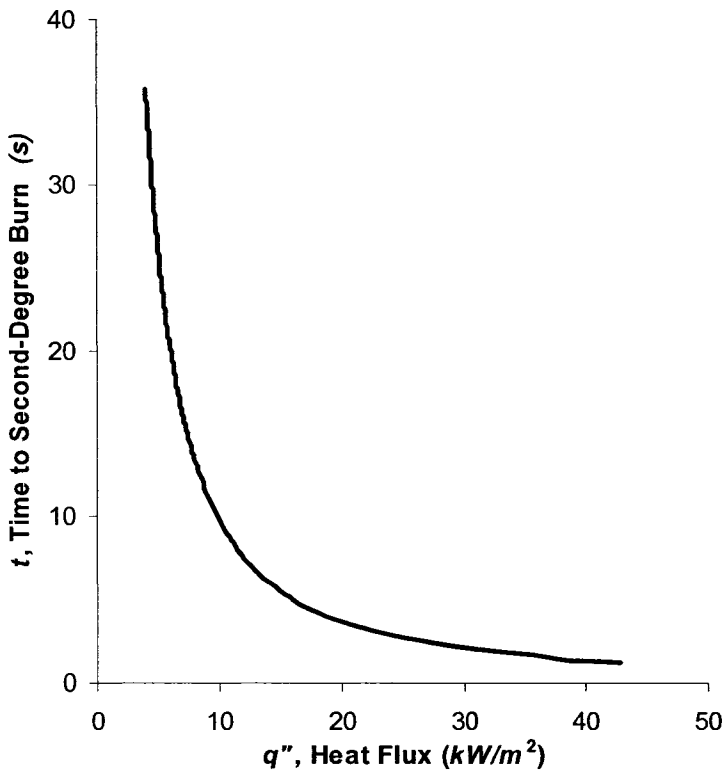

Figure 2.2 Stoll Criterion – time to produce second-degree burns for various incident heat fluxes on bare human skin (Source [4])

The time and skin temperature – minimal blistering within 24 hours - at which intolerable pain occurred were recorded [6]. Her results can be translated into a relationship that calculates the amount of energy needed to produce second-degree burns. Many standard tests for FR fabrics (see section 2.1.2) such as ASTM F1939

and ASTM F1930 [4] use that relationship based on the energy absorbed by test sensors. Figure 2.2 shows the time required to produce second-degree burns for various heat fluxes (Stoll criterion) based on Equation 2.1.

$$q" = 50.123t^{-0.7087} \tag{2.1}$$

Where incident heat flux, $q"$, is in kW/m^2 and time, t, in seconds. The lower limit of injurious temperature is approximately 44°C (at the basal interface). Injury will occur anytime and all the time this interface remains above that limit. This means that injury happens during cooling as well as heating [7]. At this temperature, irreversible damage may be caused to sweat glands and hair follicles.

2.1.2 Test Methods for Single Layer Fabrics

As FR fabrics were developed for industry, it became necessary to estimate the level of protection they provided against skin burns. A variety of tests may be performed on fabrics to determine if they can be considered FR. The most common way to test FR fabrics is to place them in a horizontal plane and place a vertical open flame directly beneath them as shown in Figure 2.3. This test is commonly known as "bench top" test for protective fabrics. In Figure 2.3, q_{conv} and q_{rad} represent convective and radiation heat flux, respectively. Many standard tests are based on this geometry and orientation of flame and sensor. Included are [8]:

- Standard Test Method for Thermal Protective Performance of Materials for Clothing by Open Flame Method (ASTM F1060 – 2001)
- Workwear For Protection Against Hydrocarbon Flash Fire (CAN/CGSB – 155.20 – 2000)
- Canadian General Standards Board (CAN/CGSB – 155.22 – 1997)
- Standard Test Method for Thermal Protective Performance of Materials for Clothing By Open Flame Method (ASTM D4108 – 1987, Not re-approved in 1995)
- Protective Clothing Against Heat and Flame – Determination of Heat Transmission on Exposure to Flame (ISO – 9151 – 1995)
- Protective Clothing for Structural Fire Fighting (NFPA 1971)

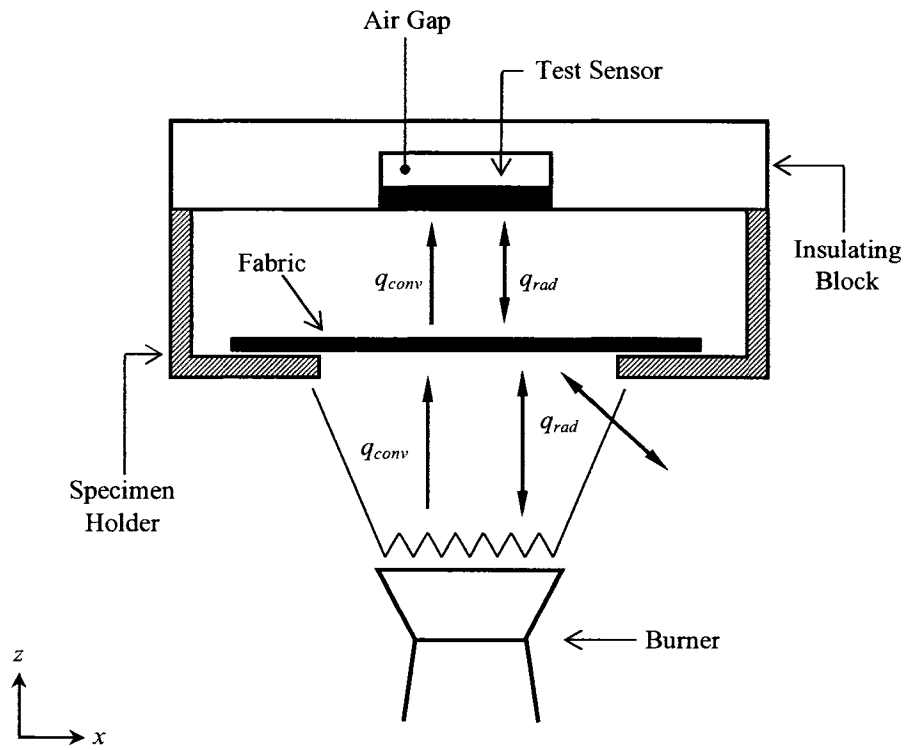

Figure 2.3 Fabric – Air Gap – Test Sensor System (Bench Top Test - Source [9])

There are differences between these testing methods in the magnitude of exposure heat flux, the nature of the exposure, variations in method of mounting and restraining the fabric, the nature of the contact between the sensor and the fabric and the *end point* of the test. All the standards (except ISO – 9151) base the end point on the time it takes for the heat transferred through the fabric to cause the onset of a second degree burn in human skin based on the criteria established by Stoll and Chianta [7]. The ISO standard uses the time it takes for a 24°C temperature rise to occur in the sensor to produce the heat transfer index (HTI). HTI provides a means of ranking the transfer of a fixed amount of energy. A set temperature rise (24°C) in all ISO tests results in HTI's that can be ranked based on the same energy absorption.

In all cases the sensor is the same, a flat pure copper disk, 40 mm in diameter and 1.6 mm thick. The thermocouple(s) used to measure temperature vary. Four iron-constantan thermocouples (Type J) embedded in the copper disk are used in most cases. ISO tests specify the use of only one copper-constantan thermocouple (Type T) and a sensor mass of 18 ± 0.05 g. To ensure good absorption of radiant energy, the sensor is painted with a flat black paint with an absorptivity greater than 0.9. In all cases, the heat flux applied to the lower surface of the fabric is specified and may vary from 80 to 84 kW/m^2. However, as the fabric heats up, it radiates heat to the surroundings and the net heat transfer into the fabric can fall down to 50 kW/m^2 or less. For further details see reference [8].

2.1.3 Thermal Protective Clothing

Selecting appropriate materials and garments designed for single layer coveralls involves many aspects. Some of the desired properties of thermal protective clothing are as follows [8]. The constituent fibres should be flame resistant and non-melting. They should not emit toxic gases at high temperatures. The fibres should be shrink resistant, and maintain their strength and flexibility even at high temperatures. They should also have a low thermal conductivity so that they transmit as little heat as possible to the underlying skin. Fabrics made of these fibres should shrink very little and not split when exposed to flames, have low air permeability (so as to decrease convective heat transfer through fabrics), and be free of flammable finishes or coatings. The garment itself should have a proper fit and be easy to maintain. Closures and waistbands should be designed so as to reduce possible "chimney" effects during exposures. This study focuses on three common protective fabrics: Indura®, Kevlar®/PBI and Nomex® IIIA. The reason for testing them was their availability and prominence in coverall usage.

2.2 Heats and Mass Transfer on Flat Surfaces

The heat transfer rate from a jet impinging onto a flat surface is a complex function of parameters such as Nusselt number (*Nu*), Reynolds number (*Re*), Prandtl number (*Pr*), non-dimensional nozzle-to-plate spacing (*z/d*), non-dimensional radial displacement from the stagnation point (*r/d*) and free stream turbulence intensity (*I*) – not measured in the present investigation. This section offers a review of published work intended to explain the complexity of such phenomenon. Although the literature

serves as an important guideline in some aspects of the present work, no database was found that presented similar objectives to the ones here (see Section 1.2).

2.2.1 Gas Jets Impinging on Flat Surfaces

Over the past decades numerous studies have been reported on the heat transfer of impinging jets on flat surfaces. Table 2.1 (Ref. [10-23]) lists investigations that considered impinging circular jets testing a variety of experimental parameters. Because the literature on this subject is very broad, only the most relevant to the present study will be discussed in detail.

An appropriate starting point for studying impinging jets is the work presented by Martin (1977). He did a comprehensive survey of literature that is devoted to heat and mass transfer of impinging gas jets on flat plates [24]. Although his compilation is very useful as a general reference, it lacks focus on important issues such as local variations of heat transfer coefficients. Furthermore, the discussions he presented centre on steady state solutions that intrinsically differ from the transient results of this research.

Early works by Gardon and Akfirat (1965) address the issue of local heat transfer and the flow conditions with which they are associated. Their work revealed the existence of a maximum at the stagnation point with nozzle-to-plate spacing variation alone as well as several secondary peaks at radial distances. They concluded that the heat transfer characteristics of impinging jets could not be explained in terms of velocity and position-dependent boundary layer alone, but by accounting for the influence of turbulence. The latter appeared to be uniquely dependent on the jet

Reynolds number (nozzle), manifesting itself by transition from laminar to turbulent boundary layer flow or by purely local enhancement of the rate of heat transfer across the boundary layer [17].

Goldstein et al. (1986) investigated the radial distribution of the recovery factor (ratio of the recovery temperature to the total temperature) and local heat transfer for an air jet impinging on a flat isothermal plate under steady state conditions. They discovered that the recovery factor depends on the nozzle-to-plate spacing but is independent of Reynolds number. Maximum heat transfer (obtained in their experiments) occurred in the stagnation region with the jet nozzle set at 8 diameters away ($z/d \approx 8$). This can be related to penetration of turbulent-induced mixing from the shear layer. Mohanty et al. [10] used heat flux sensors to obtain local heat transfer measurements of a round air jet impinging normal to a flat surface. Results from 3 different nozzle diameters and 50 nozzle-to-plate distance ratios were obtained (for a Re_d range of 4,860-34,500). Their experimentation consisted of a blower-nozzle arrangement for creating airflow; a brass plate with variable heating arrangement and insulations; flow measuring devices and three-wire differential thermocouple heat flux sensors for direct measurement of local heat transfer coefficients. Mohanty [10] and Goldstein's [12] studies are fundamentally different from the present work in that the temperature of both the flat plate and the air jet were kept constant so as to create steady state solutions. Nevertheless, the rate of decay (of heat transfer) with radial distance found in their work was used as a basis of comparison for the transient solution of the present study.

Huang and El-Genk (1993) carried out a similar experiment to the one performed by Mohanty et al. Their experimental set up also included a uniformly heated flat plate and an impinging circular air jet (at uniform temperature) so that steady solutions were obtained. Huang and El-Genk, however, focused on determining local and average Nusselt numbers for small values of both Reynolds numbers and jet spacing, which made their research of interest for the preset study. They developed a correlation, which extends the existing database to values as low as Re = 6000 and spacing of one jet-diameter. Their research showed that the maximum Nusselt number still occurred at the stagnation point for considerably small Reynolds numbers ($Re \leq 1.3 \times 10^4$, z/d = 1) and that the peak shifted outwards as Re increased [11].

Siba et al. (2003) studied the flow and heat transfer characteristics of a high turbulence air jet impinging on a flat plate. Their work is of particular interest because they experimented with a flat plate whose thermal boundary conditions were non-uniform (i.e. transient solution). Their plate was heated to a predetermined temperature (30-40°C above room temperature) and was cooled down by the impinging air jet. They found that the turbulent fluctuations of the free stream velocity were the primary aerodynamics influencing heat transfer [19]. Although such experimentation allowed results that are somewhat comparable to the present work, Siba only focused on 1 nozzle-to-plate spacing (z/d=10). Furthermore, their research dealt mostly with the effects of high turbulence induced by the jet and not local heat transfer rates.

Table 2.1 Summary of Investigations of impinging round jets onto flat surfaces.

Ref.	Author(s)	Geometry	*Re* Range	*z/d* Range	Measurement	Fluid
[10]	Mohanty and Tawfek	Cool air nozzle, heated plate	4,860-34,500	4-58	S.S.* local heat transfer	Air
[11]	Huang and El-Genk	Cool air jet, heated circular plate	6,000-60,000	1-10	S.S. local and average *Nu*	Air
[12]	Goldstein, Behbahani and Heppelmann	Rectangular flat plate, compressed air jet	61,000-124,000	2-12	S.S. local *Nu* and recovery factor	Air
[13]	Perry	Hot air jet, water-cooled flat plate	7,000-30,000	≥8	S.S. average at various angles	Air
[14]	Popiel, Meer and Hoogendoorn	Tunnel burner, isothermal plate	1,050-1,860	2-20	S.S. local heat transfer	Combustion Products
[15]	Vander, Incropera and Viskanta	Long tube, rectangular plate	23,760-78,690	8.7	S.S. local heat transfer	Water at 30, 40 and 50°C
[16]	Tawfek	Air nozzle, isothermal flat plate	3,400-41,000	6-58	S.S. heat transfer and surface pressure	Air
[17]	Gardon and Akfirat	Air nozzle, isothermal flat plate	450-22,000	1-50	S.S. local heat transfer , turbulence	Air
[18]	Meola, Renzis and Carlomagno	Air nozzle, isothermal flat plate	15,000	2-10	S.S. local heat transfer	Air
[19]	Siba, Ganesa-Pillai, Harris and H-Sheikh	Heated flat plate, cool air jet	16,100-29,600	10	US.+ local heat transfer, turbulence	Air
[20]	Goldstein and Seol	Isothermal flat plate with 16 air jets	7,100-40,000	1-8	Recovery Factor, effectiveness and S.S. local *Nu*	Air
[21]	Hansen and Webb	Isothermal plate-6 surface finishes, jet	4,700-33,000	¼-14	S.S. local *Nu* (roughness effects)	Air
[22]	Beitelmal and Saad	Isothermal plate-2 surface fihishes, jet	9,600-38,500	1-10	S.S. local *Nu* (roughness effects)	Air
[23]	Tawfek	Isothermal flat plate, variable angle air jet	3,800-40,000	7-30 (90-20° Angles)	S.S. local *Nu*, upon curve surface	Air

* S.S. - Steady State
+ US. - Unsteady

2.2.2 Flames Impinging on Flat Surfaces

A considerable number of investigations have been conducted to study the flow and heat transfer characteristics of impinging air jets. However, no studies were found that discussed the performance of FR fabrics under the influence of air jets. In a greater scope, the present research is a step towards discovering similarities between the characteristics of an impinging air jet and those of an impinging flame. Vistanka (1993) suggested that the aerodynamics of an axisymmetric impinging flame jet were similar to those of an isothermal air jet. He found that an impinging flame, like an air jet, also has three characteristic regions: free jet, stagnation and wall jet regions. However, the influence of Reynolds number and unreacted gases in the central core of the flame, showed very different results that do not compare well to the air jet case [25]. A description of free jets and their behaviour when interacting with solid surfaces is presented in Chapter 3.

Dong et al. (2001) performed an experimental study to determine the heat transfer characteristics of a premixed butane/air round flame jet impinging on a flat rectangular plate at low Reynolds number. The range of Reynolds numbers was selected to cover the laminar to transitional flow conditions ($800 \leq Re_d \leq 2{,}500$). They tested nozzle-to-plate spacings of z/d = 1 to 8. All of their experiments were carried out at steady state conditions using a water-cooled plate. They found that Reynolds number significantly influenced the heat transfer characteristics, which were enhanced in both the stagnation region and the wall jet region by increasing *Re*. They found that the maximum heat flux never occurred at the stagnation point, but at a distance of 1-1.5 radii away from it. This was due to the influence of a cool central

core with unreacted gases. It was found that the location of the maximum heat flux moved by varying *Re*. In regards to nozzle-to-plate spacings, they concluded that the stagnation point heat flux was practically uninfluenced at low Reynolds numbers (1500) and small spacings (up to $z/d = 8$), [26].

Kremer et al. (1973) examined a turbulent premixed methane/air flame jet, impinging upwards obliquely to a plate with the jet exit angle ranging from 5° to 90°. Their study showed very different results to the ones for low-turbulence flames. Their work dealt with highly turbulent flames (*Re* 22,700) and large nozzle-to-plate distances (z/d= 30 – 50). Their experiments showed that at high Reynolds numbers and large nozzle-to-plate spacings, a radial heat transfer distribution similar to the results in air jets was found (with a maximum at the stagnation point). As the exit angle became smaller, the location of maximum heat flux was shifted away from the stagnation point. This was explained as the change in fluid flow and combustion zone. In addition, they found that both, the axial heat flux in the flame and the radial heat flux distribution in the plate decreased with reduction of the impingement angle. For further details see Reference [27].

2.2.3 Heat Transfer in Air Gaps

Part of the present investigation deals with exposure of fabrics spaced away from the testing plate by 6 mm. In most horizontal enclosures found in bench top tests (air gap in Figure 2.3) the temperature difference across the enclosure increases by several hundred degrees Celsius in a few seconds. Torvi et al. [28] have used flow visualization methods to study the heat transfer in horizontal air spaces between solid

boundaries and the test sensors (in bench top tests). They compared the nature of convection cells and Rayleigh number histories to the exposed heat fluxes. The goal of their studies was to successfully create a model to predict the effects of small enclosures (ranging from 6.4-19.0 mm in width) under high heat flux conditions (60-80 kW/m^2). They found that the maximum temperature reached in each case was similar (unaffected by the gap). However, the time it took to reach such temperatures varied depending on the width of the enclosure. This was reflected in a delay in the time-temperature history [28].

2.3 Overview of the Research in this Thesis

As seen in the literature review, a considerable amount of research in the area of air jets impinging on flat plates has been performed. However, no model or experimentation was found that successfully provided results on transient heat transfer of impinging air jets through thin fibrous layers. Even some of the studies that dealt with transient heat transfer of impinging jets did not focus on the local heat transfer characteristics. Furthermore, the effects of having thin fibrous materials laid in contact and at a distance away from the impinging surface have never been looked at using air jets. This experimental work is part of a larger research group at the University of Alberta where the effects of other parameters are considered such as shape, moisture fabric type and fabric shrinkage. The goal of these projects is to further knowledge in the area of protective clothing and test protocols used in the evaluation of materials, clothing and protective equipment.

CHAPTER 3: METHODOLOGY, EXPERIMENTAL APARATUS AND PROCEDURE

In this chapter methodology, apparatus and procedure of the present experimental work will be described in detail. The first section of this chapter contains information regarding the characteristics of the flat plate used, theory of transient heat transfer into a semi-infinite solid and a brief discussion on the hydrodynamics of impinging flows. The second section is a detailed description of the experimental apparatus including the nozzle, flat plate and data acquisition system. The chapter concludes with a comprehensive description of the tests procedure.

The main objective for testing was to gather heat transfer data from a vertical warm jet of air impinging on a horizontal surface (simulating bench top tests with flame as described in Section 2.1.2). The horizontal surface was a square flat plate made of skin simulant (colerceran[2]) instrumented to measure surface temperature. It had 16 copper-constantan thermocouples mounted on its surface in the vertical and horizontal axes (cross pattern). This allowed the gathering of a heat transfer profile across the flat surface. Data was stored using a computer-controlled data acquisition system for all thermocouples in real time. Layers of three types of FR conditioned[3] fabric (Indura®, Nomex® IIIA and Kevlar®/PBI) were located in two positions relative to the horizontal surface: in contact and at 6 mm away to study the effects of air gaps. The results from these experiments will be discussed in Chapter 4.

[2] See Section 3.1.1
[3] 20 ± 2°C, 65 ± 2% Relative Humidity – Section 3.1.4

3.1 Methodology

Coloceran and commercial garment fabrics were used in this study in order to further knowledge in the area of protective clothing and test protocols used in the evaluation of materials, clothing and protective equipment. Although there is a lot of background literature in this area, it is still important to define some of the theoretical limitations and criteria for clarity purposes. This section contains information regarding the characteristics of the flat plate material including semi-infinite solid assumptions, how the one dimensional heat flux is derived from surface temperature history and a brief overview of the hydrodynamics of impinging flow.

3.1.1 Skin Simulant Materials

Typically, when skin comes in contact with different materials, heat flowing from the skin may increase or decrease depending on the properties of that material. The problem involves transient conduction as the temperature of the material surface gradually changes to a new equilibrium value. Cornwell [29] developed a theoretical relation that provides a useful index to compare the "coldness" felt on touching different materials. This relation is based on the thermal properties of each material. It can be referred to as *contact coefficient*, b ($J/m^2 \cdot K \cdot s^{1/2}$), or *thermal inertia*, b^2 ($J^2/m^4 \cdot K^2 \cdot s$).

$$b^2 = \rho c k \tag{3.1}$$

Equation 3.1 shows this relationship, where c, k and ρ are specific heat, thermal conductivity and density, respectively. A decisive factor in choosing an appropriate

skin simulant is that its thermal inertia (or contact coefficient), should match that of the skin. The skin simulant utilized in this study is an inorganic mixture of calcium, aluminium, silicate with asbestos fibres and a binder (*colerceran*) [30]. It is easily machinable to facilitate the installation of thermocouples.

Table 3.1 Thermal Properties of Human Skin and Skin Simulant - Source [30].

Property	**Human Skin**		**Skin Simulant**
	Epidermis	*Dermis*	
k *(W/m·K)*	0.255	0.523	0.970
c *(J/kg·K)*	3598	3222	1205
ρ *(kg/m^3)*	1200	1200	1877
$b^2 \cdot 10^6$ *(J^2/m^4·K^2·s)*	1.10	2.02	2.19
b *(J/m^2·K·s$^{1/2}$)*	1050	1414	1483

The thermal properties of this particular skin simulant and those of human skin are presented in Table 3.1. Clearly, the thermal inertia of the skin simulant used in this study closely resembles that of human skin; in particular those of the dermis where second-degree burns arise (see Section 2.1.1.1 for details on skin burn classification).

3.1.2 Semi Infinite Solid Theory

This study is concerned with transient heat transfer from an impinging air jet to a flat plate as shown in Figure 3.1.

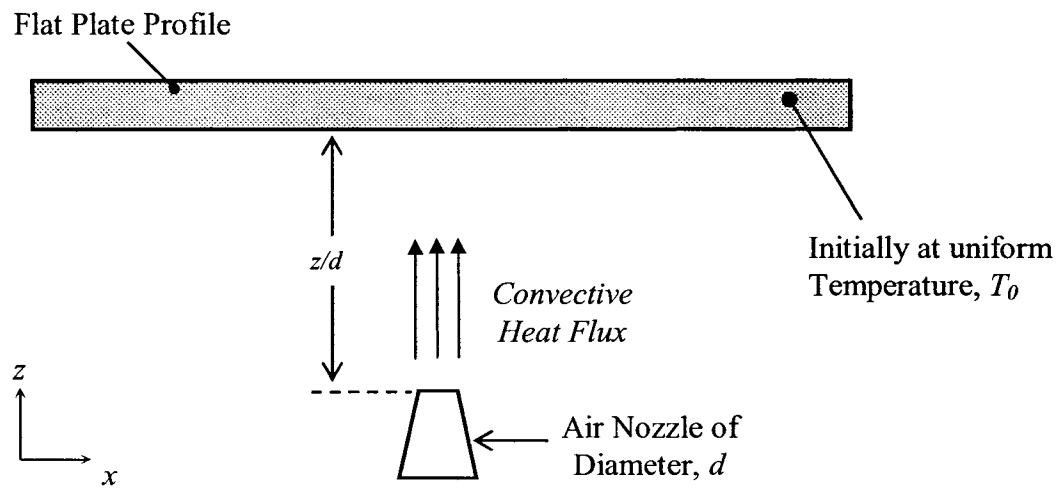

Figure 3.1 Profile of skin simulant flat plate being impinged by warm flow

The mathematical description of transient heat conduction within the solid (flat plate) yields a second-order, parabolic, partial differential equation known as the heat diffusion equation. This equation is a combination of the energy equation and Fourier's law. A number of useful solutions have been developed for cases where heat flows in only one direction – so that temperature, T, is only a function of vertical direction, z, and time, t. Equation 3.2 shows the heat diffusion equation for the one dimensional case, assuming constant properties .

$$\frac{\partial T}{\partial t} = \kappa \frac{\partial^2 T}{\partial z^2} \tag{3.2}$$

Where $\kappa = k/\rho c$ is the thermal diffusivity and has units of m^2s^{-1}. Solutions to this equation are useful because they give considerable insight into the transient behaviour of temperature and heat flow [31]. In the present study, the surface of the skin simulant flat plate (of thickness 21 mm) is exposed to a sudden change in convective heat flux from an impinging air jet. The plate is assumed to have an initial isothermal temperature, T_0. The sudden change in surface heat flux will create a surface temperature rise, which will result in a non-linear temperature gradient through the plate.

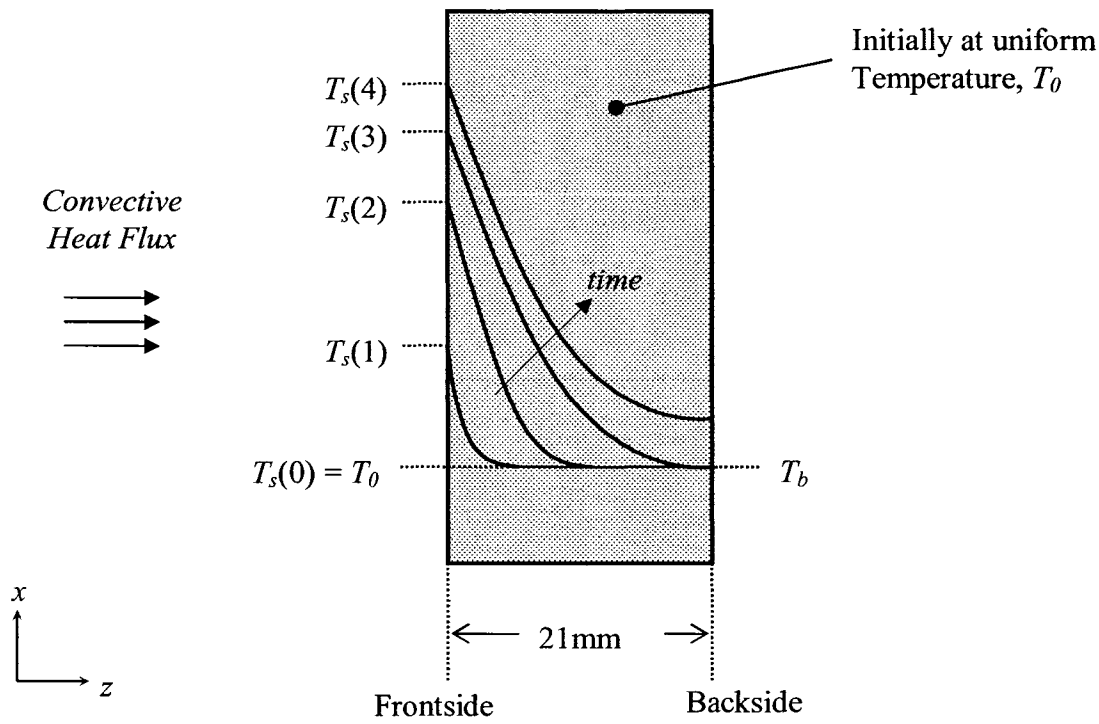

Figure 3.2 Non-linear temperature gradient of skin simulant flat plate exposed to a sudden change in convective heat flux

Figure 3.2 shows temperature gradients at different times after the plate has been suddenly exposed to convective heat flux. $T_s(1)$, $T_s(2)$, $T_s(3)$ and $T_s(4)$ represent arbitrary frontside surface temperatures at any given time after the plate has been exposed. The flat plate is said to behave like a semi-infinite solid, during and until the temperature at the backside of the plate has been affected by the sudden rise in front side surface temperature (i.e. $T_b \leq T_0$). The length of time for which such condition is valid depends on the thermal properties and thickness of the skin simulant. Figure 3.3 shows the response of a semi-infinite solid to a step change in surface heat flux. Where $\theta = x/(4\kappa t)^{1/2}$ is the non-dimensional distance from the surface based on thermal diffusivity, κ, distance below the surface, x and time, t. The vertical axis is the non-dimensional heat flux penetration coefficient given at any time, t ($t \neq 0$). Where q_0, $Ts(t)$ and T_i represent heat flux, surface temperature at time, t and initial surface temperature, respectively (see Appendix A for details). Evidently, the temperature rise is most significant for $\theta \leq 2$.

The flat plate used in this study, had a thickness of 21 mm and thermal properties similar to those in Table 3.1. This allowed the plate to behave like a semi-infinite solid for 65 seconds after sudden exposure to convective heat flux (from the impinging jet). Sixty five seconds was the time constraint for which the results of the experiments are valid. If the experiments were to be run longer (i.e. $t > 65$ s), the skin simulant flat plate would need to be thicker or temperature sensors would need to be installed on the backside of the plate. Specific details are given in Appendix A.

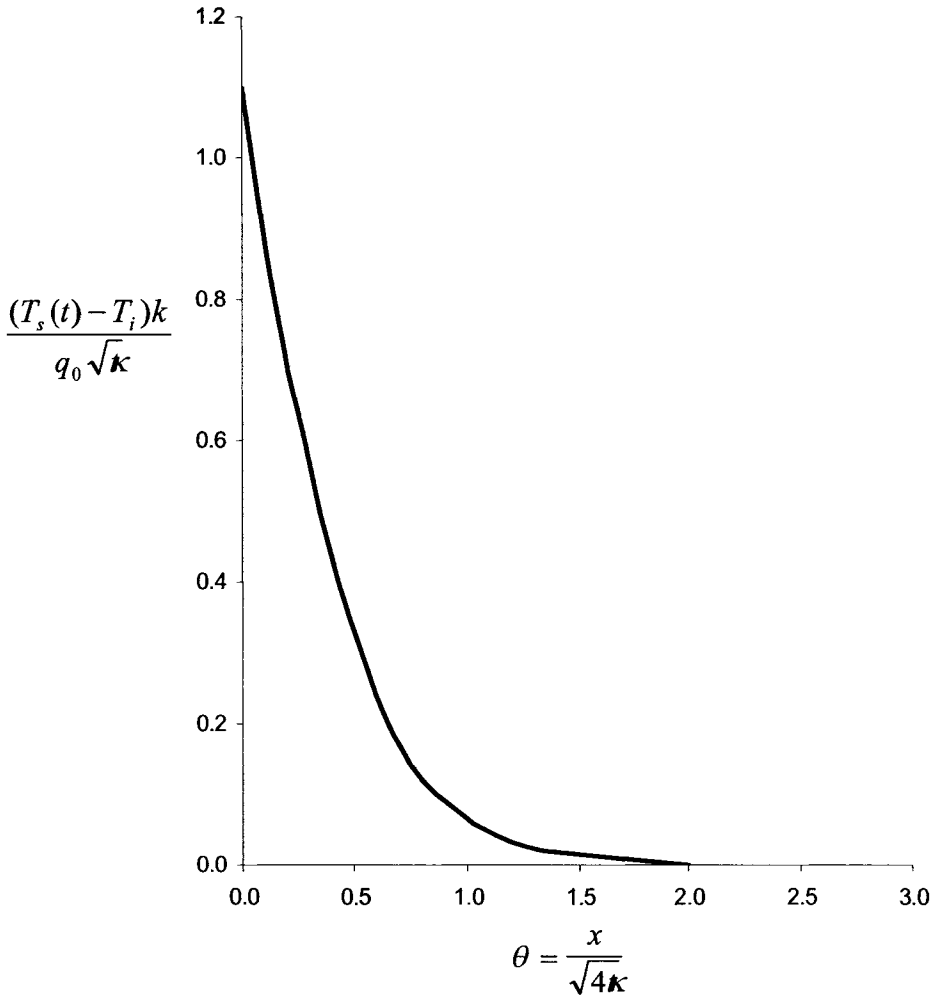

Figure 3.3 Dimensionless response of a semi-infinite solid to a step change of surface heat flux (source [31])

3.1.3 One Dimensional Skin Simulant Heat Flux Sensor

With the assumption that the skin simulant flat plate was initially at a uniform temperature, Duhamel's theorem (Equation 3.3) can be used to determine the surface heat flux history based on the surface temperature history. Surface temperature history measurements were obtained from 16 flattened copper-constantan thermocouples mounted on the surface of the plate as outlined in Section 3.2.1.1.

$$q''(t) = \sqrt{\frac{kc_p\rho}{\pi}}\left[\frac{1}{2}\int_0^t \frac{T_s(t)-T_s(\tau)}{(t-\tau)^{3/2}}d\tau + \frac{T_s(t)-T_i}{t^{1/2}}\right] \tag{3.3}$$

Where q'' is the heat flux at any given time, t. T_s represents surface temperature at any time. T_i is the initial surface temperature at $t = 0$ and τ is an integration dummy. The singularity in Equation 3.3 (when $\tau = t$) can be overcome using several methods. Vosen [32], Woodard [33], Diller [34, 35] and Cook-Felderman [36] have all suggested approximation techniques to solve it. The latter method (Cook-Felderman) was chosen in the present study due to its simplicity. A simple Matlab program was created to transform surface temperature history data into surface heat flux history using Cook-Felderman's approximation. Nevertheless, approximations from all 4 authors were tested and results showed to be comparable (specific details can be found in Appendix B).

3.1.4 Hydrodynamics of Impinging Flow

The flow pattern of jet impinging on a flat surface from a single round nozzle is shown in Figure 3.4. It can be subdivided into three characteristic regions: the free jet region, the stagnation flow region and the region of radial flow outside the stagnation zone (wall jet region) [37]. The jet utilized in this study is characterized by a uniform velocity profile at the exit of the nozzle. Immediately leaving the nozzle, the air in the jet begins to entrain the surrounding still air. With increasing distance from the exit, the potential core is seen to contract and the free boundary to broaden. This is due to momentum exchange between the jet and the surrounding air.

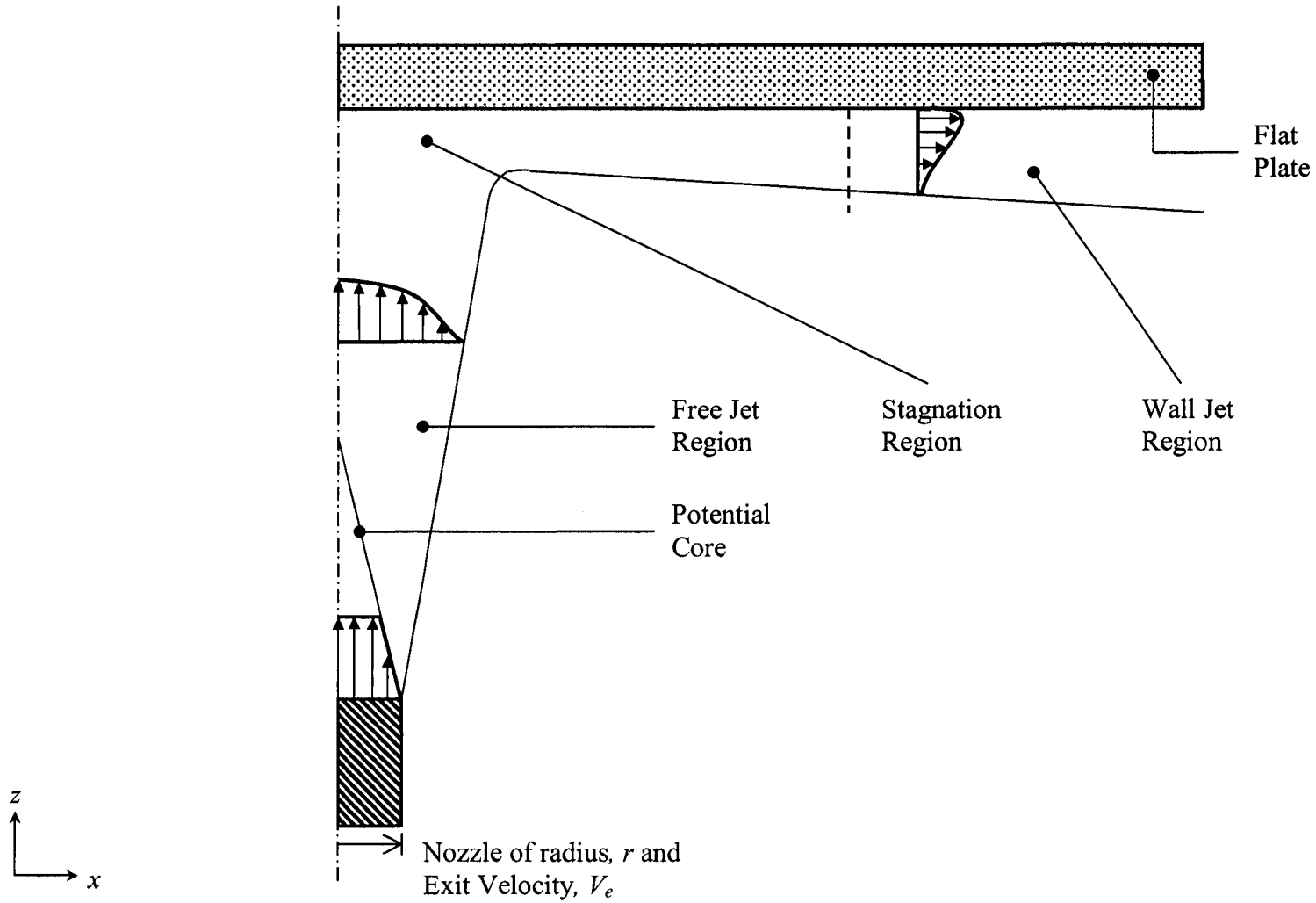

Figure 3.4 Surface Impingement of a single round jet with velocity profiles – Half view (Source [38]).

Within the stagnation zone the flow is influenced by the surface of the plate as it is decelerated (in the normal direction) up to the stagnation point; then accelerated (in the transverse direction) at the start of the wall jet region. With a heated jet, convection heat transfer occurs in both the stagnation and wall jet regions. For large nozzle-to-plate separations, the rate of heat transfer monotonically decays from a maximum value at the stagnation point as one moves radially outwards. For small separations, the distribution in characterized by a second maximum whose value increases with increasing jet Reynolds number and may exceed that of the first maximum [38]. For more information on this refer to Section 2.2.

3.1.5 FR Fabric Samples

An important part of this work was to compare the effects of adding layers of FR fabric in contact and at a fixed distance away from the skin simulant plate (6 mm). Three common FR fabrics were used: Indura®, Kevlar®/PBI and Nomex® IIIA. These fabrics were used because of their availability and prominence in coverall design. Specimens (350 X 350 mm) were cut, and conditioned for at least 24 hours at 20 ± 2°C, 65 ± 2% relative humidity at the Textiles Analysis Services laboratory located in the Department of Human Ecology (University of Alberta). Samples were then kept individually in sealed plastic bags and brought over to the Department of Mechanical Engineering (5 minutes by foot) where the experiments were conducted. Specimens were tested between 30 minutes and 4 hours after being removed from the conditioning laboratory. The delays between conditioning and testing the fabric should have minimal effects on the tests results. This has been confirmed by studies

performed by Torvi and Lee-Barker [39, 40]. Their work focused on heat transfer effects of having conditioned, dried, oven-dried and wet samples. Their results suggest that short delays (less than 4 hours) between conditioning and testing the fabric have insignificant effects on the tests results. Samples were kept in their sealed container up until they were tested as recommended by ISO 139. For further details on conditioning and comparison data please refer to Appendix C. Table 3.2 is a summary of some physical properties for the fabrics used in this study.

Table 3.2 Summary of Physical Properties of Fabrics used in this Study

Property	Indura®	Kevlar®/PBI	Nomex® IIIA
Thickness *(mm)*	0.62	0.49	0.53
Mass *(g/m^2)*	339	208	208
Density *(kg/m^3)*	542	424	392
Permeability *($cm^3/cm^2/s$)*	7.2	12.3	29.0

These properties were obtained experimentally using specialized equipment available at the Textiles Analysis Services laboratory (Human Ecology). As can be seen in the table, Indura® is the heaviest and least permeable of all the fabrics tested. Although both Kevlar®/PBI and Nomex® IIIA have the same weight, their densities and permeability are not the same. It is important to note that the values in Table 3.2

are experimental and that some of the nominal properties may vary from the ones presented here. For example, the nominal mass per unit area for Kevlar®/PBI and Nomex® IIIA is 200 g/m^2 as opposed to 208 g/m^2.

3.1.6 Shim Stock Samples

Pieces of shim stock were used for non-contact testing (i.e. only for tests with 6 mm air gap). This was done so as to compare the energy transfer across the air gap with a solid bottom boundary to that across an air gap with a porous bottom boundary. The nominal thickness of the shim stock was chosen as 0.76 mm (or 0.003 in) so that it would have approximately the same volumetric heat capacity as the fabric samples, resulting in it heating up at about the same rate. It was made of steel and coated with matte black paint (TREMCLAD® High Heat Manifold Paint).

3.2 Experimental Apparatus

The experimental apparatus used in the present study is shown in Figure 3.5. The system consisted of a round aluminium nozzle mounted vertically on a stand; two electric heaters – one in line with the air supply and another one around the nozzle; a skin simulant flat plate with 16 type-T thermocouples (copper-constantan) located at various radial distances; a four-legged stand to hold the flat plate; compressed air supply (available from Mechanical Engineering Building – 370 kPa); and a computer controlled data acquisition system. In order to control the time of impingement, a shutter was placed 8 mm away from the nozzle's exit (shutter not shown). It is made

of skin simulant like the flat plate and had one copper-constantan thermocouple located at its centre.

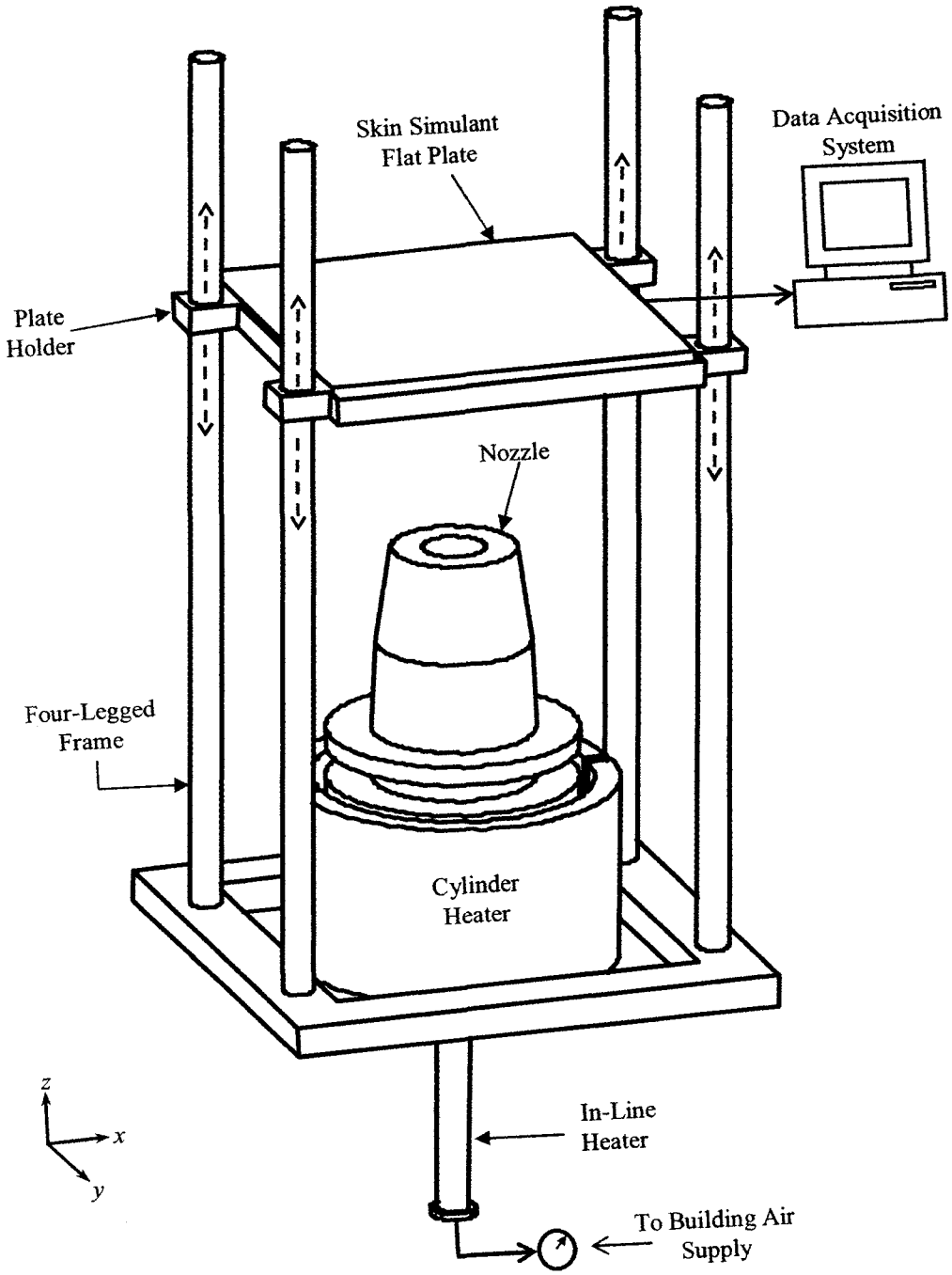

Figure 3.5 Apparatus Installation used for experiments – air nozzle, electric heaters, four-legged stand and skin simulant flat plate (shutter plate not shown).

This thermocouple was used to monitor the temperature of air exiting the nozzle before the jet was allowed to impinge on the flat plate.

3.2.1 Skin Simulant Flat Plate

The flat plate used to gather heat transfer information was made of skin simulant material (refer to Section 3.1.1). Two similar plates were built, but only one was used throughout all experiments to ensure consistency. The other one was kept as backup. The plates were square with dimensions 300 X 300 mm and a thickness of 21 mm. A schematic of the flat plate can be seen in Figure 3.6. It features 16 temperature sensors (type-T thermocouples) mounted at various radial locations, which for convenience were referred to as *r/d* locations (ratio of distance from the plate's centre to nozzle diameter, *d* of 32 mm). The flat plate was divided into four quadrants and thermocouples were located along its axes (*A-A* and *B-B*). It is important to note that a non-uniform spacing was used so more thermocouples were installed near the centre, as this is the area of most interest. Table 3.3 shows the radial distance, *r/d*, at which each thermocouple is located relative to the centre of the plate in Figure 3.6 (thermocouple "*e*"). The number of input channels in the data acquisition system (16) limited the number of thermocouples installed. This resulted in one central thermocouple, 4 on the "negative *B*-axis", 4 on the "positive *B*-axis", 4 on the "negative *A*-axis" and 3 on the "positive *A*-axis". Each of those thermocouples was designated to an input channel on the computer. Each thermocouple was tested and calibrated (see Section 3.2.1.1.)

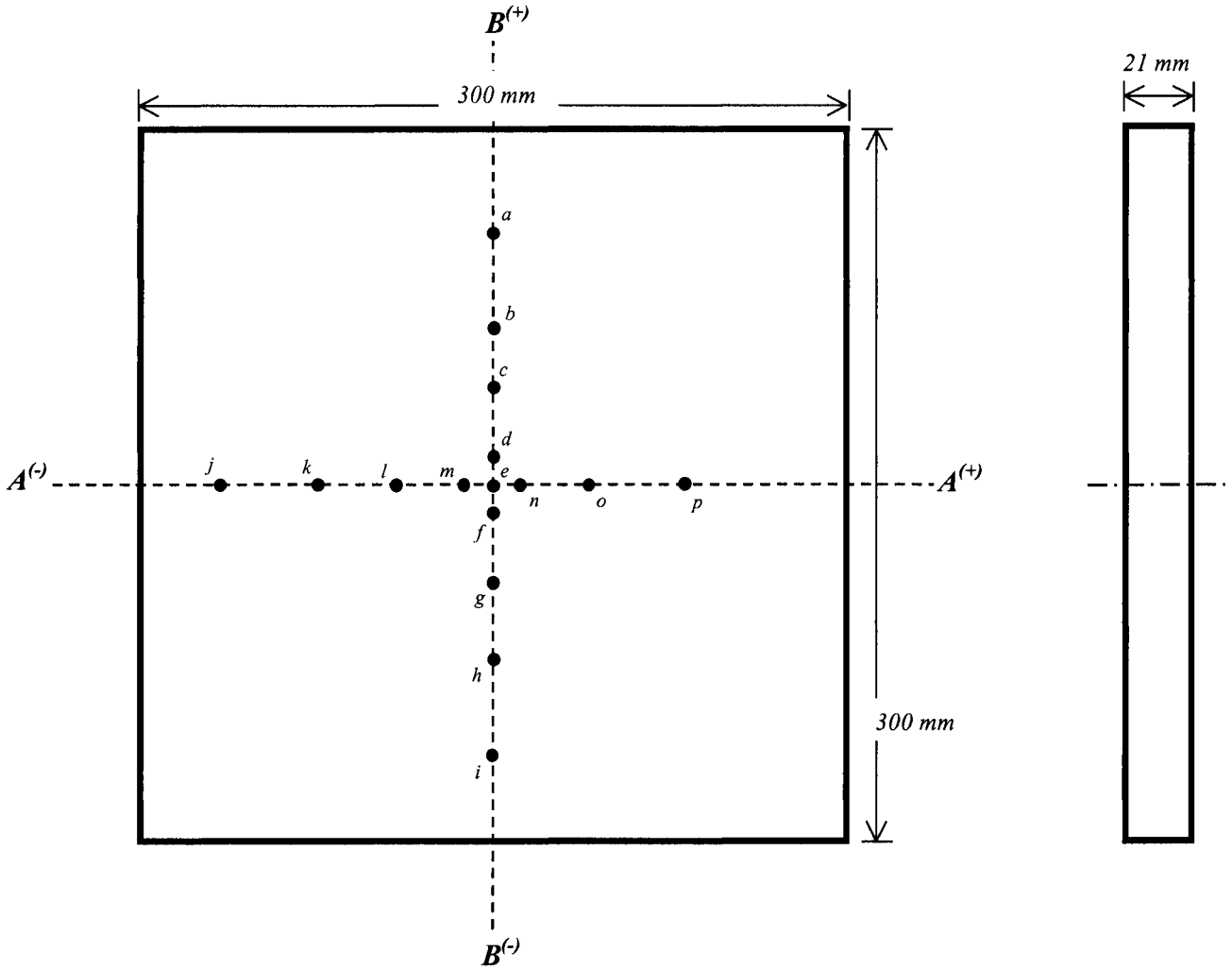

Figure 3.6 Skin simulant flat plate showing 16 copper-constantan thermocouples. Plate divided into 4 quadrants by axes *A-A* and *B-B*. See Table 3.3 for *r/d* correspondence.

Table 3.3 Radial distance, *r/d*, of each thermocouple installed in flat plate relative to the centre of the plate in Figure 3.6. "*d*" represents nozzle diameter (32 mm).

Thermocouple	Radial Distance, *r/d*
a	3.12 ± 0.06
b	1.79 ± 0.06
c	0.94 ± 0.06
d	0.38 ± 0.06
e	0.00 ± 0.06
f	0.58 ± 0.06
g	1.18 ± 0.06
h	2.09 ± 0.06
i	3.39 ± 0.06
j	3.08 ± 0.06
k	1.81 ± 0.06
l	0.90 ± 0.06
m	0.34 ± 0.06
n	0.33 ± 0.06
o	0.90 ± 0.06
p	1.86 ± 0.06

3.2.1.1 Thermocouples on Skin Simulant Plate

This study was concerned with heat transfer on flat smooth surfaces. To avoid turbulence complications due to surface roughness, thermocouple-joint thickness and bonding to the surface were critical. Thermocouple-joints were flattened using an Instron® machine down to 76-100 μm (0.003-0.004 in) and bonded to the plate's surface using high-performance cyanoacrylate resins, which are commercially available (described in detail in Appendix D). Holes of 2.5 mm in diameter were drilled near the desired gauging locations. The edges of those holes were smoothed down to avoid sharp ends, which could cause breakage of thermocouple wires. The plate's surface was then sanded down so as to be free from pits and irregularities. A commercial degreaser (CSM-1A), conditioner (M-Prep A) and neutralizer were

applied to the gauging area to prepare for thermocouple bonding. Adhesive was then applied to thermocouple-joints and gauging area as described in the installation system guidelines, which included curing in an industrial oven for a specific period of time (see Appendix D). Holes were refilled and smoothed using high-temperature cement. Figure 3.7 shows a cross sectional view of one thermocouple installed in the skin simulant flat plate. Thermocouples were then tested and calibrated by using a simple Q-Basic routine along with a calibration lamp system that produced a constant adjustable heat flux. The thermocouple response to a change in temperature, T, is directly proportional to $B(t)^{1/2}$, where t represents time and B is a constant that depends on the physical characteristics of each thermocouple. The performance of each thermocouple was analysed and calibration factors were obtained for all 16 sensors (Appendix I for a complete list of calibration factors).

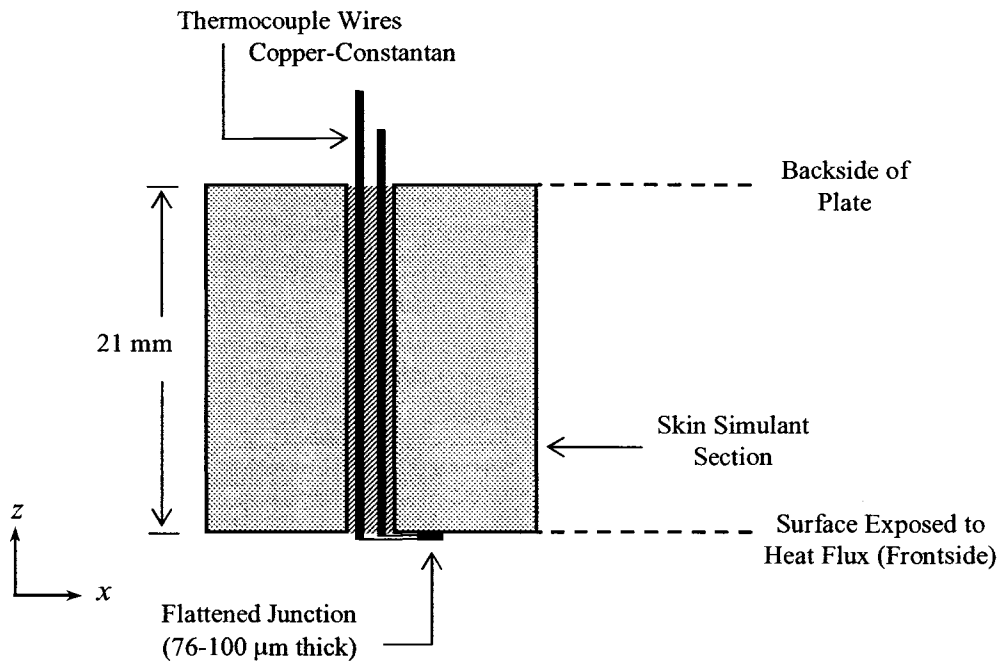

Figure 3.7 Cross sectional view of one copper-constantan thermocouple installed in the skin simulant flat plate.

3.2.2 Air Nozzle

To allow this research to focus on the parametric study of flame-resistant fabrics and nozzle-to-plate separation testing, the temperature and Reynolds number of air exiting from the nozzle were kept constant. The particular nozzle used for the experiments has an exit inner diameter of 32 mm. Its design is based on axisymmetric wind tunnel contractions studies by Morel [41] so that no local separation occurs at the inlet. This provides a uniform exit velocity profile. A schematic of this nozzle can be seen in Figure 3.8. When connected to the building air supply at maximum line pressure (370 kPa), it produced a constant uniform velocity similar to the velocity profile shown in Figure 3.4 (at the nozzle's exit). The resulting air velocity was 13.0 ± 1.5 m/s, which translated into a Reynolds number, Re_d, of 21,132. Air velocity was measured using a 0.28 mm (0.011 in) diameter pitot tube at various locations across the nozzle's diameter (8 mm away from the exit).

In order to warm up the air to a quasi-steady temperature (102 ± 4° C), two electric heaters connected in parallel were used. One in-line heater (by Omegalux®) preheated incoming air from the supply. The second one was a hollow cylinder-like heater that was installed around the jet to maintain the metal temperature and avoid heat loss before air exited the nozzle. Together, both heaters had a power consumption rating of 1.2 kW. Two kinds of insulation were used around the second heater to improve the energy transfer to the air stream. A diagram of the nozzle-heater assembly can be seen in Figure 3.8. A change of 1° C per minute (jet air temperature) was selected to be an appropriate quasi-steady value for the test run time of 65 seconds.

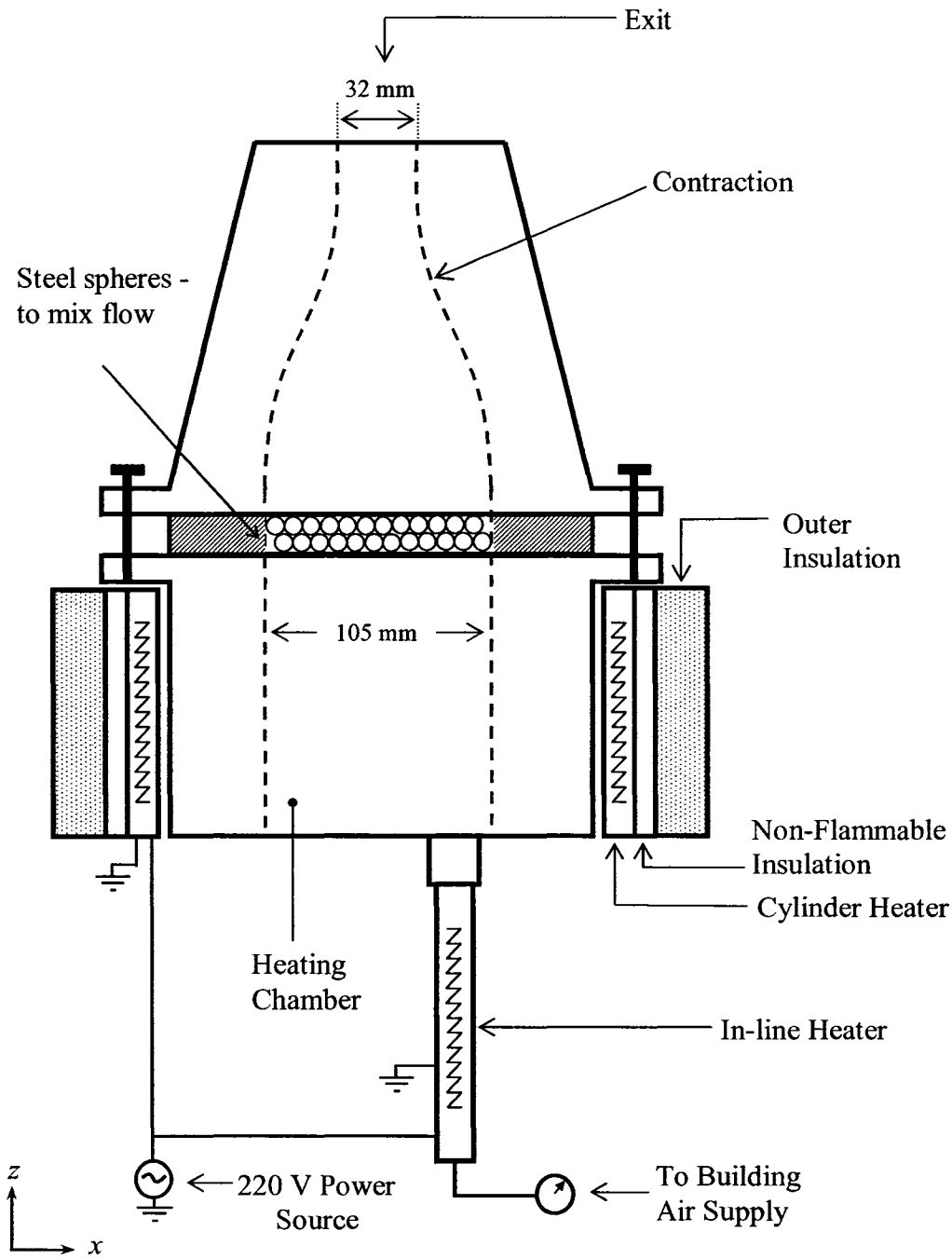

Figure 3.8 Cross Sectional view of nozzle and heaters assembly

Figure 3.9 is a plot of the temperature profile of the jet at two different locations from the nozzle's exit: at 8 mm (0.25*d*) and at 50 mm (1.56*d*). As can be seen from the plot, for 0.25*d*, the air is hotter near the wall of the jet (expected from the effects of the heater) and has a more uniform profile than for 1.56*d*. The average hot air temperature measured at 0.25*d* (T_e in Figure 3.9) was used as the reference temperature for calculating convective coefficient, *h*. The average value of T_e was 102 ± 4°C for all tests.

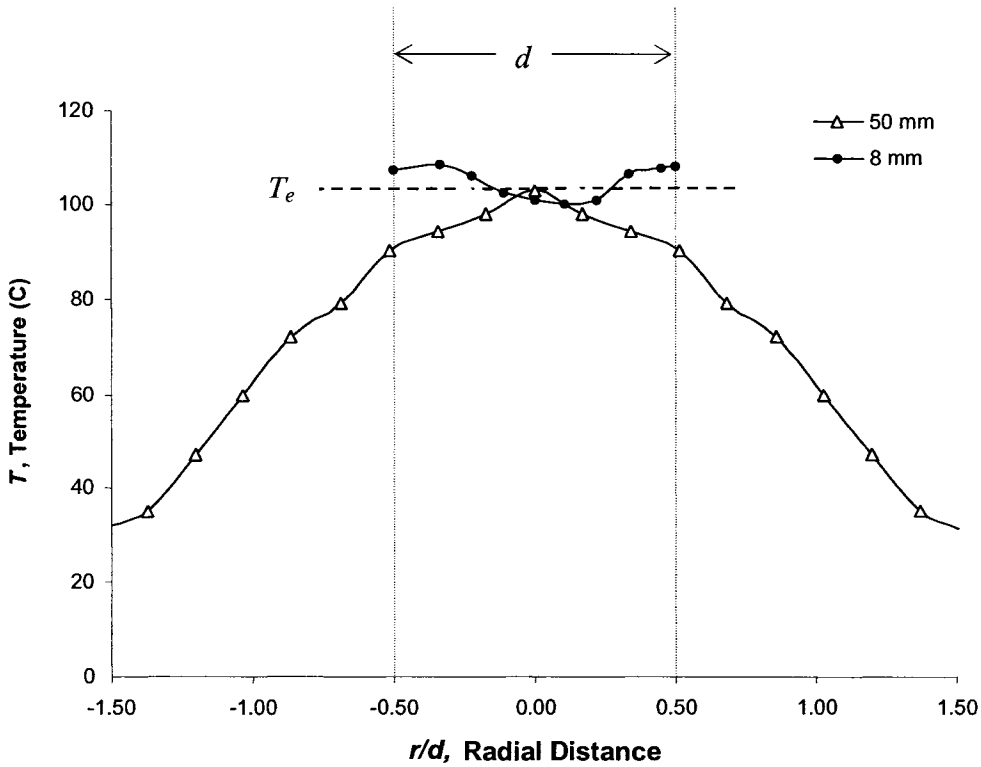

Figure 3.9 Temperature profile of air jet measured at 2 distances relative to the nozzle's exit: at 8 mm (0.25*d*) and 50 mm (1.56*d*), where *d* represents nozzle diameter (32 mm) and T_e the average temperature at 0.25*d*.

3.2.3 Computer-Controlled Data Acquisition System

The system consisted of a 486SX processor, 33 kHz and 32 bits. It featured an input card with an analogue to digital converter (A/D) with 16 input channels. Each channel was assigned to one thermocouple mounted on the surface of the skin simulant plate. A simple Q Basic routine was utilized to translate input voltage into temperature using the appropriate conversion tables for copper-constantan thermocouples. This routine along with more information on the data acquisition system can be found in Appendix E.

3.3 Experimentation Procedure

A total of 58 experiments were performed yielding over 56,000 data points. Tests were conducted in the following manner. The air supply valve was fully opened and line pressure recorded (370 kPa for all tests). Then, both electric heaters were turned on and the temperature of the air exiting the nozzle was allowed to reach quasi-steady state. This means that air temperature did not vary more than 1 degree Celsius per minute. This temperature was monitored using a copper-constantan thermocouple installed at the centre of the nozzle's shutter. The shutter was always placed 8 mm away from the nozzle's exit. Reaching quasi-steady state took about 35 minutes each time. Once quasi-steady state was achieved the data acquisition system was allowed to run, recording temperatures of all 16 thermocouples in real time every 0.08 s. The nozzle's shutter stayed closed for the first 5 seconds of the experiments. This means that no warm air impinged on the flat plate and the data acquisition system recorded room temperature for all 16 thermocouples during that time. After 5

seconds, the shutter was opened and warm air was allowed to impinge onto the flat plate's surface (time to open the shutter is 4 seconds). The test duration was limited by the semi-infinite solid assumption (related to the thickness and thermal properties of the plate) to 65 seconds. Experiments were performed for nozzle-to-plate separations (z/d) from 1 to 10 nozzle diameters in increments of $z/d = 1$. A digital Vernier was used to mark all 10 positions on the four-legged stand. The time between runs was typically 2 hours or until all of the thermocouples reached room temperature.

Once information from the base plate was obtained, layers of three different types of conditioned fabric (20 ± 2°C, 65 ± 2% Relative Humidity – Section 3.1.5) were clamped so as to be in uniform contact with the plate as shown in Figure 3.10b. Four heavy-duty clips on all sides of the flat plate permitted this without over stretching (damaging) the fabric. Again, data was collected for nozzle-to-plate separations from 1 to 10 (for fabrics: Indura®, Kevlar®/PBI and Nomex® IIIA). No fabric sagging was noticed for the experiments with the fabric in contact.

In order to study the effects of air gaps in between the fabric and the flat plate, a solid acrylic frame of 6 mm thickness was placed beneath the flat plate as shown in Figure 3.10a. The frame allowed spacing to be even on all sides and provided additional support to the fabric clamps. The conditioned fabric was then placed on the acrylic frame and tested. During the performance of these tests, it was noticed that the air gap between the fabric and the plate provided enough damping (to the particular jet temperature and Reynolds number) so that any experiment beyond $z/d = 3$

produced virtually undetectable changes. It is for this reason that data was collected only up to distances of $z/d = 3$.

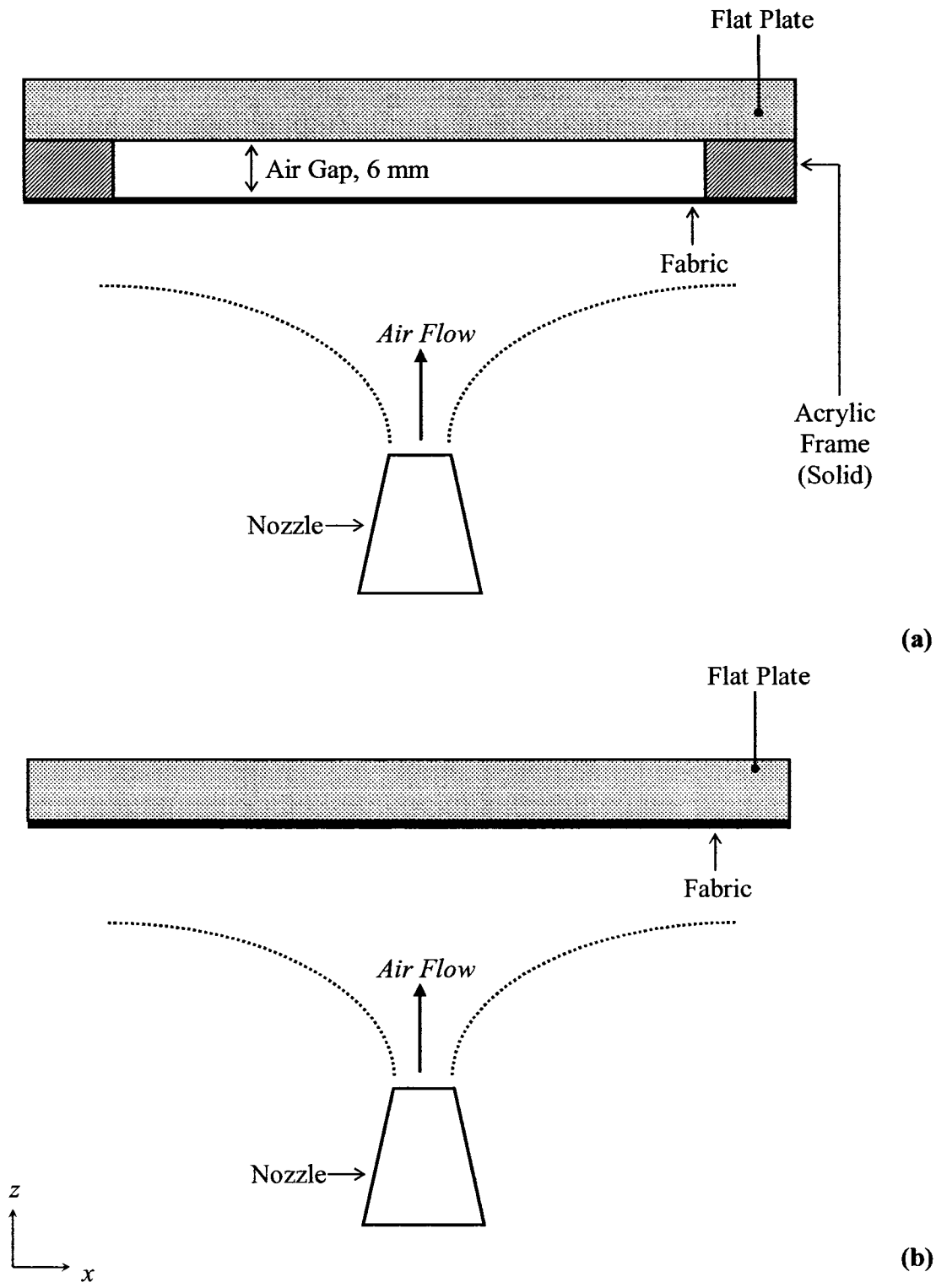

Figure 3.10 **(a)** Testing Geometry: Fabric – Air Gap – Skin Simulant Flat Plate (non-contact tests). **(b)** Testing Geometry: Fabric– Skin Simulant Flat Plate (contact tests)

In these tests fabric sagging was noticed under the influence of the jet. This will have an effect on the size of the gap and consequently on the overall heat transfer. In a similar manner, shim stock was tested using the acrylic frame. Tests for nozzle-to-plate separations of 1, 2 and 3 were performed in this case as well.

3.3.1 Calculations Procedure

The impinging nozzle was positioned concentric with the skin simulant plate, and was moved along the perpendicular axis of the plate to simulate different *z/d* ratios. The local Nusselt number, *Nu*, at each radial location, *r/d*, was derived from the surface heat flux history as described earlier. Given a heat flux at a particular location and time, Newton's law of cooling (Equations 3.4) can be used to calculate the local heat transfer coefficient, *h*. Then, using the definition of Nusselt number based on nozzle diameter, *d* (Equation 3.5), local results at any given time and *r/d* location can be obtained.

$$q'' = h\,(T_e - T_s) \tag{3.4}$$

$$Nu = \frac{hd}{k} \tag{3.5}$$

Where q'' is surface heat flux history (local) derived from the surface temperature history. Symbol T_s is the surface temperature at any given time. Symbol T_e is the jet exit temperature as defined in Section 3.2.2. h and d are the local heat transfer coefficient and nozzle diameter, respectively. Air thermal conductivity, k, is evaluated

at the average local film temperature, $T_{avg} = (T_e+T_s)/2$. Some authors define k in terms of the adiabatic temperature to account for compressibility effects [11]. In this case, the adiabatic temperature would be very close to T_e because the flow Mach number at the nozzle exit is only about 0.03. See Appendix E for details on computer code created to convert temperature data into Nusselt number.

CHAPTER 4: RESULTS AND DISCUSSIONS

Experiments were performed using the procedures and apparatus described in Chapter 3. Results from those experiments are presented and discussed in this chapter. In the first section, experimental results from all tests will be shown separately (by category). This includes heat transfer results obtained with the skin simulant plate alone at 10 different nozzle-to-plate spacings (*z/d*). Also, the results obtained by adding the FR fabric in contact and 6 mm away from the skin simulant flat plate. The results of having a sheet of steel shim stock placed 6 mm away from the plate will also be presented. In the second section of this chapter, those results are compared and discussed. A comparison of some of the present experiments with published data explaining the similarities and differences between the two is also included in this here. The chapter concludes with the repeatability test results.

4.1 Experimental Results

Results in this section are presented in terms of dimensionless Nusselt number, *Nu*, nozzle-to-plate separations, *z/d*, radial distance from centre of plate, *r/d*, and incident heat flux, *q"*. The results show the variation of Nusselt number across the plate (axis B-B in Figure 3.6) and the incident surface heat flux history of the plate at various radial locations (thermocouples *"e", "f", "g", "h"* and *"i"* in Figure 3.5). Section 4.1.1 shows the results obtained with the skin simulant flat plate alone at 10 different *z/d* spacings. Sections 4.1.2 and 4.1.3 show the results when FR Fabric is placed in contact and at 6 mm away from the flat plate, respectively. Section 4.1.4

shows the results obtained by adding a sheet of steel shim stock 6mm away from the plate.

4.1.1 Results from Skin Simulant Flat Plate Alone at Different *z/d* Spacings

Figure 4.1 shows the variation of Nusselt number as a function of radial position, *r/d*, in axis B-B (refer to Figure 3.6 in Chapter 3). This plot is for a nozzle-to-plate separation of 1 nozzle diameter (*z/d* = 1). The *x*-axis of the plot is divided into positive and negative *r/d* values to show both sides of the impingement point. The stagnation point is located at *r/d* = 0.00. A spline was used to follow the trend of the data, which does not show the symmetry expected on both sides of the *x*-axis. The Nusselt number variation is presented at 3 different points in time after the jet was allowed to impinge on the surface of the plate. The times chosen were 20, 40 and 65 seconds. It is clear from the figure that Nusselt number slightly decreases at all locations as time increases. It is interesting to note that the maximum Nusselt number occurs slightly off the stagnation point at about *r/d* ≈ 0.3. Then, it starts to decrease until it plateaus and shows signs of a second peak (much lower than the first one) at about *r/d* ≈ 1.9. After that, the Nusselt number decreases monotically to the farthest sensor located at about *r/d* ≈ 3.5. Figure 4.2 is a surface heat flux history plot for thermocouples "*e*", "*f*", "*g*", "*h*" and "*i*" (as labelled in Figure 3.6). This plot is for a nozzle-to-plate separation of 1 nozzle diameter (*z/d* = 1). After the hot air jet is allowed to impinge on the surface of the plate (after 5 seconds) a drastic "jump" in surface heat flux is noted. It starts to decrease as time increases. It is important to note that this decay happens more rapidly at the first 8 to 10 seconds after the plate has been exposed. As it is expected from Figure 4.1, the central thermocouple "*e*" (*r/d* =

0.00) does not present the highest surface heat flux. Rather, thermocouples located next to it show slightly higher rates of heat transfer. Interestingly, the heat flux histories for all thermocouples located within $r/d \approx \pm 2$ show values that are close to each other, except for the farthest thermocouple. The farthest thermocouple, "*i*", (r/d = 3.39) shows much lower surface heat flux history values and a less dramatic decay.

Figure 4.3 shows the variation of Nusselt number as a function of radial position, r/d, for a nozzle-to-plate separation of 2 nozzle diameters (z/d = 2). Like Figure 4.1, Figure 4.3 shows a peak Nusselt number value that is off centred. However, there are no signs of a second peak. It is interesting to note that Nusselt numbers at all locations are consistently higher than those for z/d = 1. The plot still monotically decays as r/d increases. Figure 4.4 is a surface heat flux history for z/d = 2. The trend is very similar to that of Figure 4.2. However, it is noted that the surface heat flux history trends of the various thermocouples start to separate slightly from each other unlike the z/d = 1 case.

Figure 4.5 shows the variation of Nusselt number as a function of radial position, r/d, for a nozzle-to-plate separation of 3 nozzle diameters (z/d = 3). A completely different distribution is found in this case. The maximum *Nu* occurs at the stagnation point showing values that are considerably higher than those in cases z/d = 1 and 2. There are no signs of secondary peaks in this plot and the decay is exponential (see Appendix F) along both sides of the axis B-B. Figure 4.6 is the corresponding surface heat flux history for the z/d = 3 case. The trends are similar to the ones presented in previous cases. However, it is important to note that the

histories at different locations separate from each other even further than at smaller z/d ratios.

Figures 4.7 and 4.8 present the $z/d = 4$ case. The heat transfer distribution in Figure 4.7 show many similarities with the $z/d = 3$. In this case, however, the Nusselt numbers are even higher than before, suggesting better heat transfer. It peaks at the stagnation point with Nu values close to 200 (the highest obtained during experimentation). Figure 4.8 shows yet more surface heat flux history separation at the different radial locations.

Figure 4.9 is the Nusselt number distribution for a nozzle-to-plate separation of 5 nozzle diameters ($z/d = 5$). It peaks at the stagnation point at a Nu value close to 160. Note the smoother decay as one goes further from the centre. Figure 4.10 is the surface heat flux history for $z/d = 5$. The histories are separated more evenly which explains the smoother decay in the Nu distribution.

Figure 4.11 shows many similarities with the $z/d = 3$, 4 and 5 cases. In all cases, the Nusselt number peaks at the stagnation point. Interestingly, the plots at 20, 40 and 65 seconds are more separated of each other than in previous cases. The decay of Nu is also less steep. Figure 4.12 is the surface heat flux history for $z/d = 6$. The plot shows evenly spaced histories with a slightly steeper decay. This may explain the more significant separation at 20, 40 and 65 seconds in the previous plot.

Figures 4.13 and 4.14 show the Nusselt number distribution and surface heat flux history, respectively, for the $z/d = 7$ case. The general behaviour of both plots is comparable to the cases shown above. Heat flux in Figure 4.14 shows more "noise"

than before. This may be due to larger nozzle-to-plate separations (see Section 4.2.1). The histories at the different radial locations are spaced evenly like in previous cases.

Figure 4.15 is the Nusselt number distribution for a nozzle-to-plate separation of 8 nozzle diameters (z/d = 8). It peaks at the stagnation point and monotically decays as r/d increases. The decay, however, is not as steep as those found in cases z/d = 3, 4 or 5. Figure 4.16 is the surface heat flux history for z/d = 8. The plot is shows even separation of histories at the different radial locations.

Figures 4.17 and 4.18 show the Nusselt number distribution and surface heat flux history, respectively, for the z/d = 9 case. The plots are consistent with preceding cases except the rates of heat transfer are lower. Figure 4.18 shows more "noise" but the trend is consistent with that would be expected. Similarly, Figures 4.19 and 4.20 show the Nusselt number distribution and surface heat flux history, respectively, for the z/d = 10 case. This is the largest nozzle-to-plate separation tested in the scope of this study. Again, the rates of heat transfer are lower than those found in smaller separations. Noise becomes a factor of error in surface heat flux history readings. Figure 4.21 shows the Nusselt number distribution for z/d's (1, 2, 4, 6, 8, and 10) at 65 seconds (end of test). It is interesting to note that the maximum Nusselt number happened when z/d = 4. This occurred at the stagnation point, r/d = 0.00. However, further from the stagnation point, at about r/d $\approx$ 2, the maximum heat transfer actually happened when z/d = 1. As z/d increases, the decay becomes less drastic. Semi-log plots of the Nusselt number distribution decay can be found in Appendix F. From these relationships, it was shown that when $z/d \geq 4$ a linear behaviour occurred, which strongly suggests an exponential relationship between Nu and r/d.

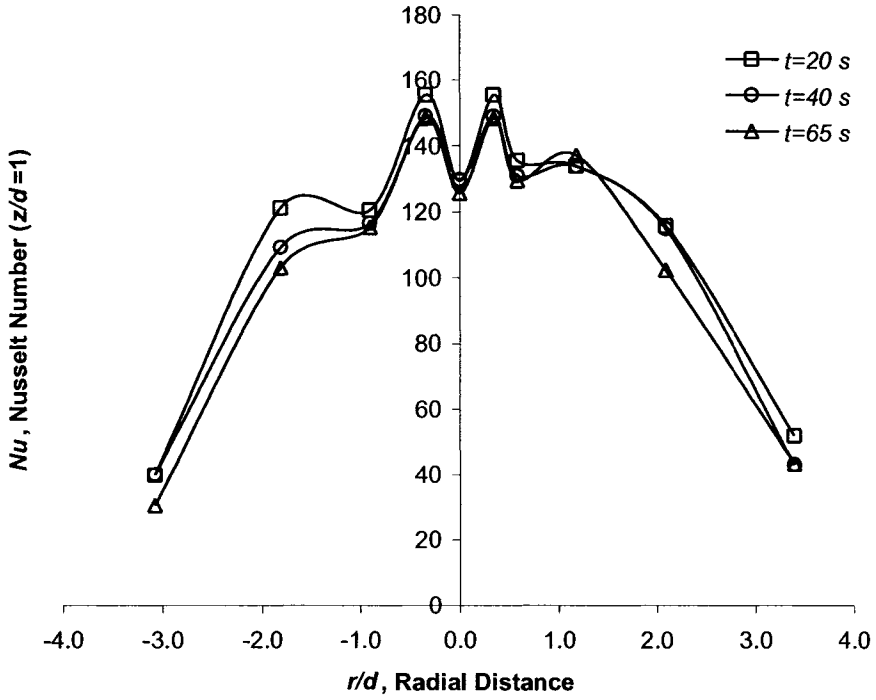

Figure 4.1 Nusselt number as a function of radial distance on plate at three different points in time during the experiment for z/d=1.

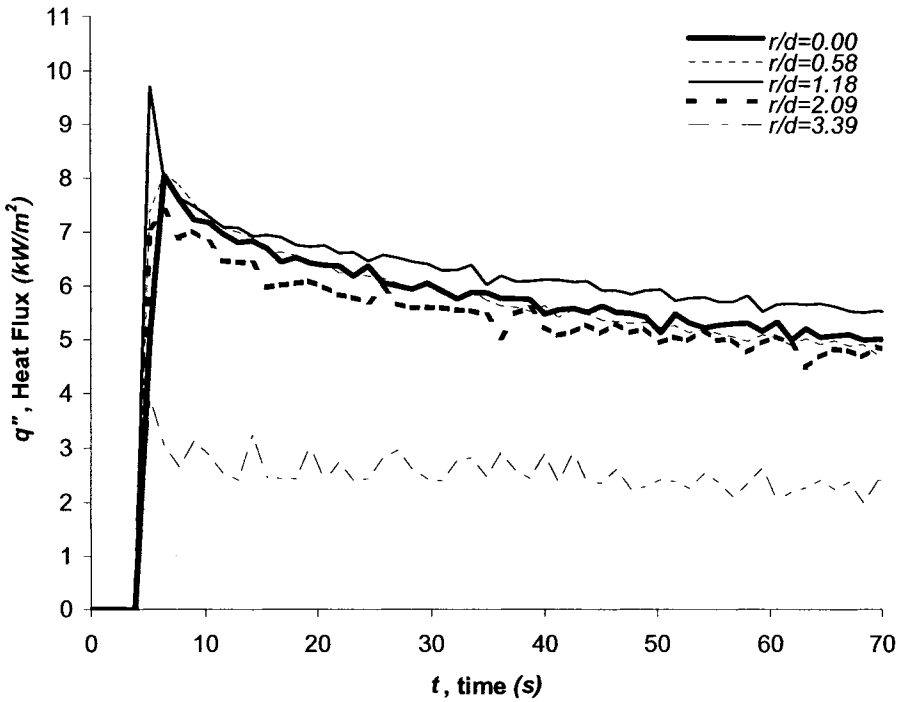

Figure 4.2 Surface heat flux history measured at different radial locations for z/d=1.

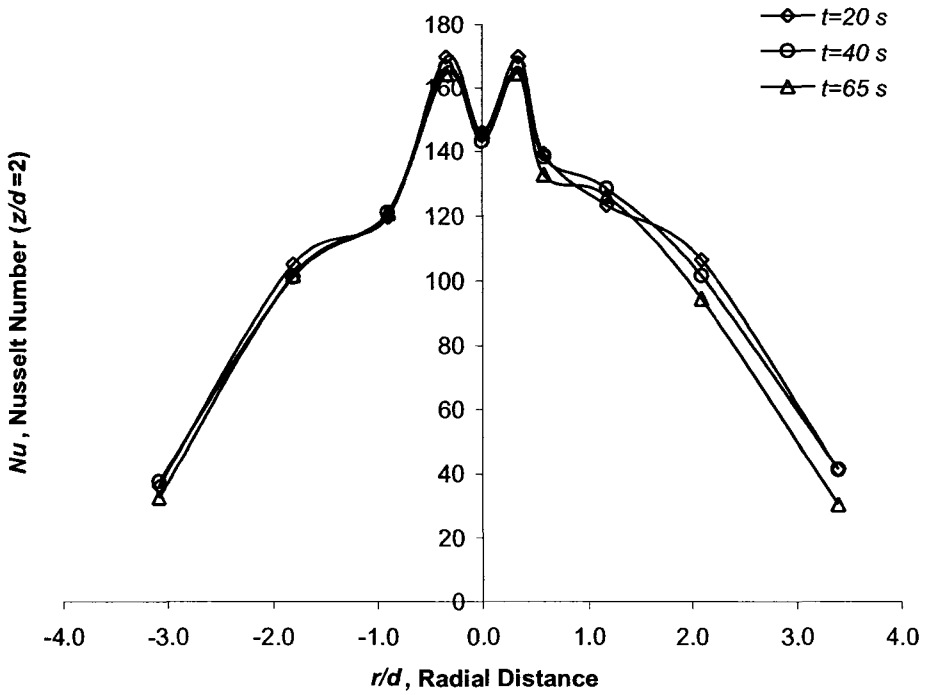

Figure 4.3 Nusselt number as a function of radial distance on plate at three different points in time during the experiment for z/d=2.

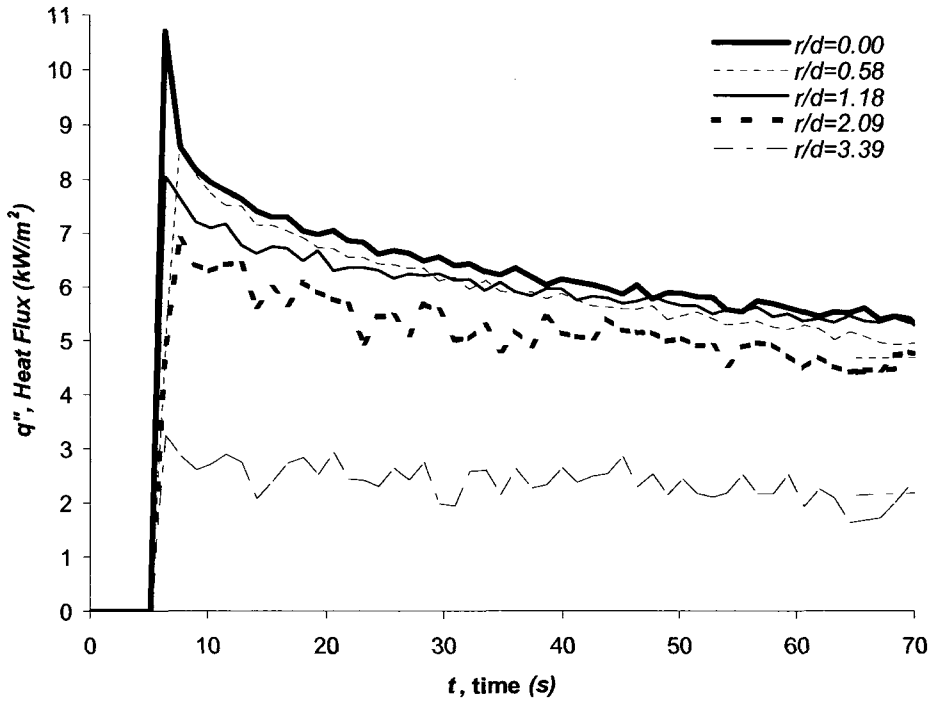

Figure 4.4 Surface heat flux history measured at different radial locations for z/d=2.

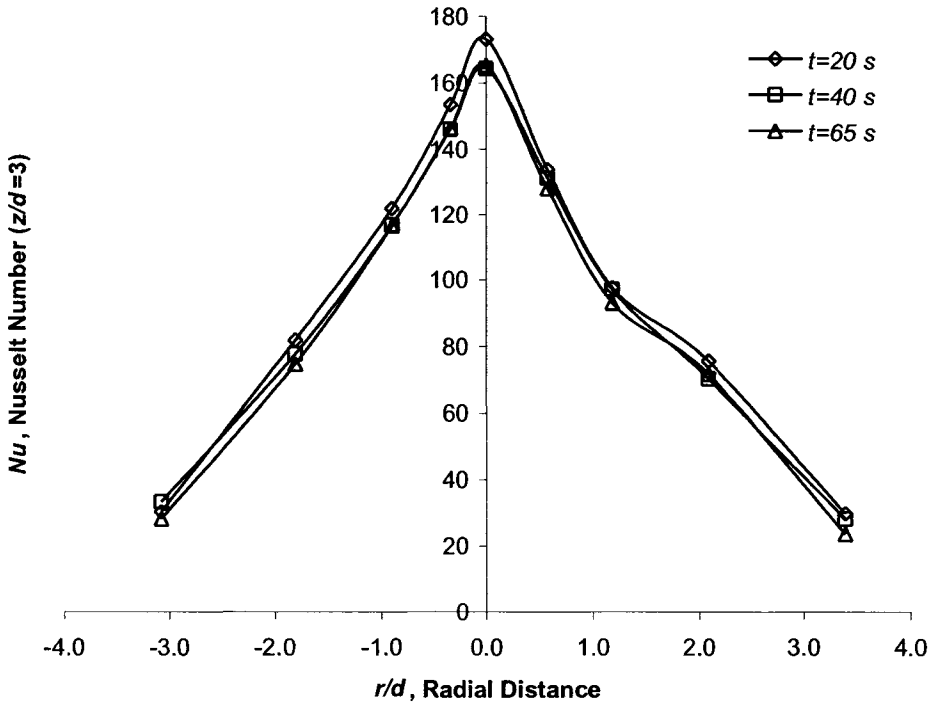

Figure 4.5 Nusselt number as a function of radial distance on plate at three different points in time during the experiment for z/d=3.

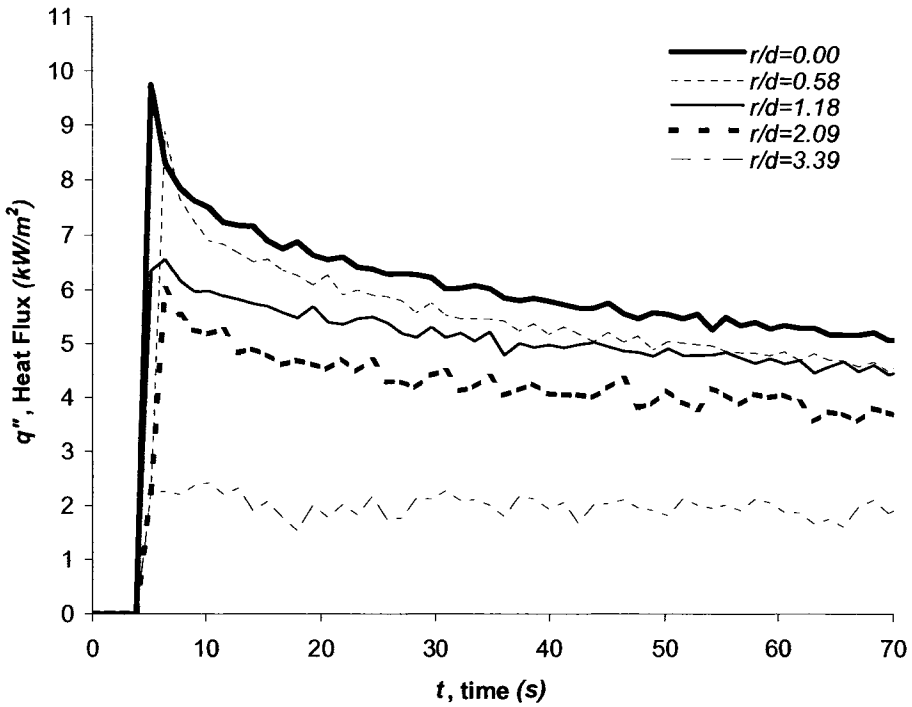

Figure 4.6 Surface heat flux history measured at different radial locations for z/d=3.

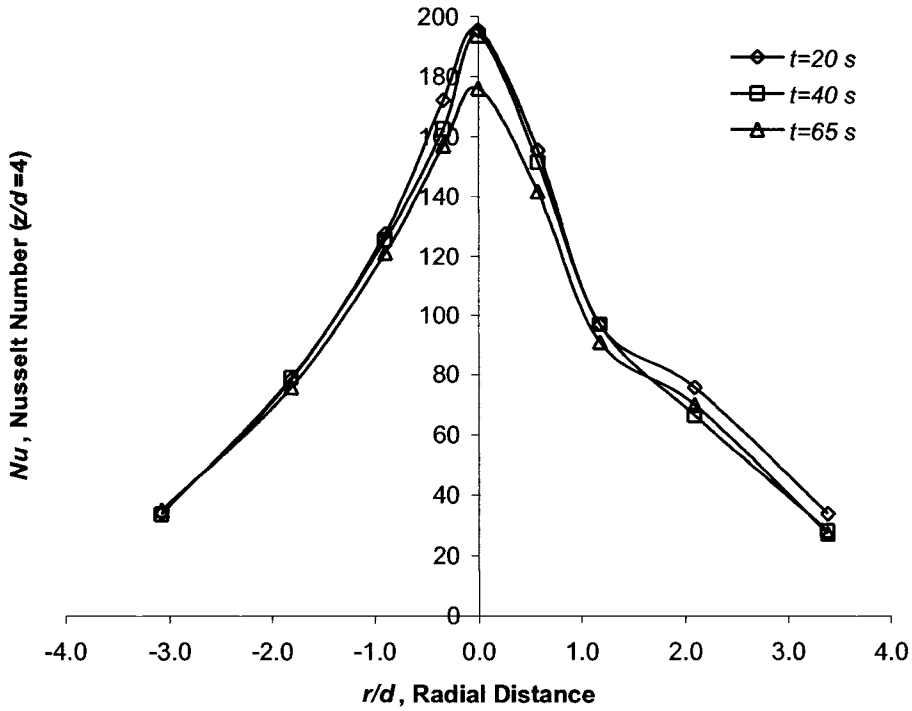

Figure 4.7 Nusselt number as a function of radial distance on plate at three different points in time during the experiment for z/d=4.

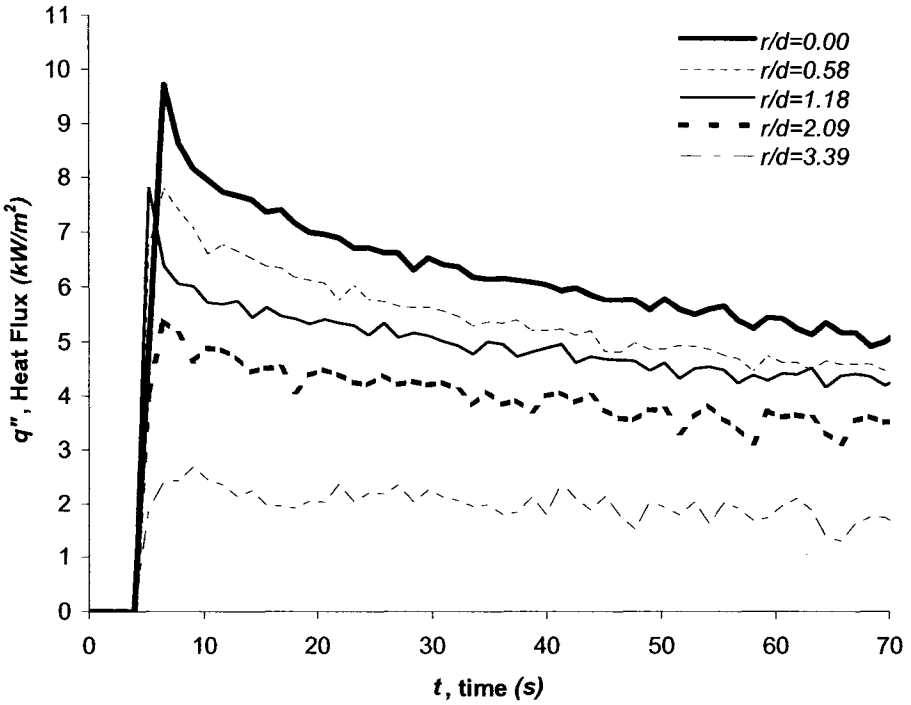

Figure 4.8 Surface heat flux history measured at different radial locations for z/d=4.

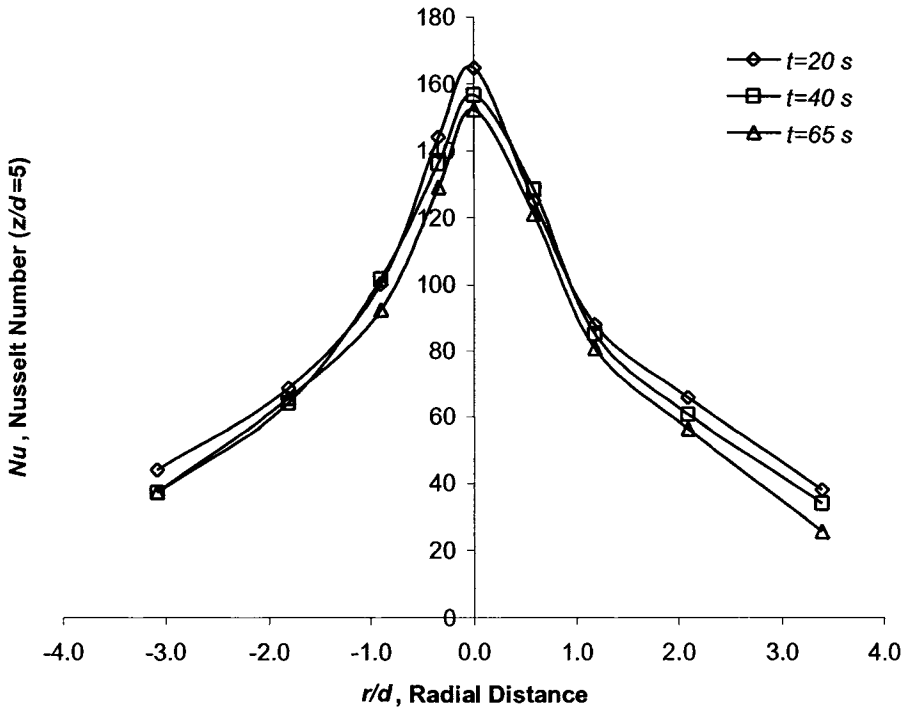

Figure 4.9 Nusselt number as a function of radial distance on plate at three different points in time during the experiment for z/d=5.

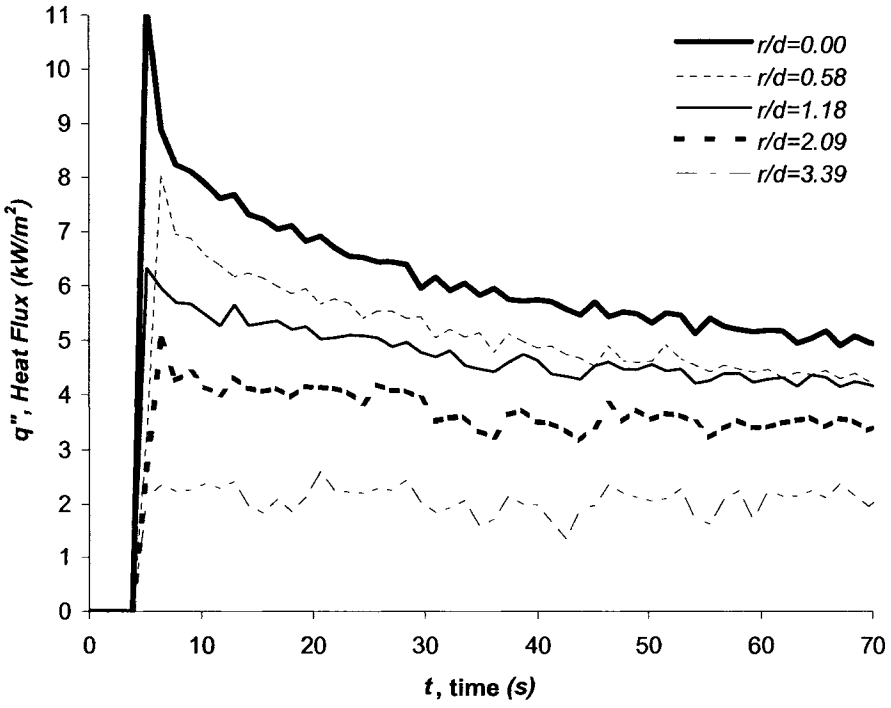

Figure 4.10 Surface heat flux history measured at different radial locations for z/d=5.

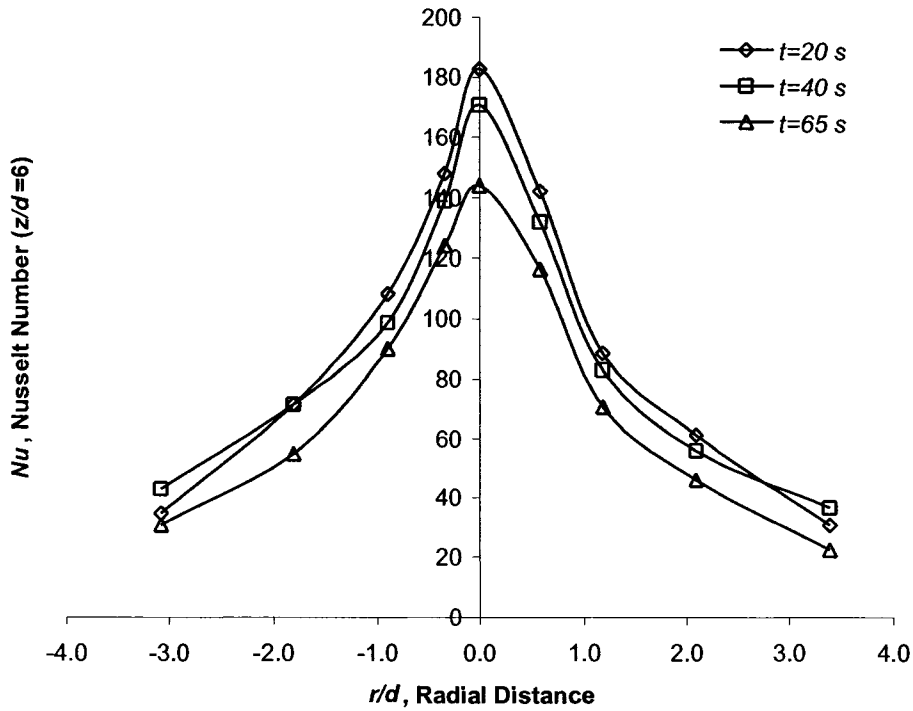

Figure 4.11 Nusselt number as a function of radial distance on plate at three different points in time during the experiment for z/d=6.

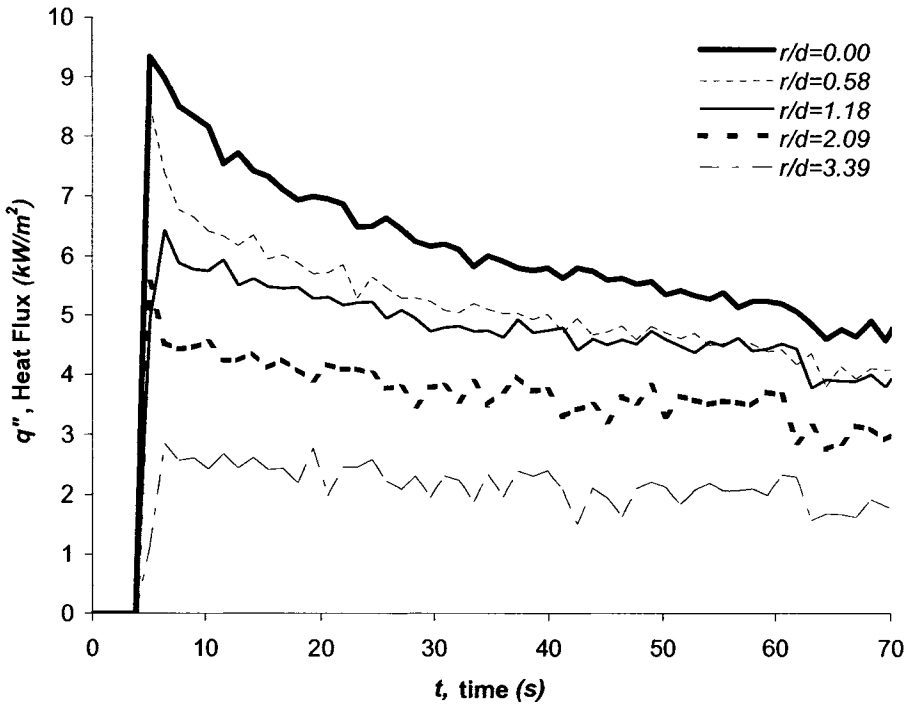

Figure 4.12 Surface heat flux history measured at different radial locations for z/d=6.

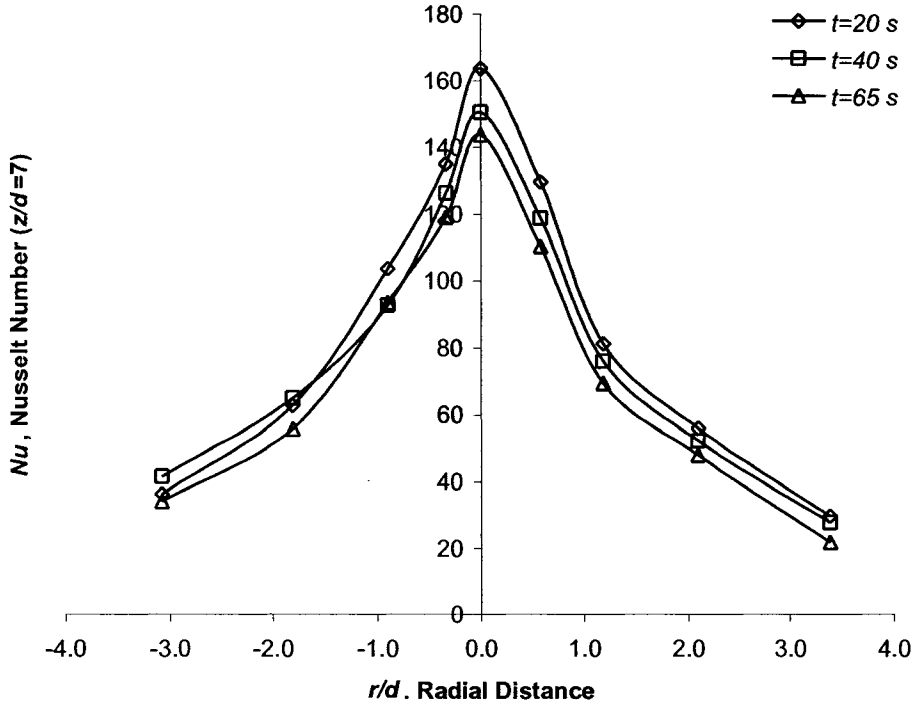

Figure 4.13 Nusselt number as a function of radial distance on plate at three different points in time during the experiment for z/d=7.

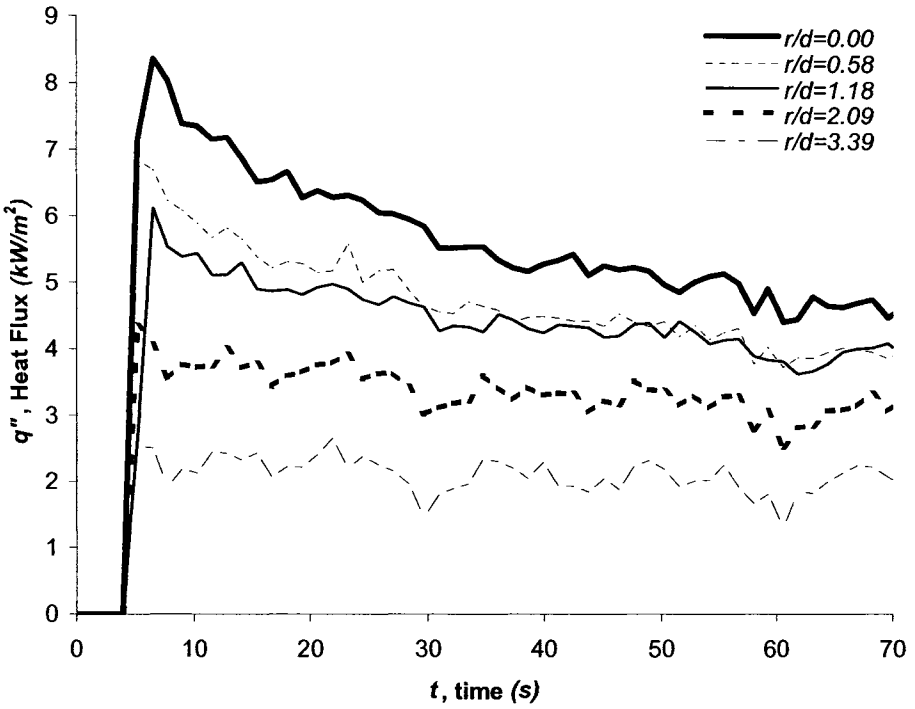

Figure 4.14 Surface heat flux history measured at different radial locations for z/d=7.

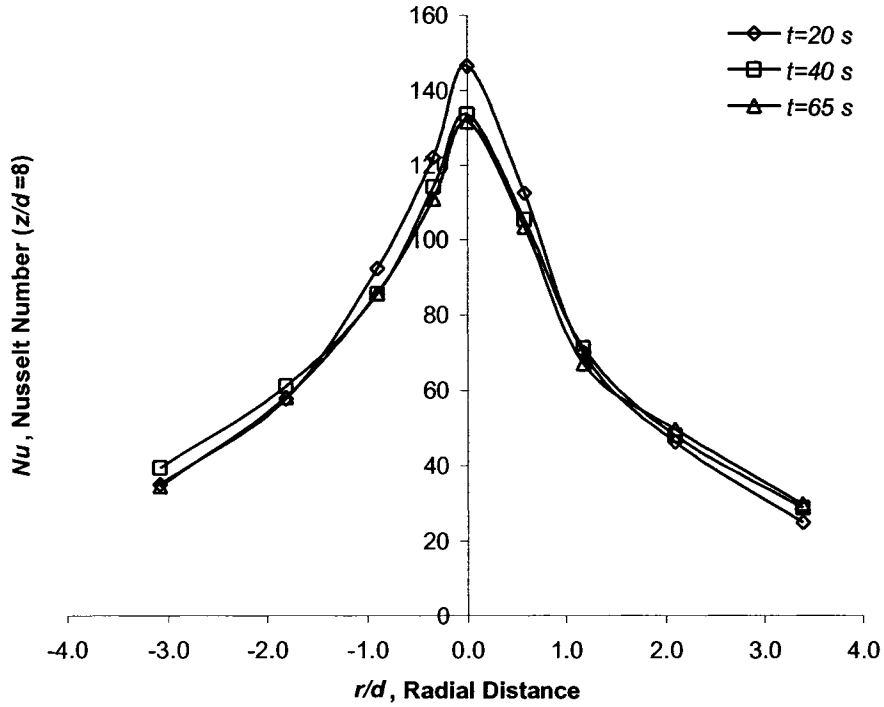

Figure 4.15 Nusselt number as a function of radial distance on plate at three different points in time during the experiment for z/d=8.

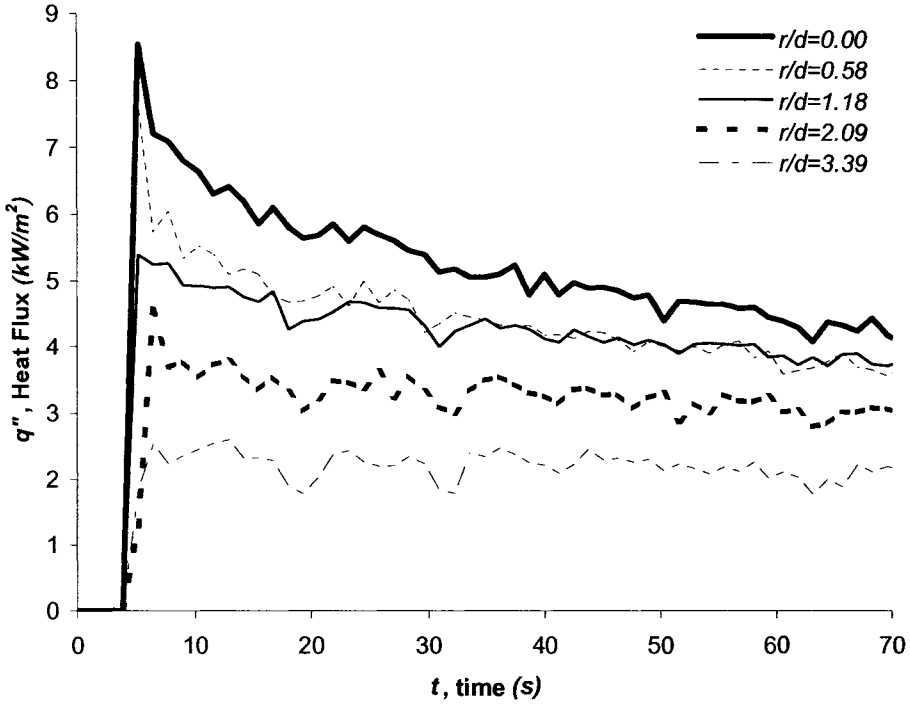

Figure 4.16 Surface heat flux history measured at different radial locations for z/d=8.

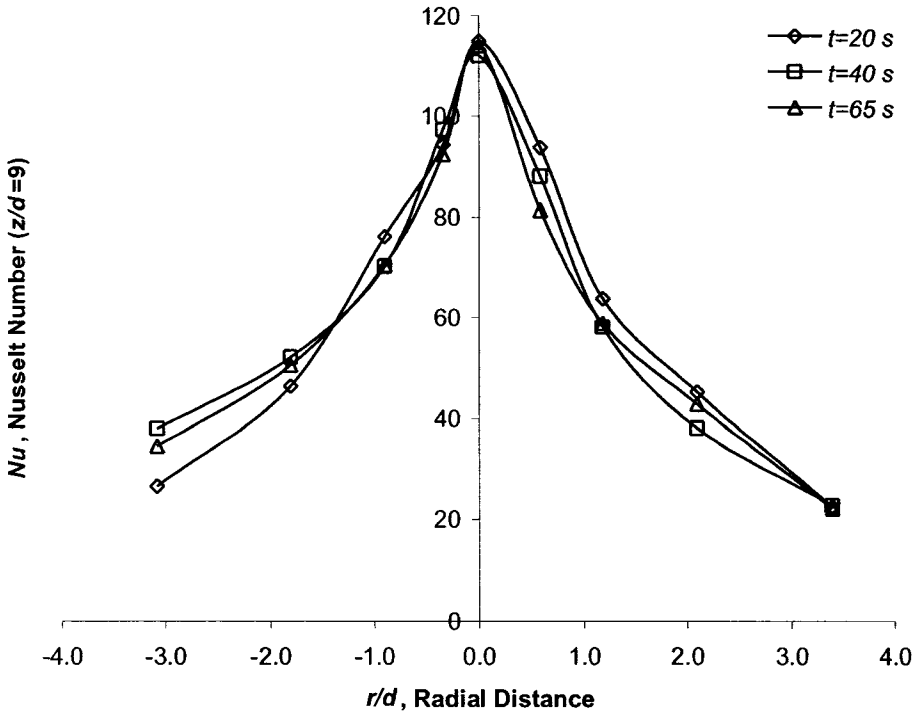

Figure 4.17 Nusselt number as a function of radial distance on plate at three different points in time during the experiment for z/d=9.

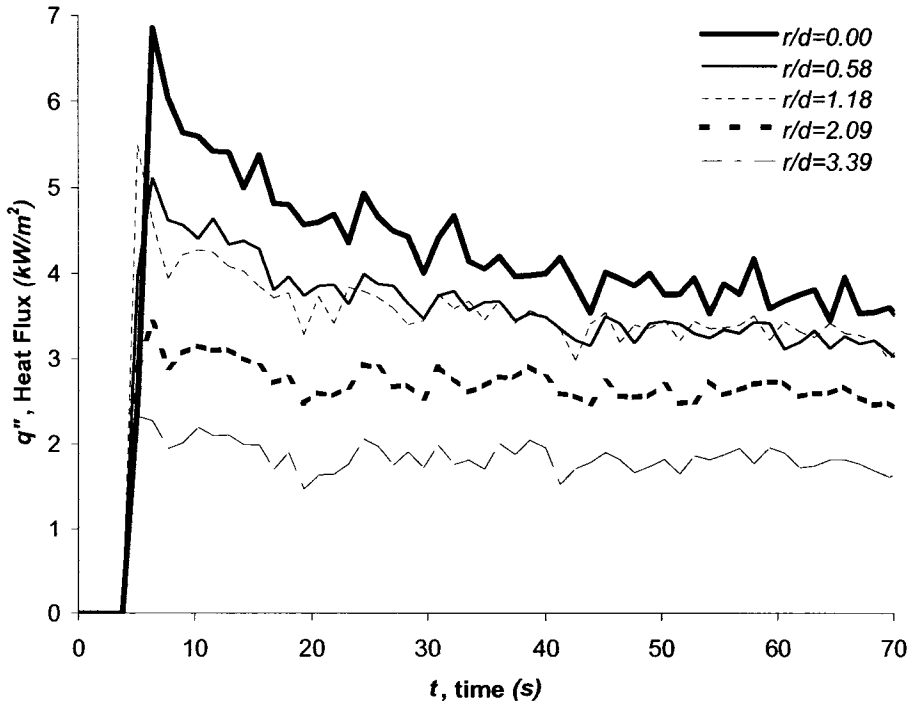

Figure 4.18 Surface heat flux history measured at different radial locations for z/d=9.

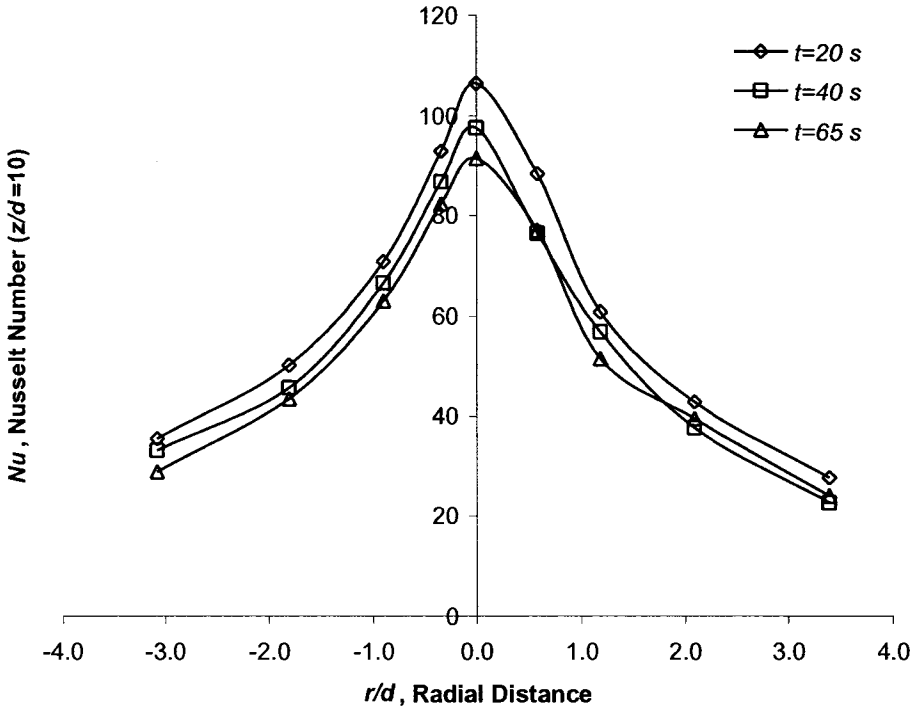

Figure 4.19 Nusselt number as a function of radial distance on plate at three different points in time during the experiment for z/d=10.

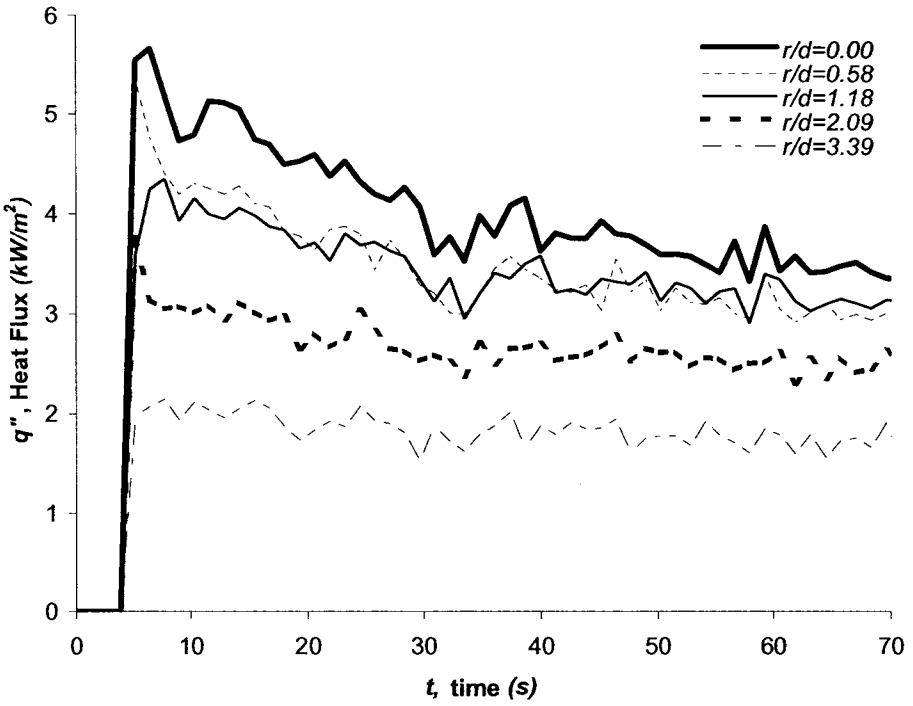

Figure 4.20 Surface heat flux history measured at different radial locations for z/d=10.

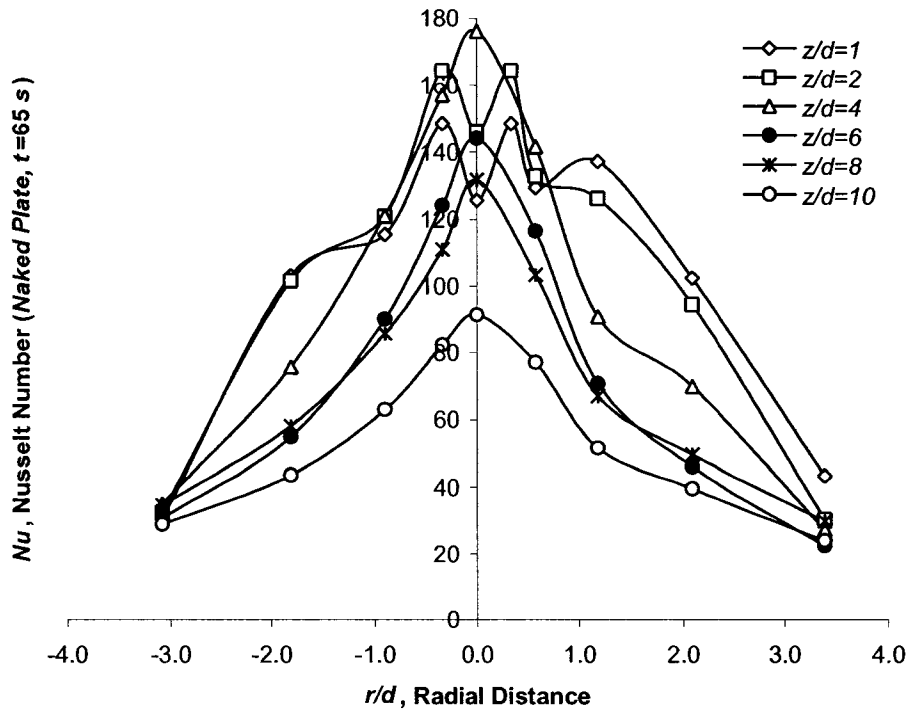

Figure 4.21 Nusselt Number Profile at different nozzle-to-plate distances after 65 seconds.

4.1.2 Results of Adding FR Fabric in Contact with Flat Plate

Samples of three different types of FR fabrics were placed in contact with the skin simulant flat plate as shown in Figure 3.10b. The FR fabrics were conditioned as explained in Section 3.1.5. The test procedure was the same as the one outlined in the previous chapter. Results for a nozzle-to-plate separation range of 1 to 10 are presented here. Figures 4.22 through 4.27 show the Nusselt number distribution when FR fabric is placed in contact with the skin simulant flat plate. The plots are for nozzle-to-plate separations of 1, 2, 4, 6, 8 and 10 nozzle diameters, respectively. Each figure shows the 3 types of fabric tested at a given *z/d*: Indura® (339), Kevlar®/PBI (208) and Nomex® IIIA (208). The data were plotted at 65 seconds after the jet was allowed to impinge on the surface of the plate/fabric system (end of test). A spline

was used to follow the trend of the data, which does not show the symmetry expected on both sides of the x-axis.

Figure 4.22 shows the Nusselt number variation with r/d for a $z/d = 1$. All 3 fabrics showed similar behaviour under the influence of the jet. The maximum Nusselt number occurred off the stagnation point at about $r/d \approx 0.3$ for all of the fabrics. Nomex® IIIA (208) has higher rates of heat transfer at all locations, in particular closer to the stagnation point. Indura® (339) shows consistently lower Nusselt numbers than those of Nomex® IIIA (208). Kevlar®/PBI (208) lies between the two. There are no signs of a second peak on any of the curves.

Figure 4.23 shows the Nusselt number variation with r/d for a $z/d = 2$. The Nusselt number peaks off the stagnation point but the peak is not as prominent as the $z/d = 1$ case. Nomex® IIIA (208) shows higher heat transfer rates at all points followed by Kevlar®/PBI (208) and Indura® (339). As r/d increases, all three fabrics show comparable Nusselt numbers.

Figure 4.24 shows the Nusselt number variation for the $z/d = 4$ case. In this case, the maximum Nusselt number occurs at the stagnation point (for all 3 fabrics). The most significant difference between the 3 fabrics happens near the stagnation point. However, as one goes further from the centre, all three materials show similar rates of heat transfer. Again, Nomex® IIIA (208) showed slightly higher Nu's followed by Kevlar®/PBI (208) and Indura® (339). It is important to note that the overall heat transfer rates (for all 3 fabrics) is higher than the $z/d = 1$ and 2 cases shown above.

Figures 4.25, 4.26 and 4.27 show the Nusselt number variation with radial distance for cases z/d = 6, 8 and 10, respectively. In all 3 cases the data trend is similar. The maximum Nusselt number occurs at the stagnation point and monotically decays as one goes further from the centre. Also, in all 3 cases Nomex® IIIA (208) has the highest rates of heat transfer followed closely by Kevlar®/PBI (208) and Indura® (339). The Nusselt numbers are consistently lower as z/d increases.

Figure 4.28 shows the Nusselt number distribution for various nozzle-to-plate separations for Indura® (339). The maximum Nusselt number occurs when z/d = 4 followed by z/d = 2. The lowest rate of heat transfer occur when z/d = 10. Figure 4.29 also shows the Nusselt number distribution for various z/d's. In this case, the plot shows the distributions for Kevlar®/PBI (208). It is interesting to note that the data here shows that the maximum rates of heat transfer happen when z/d = 1 followed by z/d = 2 and 4. Again, the lowest rate of heat transfer happen when z/d = 10. Figure 4.30 shows Nu distribution for various z/d's for Nomex® IIIA (208). In this case, the maximum rates of heat transfer happen when z/d = 4 followed by z/d = 2.

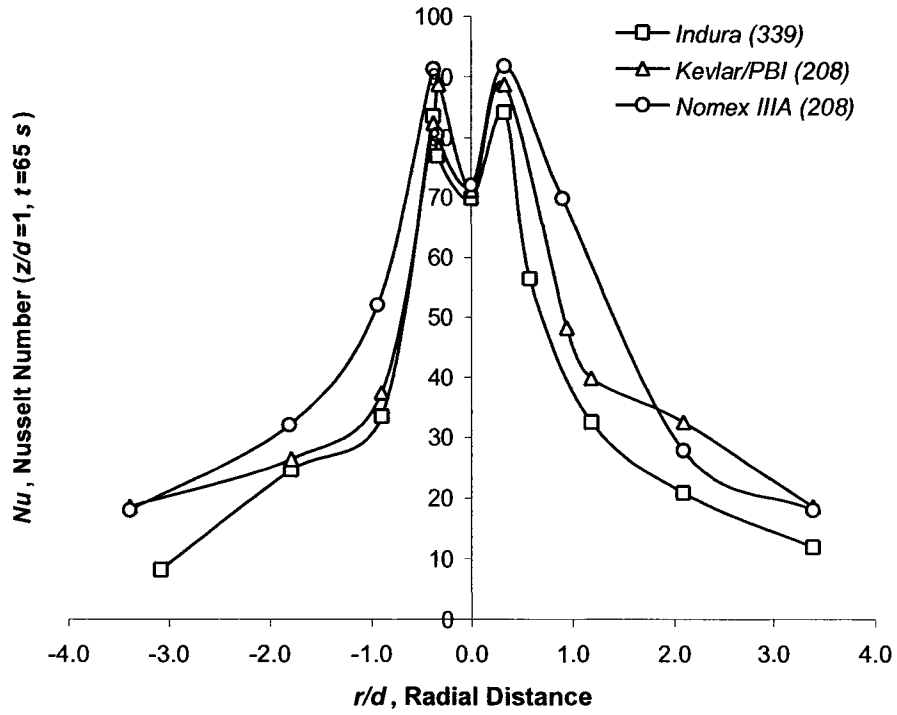

Figure 4.22 Nusselt number distribution for 3 types of fabric placed in contact with flat plate (fabric mass in g/m^2). Plots at time = 65 seconds and z/d = 1.

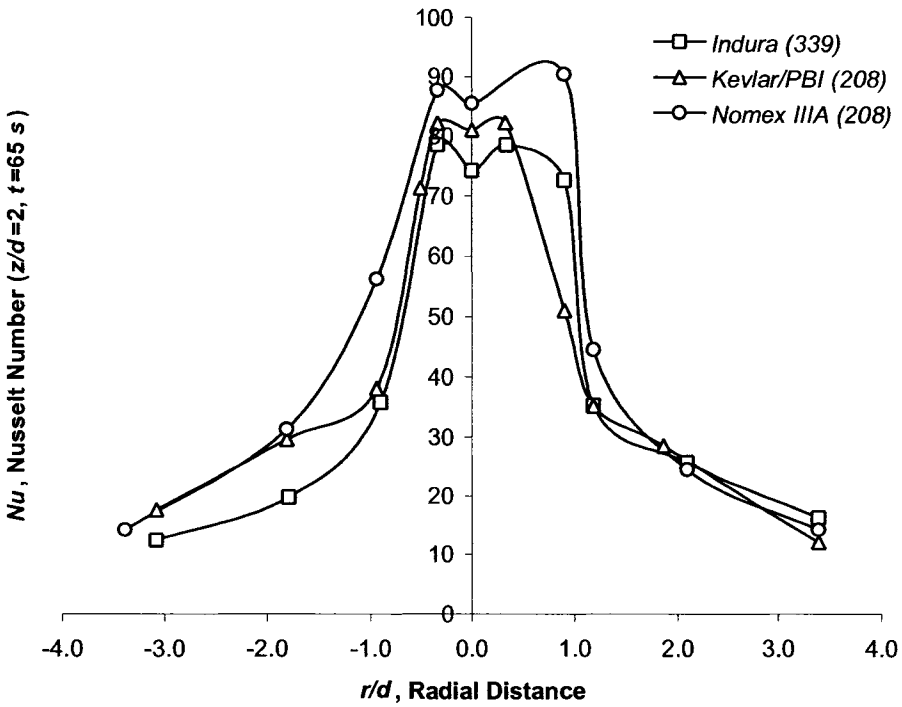

Figure 4.23 Nusselt number distribution for 3 types of fabric placed in contact with flat plate (fabric mass in g/m^2). Plots at time = 65 seconds and z/d = 2.

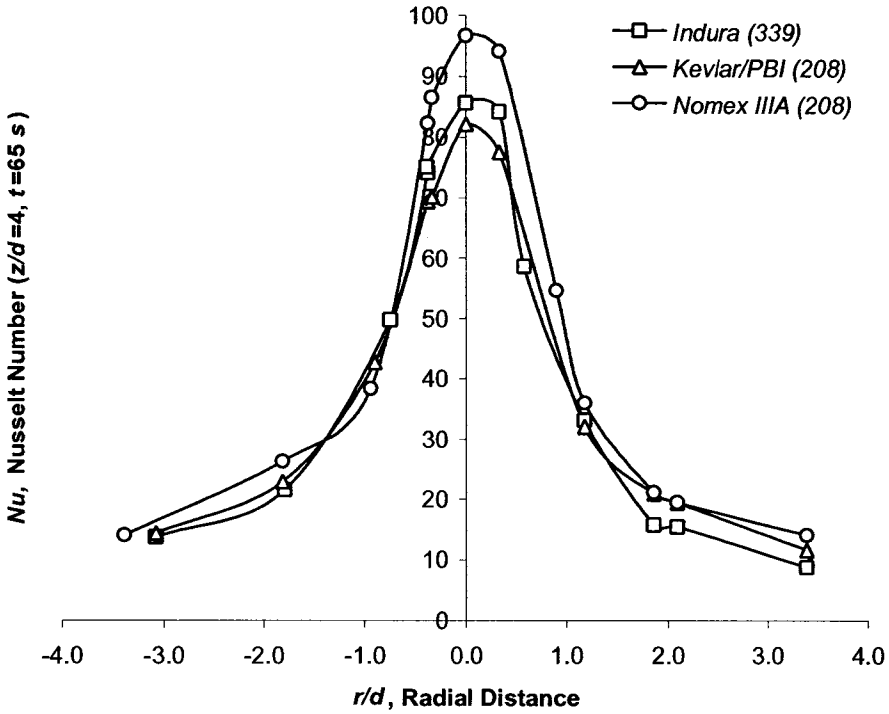

Figure 4.24 Nusselt number distribution for 3 types of fabric placed in contact with flat plate (fabric mass in g/m^2). Plots at time = 65 seconds and z/d = 4.

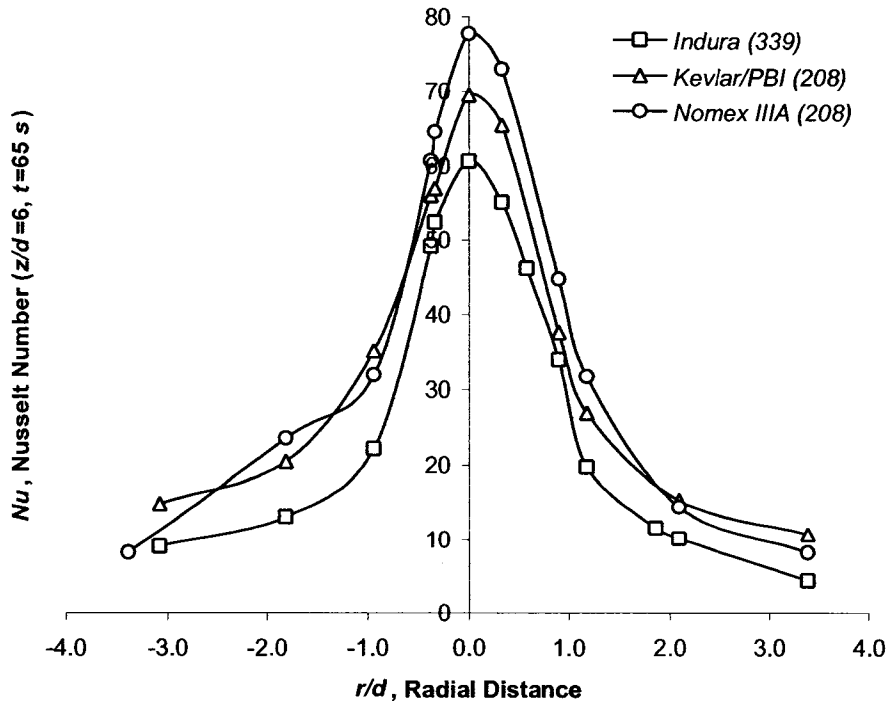

Figure 4.25 Nusselt number distribution for 3 types of fabric placed in contact with flat plate (fabric mass in g/m^2). Plots at time = 65 seconds and z/d = 6.

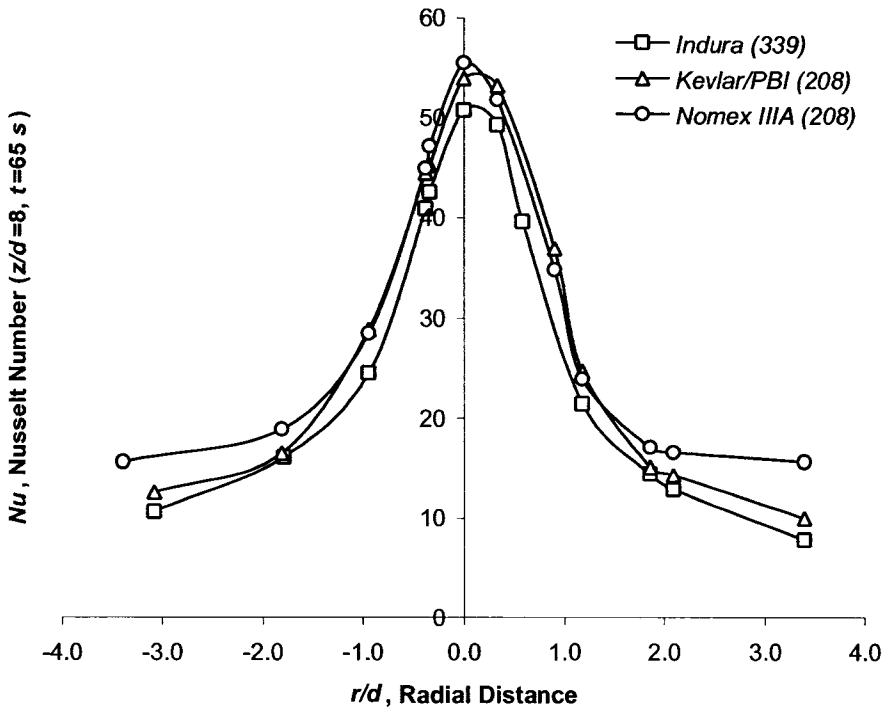

Figure 4.26 Nusselt number distribution for 3 types of fabric placed in contact with flat plate (fabric mass in g/m^2). Plots at time = 65 seconds and z/d = 8.

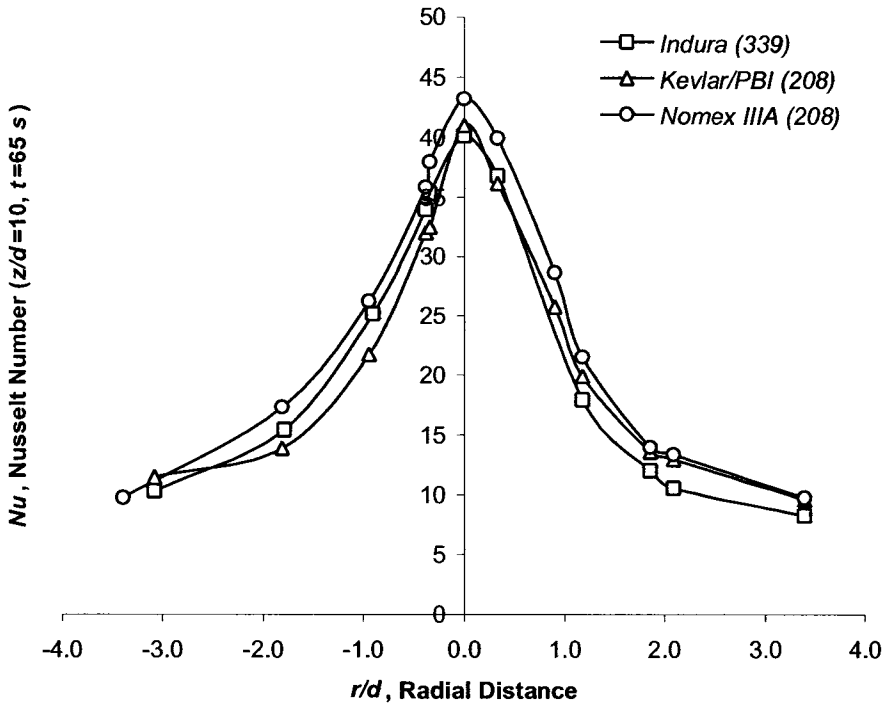

Figure 4.27 Nusselt number distribution for 3 types of fabric placed in contact with flat plate (fabric mass in g/m^2). Plots at time = 65 seconds and z/d = 10

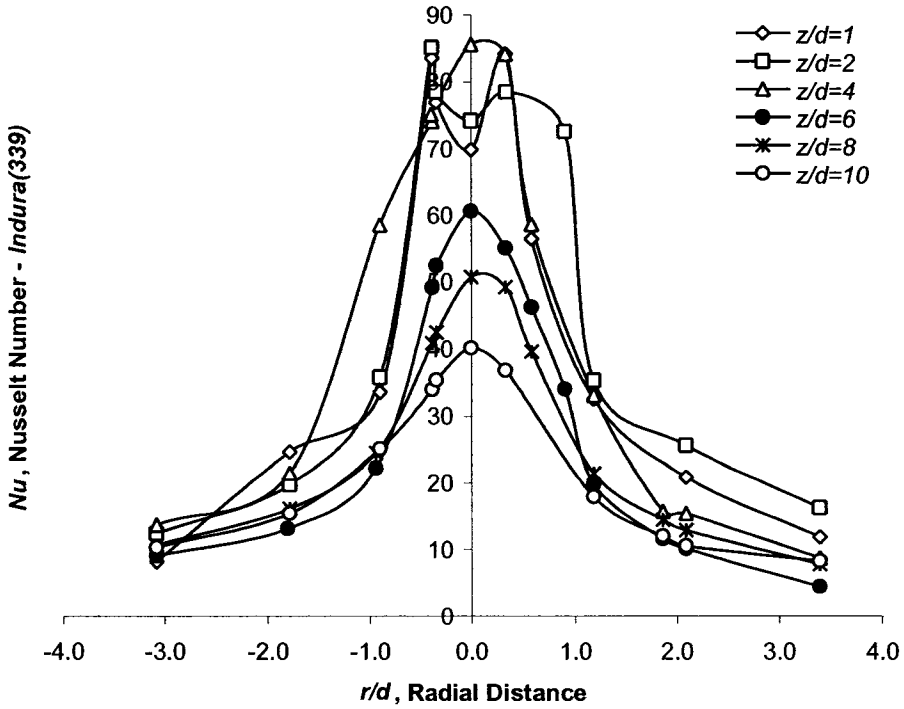

Figure 4.28 Nusselt number distribution for different z/d. Plots for Indura® (339) in contact with flat plate at time = 65 seconds.

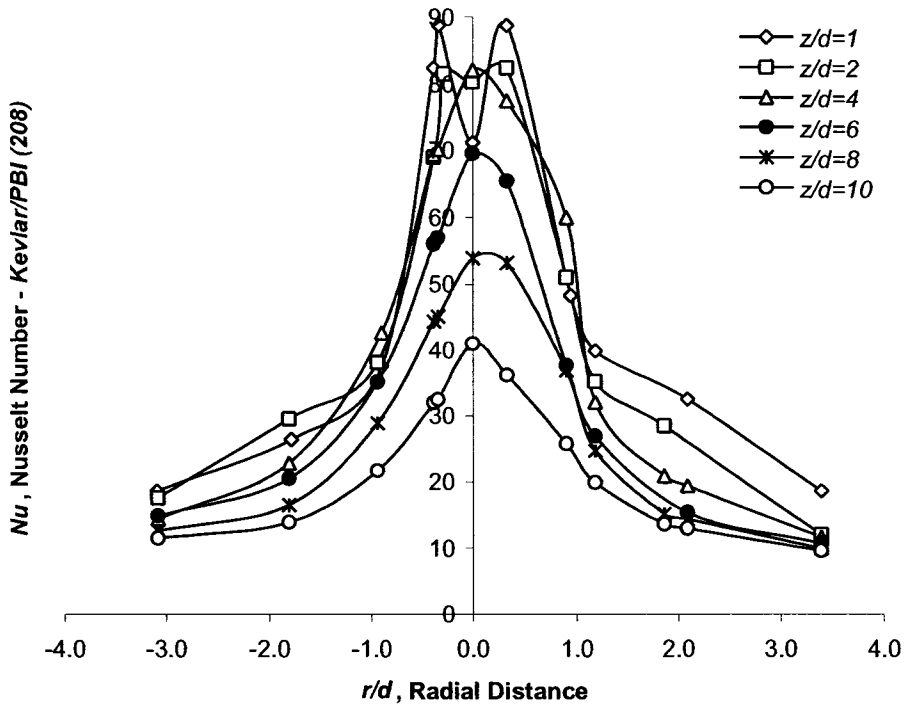

Figure 4.29 Nusselt number distribution for different z/d. Plots for Kevlar/PBI® (208) in contact with flat plate at time = 65 seconds.

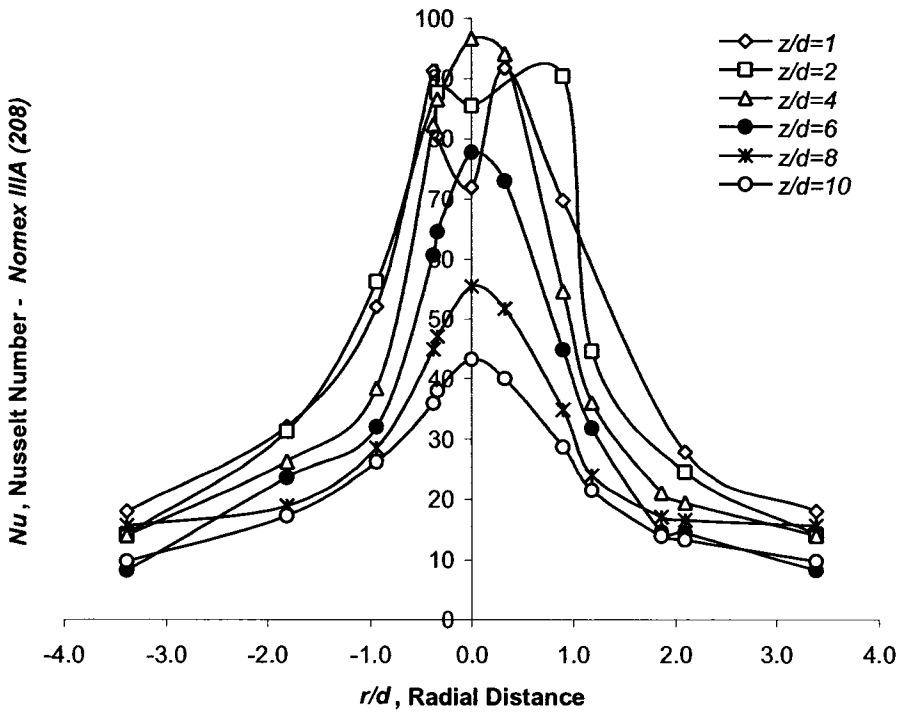

Figure 4.30 Nusselt number distribution for different z/d. Plots for Nomex® IIIA (208) in contact with flat plate at time = 65 seconds.

4.1.3 Results of Adding FR Fabric at a Space Away from Flat Plate

Fabric samples were placed 6 mm away from the skin simulant flat plate as described in the previous chapter. Three types of fabric were tested: Indura® (339), Kevlar®/PBI (208) and Indura® (208). The nozzle-to-plate separation was adjusted so that the distance *z* was measured from the nozzle's exit to the surface of the skin simulant flat plate and not the surface of the fabric (which was placed 6 mm from the plate). Three nozzle-to-plate separations were tested: 1, 2 and 3 nozzle diameters. Results beyond $z/d > 3$ were unacceptable. Figures 4.31, 4.32 and 4.33 show the results obtained for nozzle-to-plate separations of 1, 2 and 3, respectively. Each figure shows the Nusselt number distribution of all 3 FR fabrics at 65 seconds after the jet was allowed to impinge onto the surface of the plate.

Figure 4.31 is the Nusselt number distribution for a nozzle-to-plate separation of z/d = 1.0. The distribution of all 3 fabrics peaked slightly off the stagnation point. Clearly, Nomex® IIIA (208) has higher rates of heat transfer than the other 2 fabrics. The greatest *Nu* difference was found to be between Nomex® IIIA (339) and Indura® (339) – *Nu*~38. The difference in rates of heat transfer between Kevlar®/PBI (208) and Indura® (339) are not as drastic – *Nu*~10. There are no signs of second peaks in any of the curves – further explained in Section 4.2.

Figure 4.32 shows the Nusselt number distribution for z/d = 2. The distribution peaks at the stagnation point and monotically decays as r/d increases. Indura® (339) shows a flattened top. In this case, Nomex® IIIA still shows higher rates of heat transfer than those for Kevlar®/PBI (208) and Indura® (339). Furthermore, the greatest *Nu* difference was found to be between Nomex® IIIA (339) and Indura® (339) with a more pronounced difference – *Nu*~55. The difference in rates of heat transfer between Kevlar®/PBI (208) and Indura® (339) are also more pronounced than the previous case (z/d = 1) – *Nu*~30.

Figure 4.33 shows the Nusselt number distribution for z/d = 3. The distribution peaks at the stagnation point just like the previous case. However, the decay is more pronounced, especially for Nomex® IIIA. Again, Nomex® IIIA showed consistently higher Nusselt numbers than its 2 counterparts. The greatest *Nu* difference was still found with Indura® with a value of *Nu*~42. The difference between Kevlar®/PBI and Indura® was smaller but still higher than in the first case (z/d = 1) – *Nu*~22.

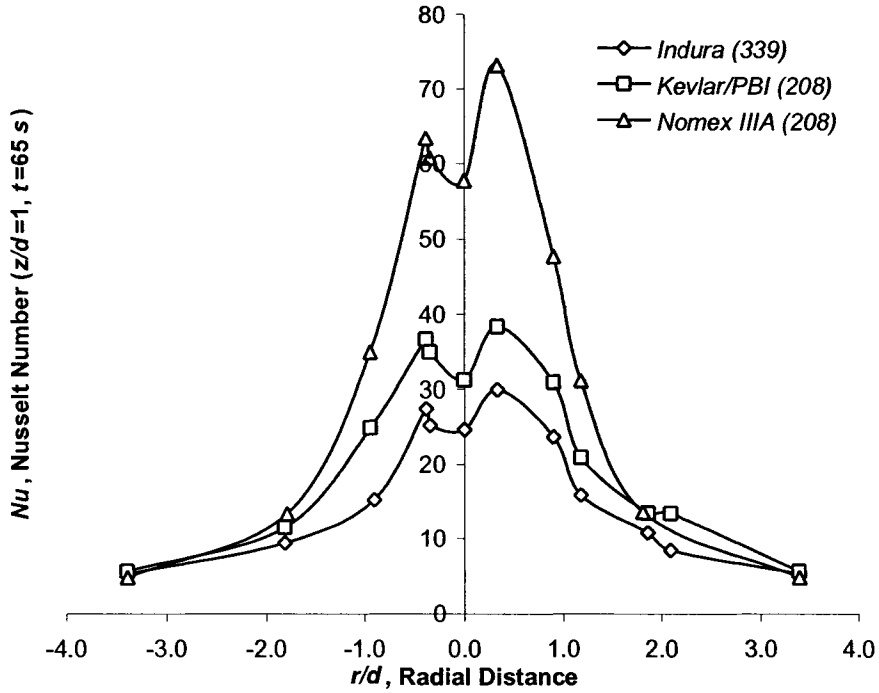

Figure 4.31 Nusselt number distribution for 3 types of fabric placed 6 mm away from flat plate (fabric mass in g/m^2). Plots at time = 65 s and $z/d = 1$.

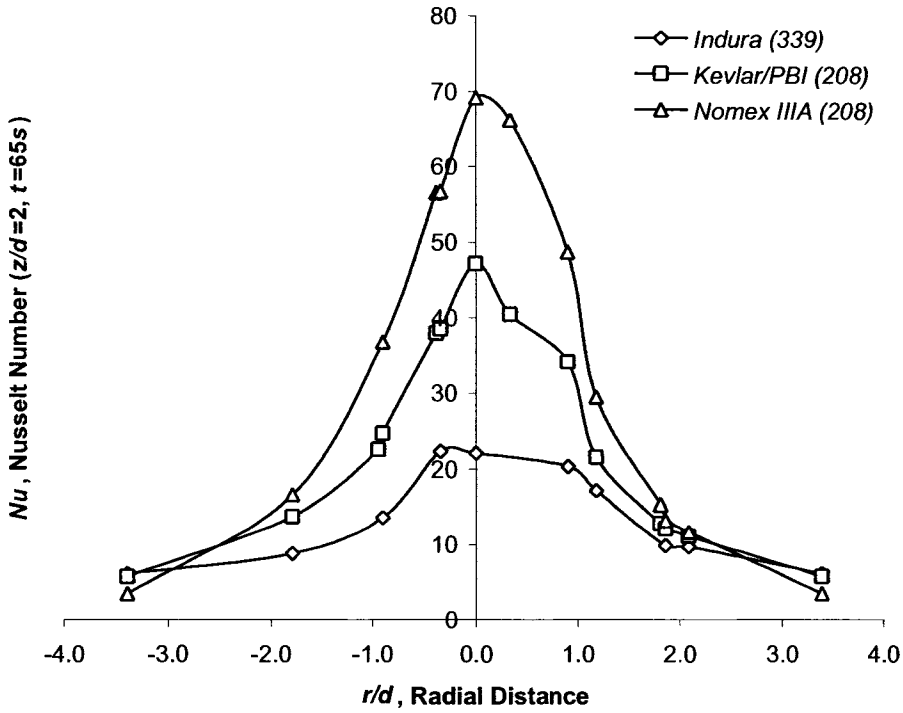

Figure 4.32 Nusselt number distribution for 3 types of fabric placed 6 mm away from flat plate (fabric mass in g/m^2). Plots at time = 65 s and $z/d = 2$.

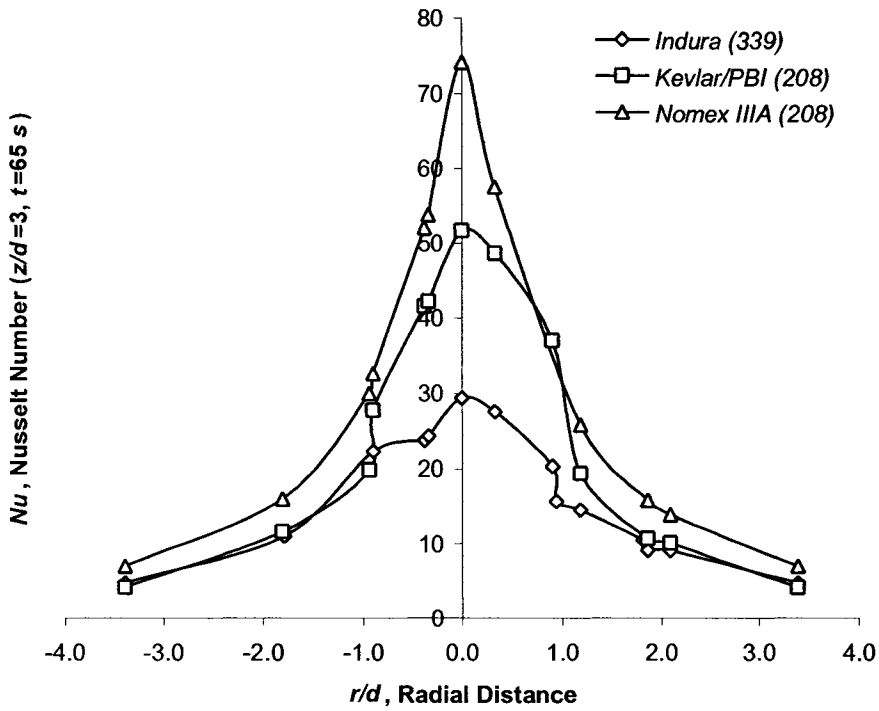

Figure 4.33 Nusselt number distribution for 3 types of fabric placed 6 mm away from flat plate (fabric mass in g/m^2). Plots at time = 65 s and z/d = 3.

4.1.4 Results of Steel Shim Stock at a Space Away from Flat Plate

A sheet of steel shim stock was used for non-contact testing (i.e. only for tests with 6 mm air gap). This was done so as to compare the energy transfer across the air gap with a solid bottom boundary to that across an air gap with a porous bottom boundary. The shim stock was placed 6 mm away from the skin simulant flat plate as described in the previous chapter. The nozzle-to-plate separation was adjusted so that the distance z was measured from the nozzle's exit to the surface of the skin simulant flat plate and not the surface of the shim stock (that was placed 6 mm from the plate). Three nozzle-to-plate separations were tested: 1, 2 and 3 nozzle diameters. The results obtained provided scattered data with no definite trend. This resulted in information that was unacceptable. The plots can be found in Appendix G.

4.2 Discussion of Results

Results presented in Section 4.1 will be discussed in this section. This section aims to explain some of the phenomena observed in those results. This discussion is divided into 4 categories for clarity: flat plate alone, contact / non-contact tests with fabric, shim stock tests and a comparison of the present results with published work from different authors

4.2.1 Flat Plate Alone

As explained in Chapter 2, there are many parameters that influence the rates of local heat transfer from an impinging air jet to a flat plate. Included are:

- Reynolds number (Re_d)
- Temperature of jet (T_e)
- Turbulence intensity (I)
- Nozzle-to-plate separation (z/d)
- Radial distance location (r/d)

In the present work Re_d and T_e were kept constant so as to focus on z/d and r/d. It is known that the dependence of Nusselt number on z/d and r/d is caused by the flow characteristics of the impinging jet near the surface of the plate [10-23, 37, 38]. As observed in Section 4.1.1, the Nusselt number profile across the flat plate changes and in general reduces as z/d increases. Near the stagnation point, depending on the z/d, there can be dramatic variations in Nu or just a decreasing value. The Nusselt number distribution in this study was evaluated at 16 different r/d ratios for 10 nozzle-to-plate spacings. The results discussed are based on the plots for thermocouples located in

axis *B-B*. It was found that both axes *B-B* and *A-A* presented similar information. Additional data may be found in Appendix H.

For $z/d \geq 3$ the flow near the stagnation point results in large local heat transfer coefficients and hence large Nusselt number values [11]. This can be observed in Figures 4.5, 4.7, 4.9, 4.11, 4.13, 4.15, 4.17 and 4.19 where the maximum local Nusselt number occurs at the stagnation point. The maximum Nusselt number occurred when $z/d = 4$. For the given Re_d, T_e and r/d, the local Nusselt numbers (at all r/d ratios) also increased with z/d until it reached a maximum value, then it decreased as z/d kept increasing.

For small z/d ratios (i.e. $z/d < 3$) there is an area within which the flow parallel to the surface is accelerated. At the end of the accelerated-flow region, the disappearance of the stabilizing streamwise pressure gradient leads to a sudden steep rise in the turbulence level [17]. This is due to transition from an accelerating stagnation region flow to a decelerating wall jet. The result is a sharp increase in the heat transfer coefficient, h (and hence higher Nu). This occurs off the stagnation point producing higher rates of heat transfer than those at the centre of the plate [11, 38]. The accelerated flow-region length depends on the characteristics of the jet/plate system set up. It is heavily influenced by the spacing z/d, which consecutively, affects the position where the maximum local Nusselt number occurs. This may explain the sharp increase in Nu at $r/d \approx 0.3$ for the $z/d = 1$ and 2 cases. Furthermore, signs of a secondary peak happen for $z/d = 1$. According to Gardon et al. secondary peaks occur in the wall jet region as a result of rising turbulence and falling velocity [17]. The

secondary peak in Figure 4.1 is almost a "plateau" suggesting a subtle change in those parameters.

As *z/d* is increased, the change in slope (with increasing *r/d*) becomes less and less evident. For larger *z/d* ratios (i.e. $z/d > 6$), the local heat transfer distribution has a smooth bell-shaped profile. This lends experimental support to Gardon's findings. He attributed this shape to the lateral variations of the thickness of a boundary layer free of transitions.

The surface heat flux history for thermocouples *"e"*, *"f"*, *"g"*, *"h"* and *"i"* (as labelled in Figure 3.6) was plotted for all *z/d* ratios. The plots are shown in Figures 4.2, 4.4, 4.6, 4.8, 4.10, 4.12, 4.14, 4.16, 4.18, and 4.20 for $z/d = 1$ through 10, respectively. It is interesting to note the sharp increase in *q"* at the start of every test. This is due to the temperature difference between the fluid and the surface of the plate. As the plate's surface heats up, the temperature difference decreases, resulting in lower heat flux rates from the moving air to the plate. When *z/d* is small, the uniform temperature profile of the jet makes the area near the stagnation point hotter than the outer edge of the plate. This causes surface heat flux histories of thermocouples *"e"*, *"f"*, *"g"* and *"h"* to have closer values than that of thermocouple *"i"*. As *z/d* increases, the temperature profile becomes parabolic (see Section 3.2.2). This results in a more pronounced surface heat flux history difference as *r/d* becomes larger. It is important to note that at large *z/d* ratios (namely 8, 9 and 10), the surface heat flux history data shows large fluctuations (referred to as "noise" in the previous section) that are not seen at small *z/d* ratios. In fact, these fluctuations are not a result of electrical noise in the readings. As the nozzle-to-plate separation increases, the free

jet region becomes larger and the fluid loses momentum. The hot fluid mixes with cold surrounding air creating eddy currents with both cold and hot air. This affects the temperature readings on the surface of the plate resulting in cold/hot fluctuations that are reflected in the surface heat flux history.

4.2.2 Contact and Non Contact Tests

Contact Tests

Samples of conditioned FR fabric were placed in contact with the skin simulant as described in Chapter 3. Three different fabrics were tested one at a time: Nomex® IIIA (208), Kevlar®/PBI (208) and Indura® (339). The fabrics were tested at the same *z/d* ratios as those with the flat plate alone. At $z/d < 3$ the highest rates of heat transfer occurred off the stagnation point. This agrees with the results from the base flat plate. The reason for such phenomenon may be due a transition from an accelerating stagnation region flow to a decelerating wall jet, which increases the heat transfer coefficient, *h*, as explained earlier. When $z/d \geq 3$ results show a monotonically decay from the stagnation point. The profile becomes more bell-shaped increasing *z/d*. This decay is also due to lateral variations of the thickness of a boundary layer free of transitions.

Nomex® IIIA was consistently the FR fabric that allowed higher rates of heat transfer. This may have been caused by its high permeability (29.0 $cm^3/cm^2/s$) and low density (392 kg/m^3), which allowed more hot air to pass through the fibres enhancing heat transfer due to convection. Indura® (339) and Kevlar®/PBI (208) showed rates of heat transfer similar to each other. The latter one seemed to provide

slightly higher Nusselt numbers, which was expected from its permeability (see Table 3.2). For contact tests, all three fabrics performed within ±12% from each other.

Non-Contact

Fabric was placed 6 mm away from the flat plate using the acrylic frame described in Chapter 3. These tests will be referred to as "non-contact" tests. The reason for testing at 6 mm away from the plate is to simulate testing with ASTM D4108, where the fabric is located ¼" away from the test sensor. The initial objective was to perform non-contact testing at z/d = 1 through 10. However, during experimentation it was noticed that beyond z/d = 3 the data obtained were scattered and unacceptable (especially for Indura® (339)). It is for this reason that for non-contact tests, results are presented only up to $z/d \leq 3$. The reason for this may be due to eddies within the gap. Torvi [28] showed that small enclosures (such as a 6 mm gap) contain large number of convection cells that may affect the heat transfer distribution across the plate.

Changing some of the parameters (such as jet Re or T_e) may have enabled one to obtain data beyond $z/d > 3$. However, it would have not been possible to compare contact/non-contact results. It is interesting to note that for z/d = 1 the maximum Nu still occurred off the stagnation point. This is more pronounced for Nomex® IIIA and may be related to the same reasons explained above (i.e. high permeability and low density). Kevlar®/PBI and Indura® provided significant lower rates of heat transfer compared to Nomex® IIIA. For z/d =2 and 3 the maximum Nu occurred at the stagnation point. This did not happen with contact tests or the flat plate alone when

z/d = 2. Again, Nomex® IIIA showed considerably higher Nusselt numbers than those for Kevlar®/PBI and Indura®.

Table 4.1 shows the Nusselt number at the stagnation point for all three fabrics located at 2 different positions relative to the flat plate. As can be seen, adding a 6 mm air gap contributes significantly to reducing the heat transfer between the plate and the warm jet. The lowest change occurred with Indura® where the non-contact test showed a reduction in heat transfer to 1/3 of the original. As z/d became larger, the Nusselt number difference at the stagnation point became smaller. This is of course due to the appearance of a maximum value at the stagnation point.

Table 4.1 Nusselt number at the stagnation point for 3 types of FR fabrics for contact (C) and non-contact (NC) tests.

	Nomex® IIIA		**Indura®**		**Kevlar®/PBI**	
z/d	***C***	***NC***	***C***	***NC***	***C***	***NC***
1	72	58	70	22	71	31
2	86	70	74	25	80	52
3	98	74	85	30	82	57

4.2.3 Shim Stock Tests

A sheet of steel shim stock was used for non-contact testing (i.e. only for tests with 6 mm air gap). This was done so as to compare the energy transfer across the air gap with a solid bottom boundary to that across an air gap with a porous bottom boundary. The shim stock was placed 6 mm away from the skin simulant flat plate as described in the previous chapter. The nozzle-to-plate separation was adjusted so that the distance z was measured from the nozzle's exit to the surface of the skin simulant flat plate and not the surface of the shim stock (that was placed 6 mm from the plate). Three nozzle-to-plate separations were tested: 1, 2 and 3 nozzle diameters. The results obtained provided scattered data with no definite trend. This resulted in adding little information. As such the results are not presented here but are included in Appendix G. Again, changing some of the parameters (such as jet Re or T_e) may have enabled these experiments to produce usable data.

4.2.4 Comparison with Other Authors

No published data were found that matched the objectives of this thesis. Most of the information available dealt with steady state experimentation (i.e. the plate and the jet were kept at constant temperatures). Steady state testing (in the present study) was not possible due to nature of the experimental set up. Furthermore, the Reynolds number at which such data were taken differs to that of the present work. Also, all of the published experimentation (even the Siba–Ganesa [19] transient case) used heated plates and room temperature jets while the present study did the opposite.

In order to gauge the appropriateness of the results obtained in this study the results from 4 different authors were compared against the present work. Figure 4.34

shows the results of: Siba-Ganesa [19], Goldstein-Behbahani [12], Sparrow-Lovell [42] and Tawfek-Mohanty [10]. The details of each of those experiments are given in Table 4.1. The plot shows the local Nusselt number to Stagnation Nusselt number ratio, Nu/Nu_0, for a nozzle-to-plate separation of 10 (z/d = 10). In the plot, it is clear that the results obtained in this study provide a more prominent decrease in Nu. This may be due to comparing transient results (present study) to steady data (Siba-Ganesa [19], Goldstein-Behbahani [12], Sparrow-Lovell [42] and Tawfek-Mohanty [10]).

Table 4.2 Experimentation details of different authors

Author(s)	Re_d	z/d	***d (mm)***
Siba-Ganesa [19]	23,700	10	11.18
Goldstein-Behbahani [12]	61,000	10	127.00
Sparrow-Lovell [42]	5,000	10	6.35
Tawfek-Mohanty [10]	4,860	10	3.00
Present	21,132	10	32.00

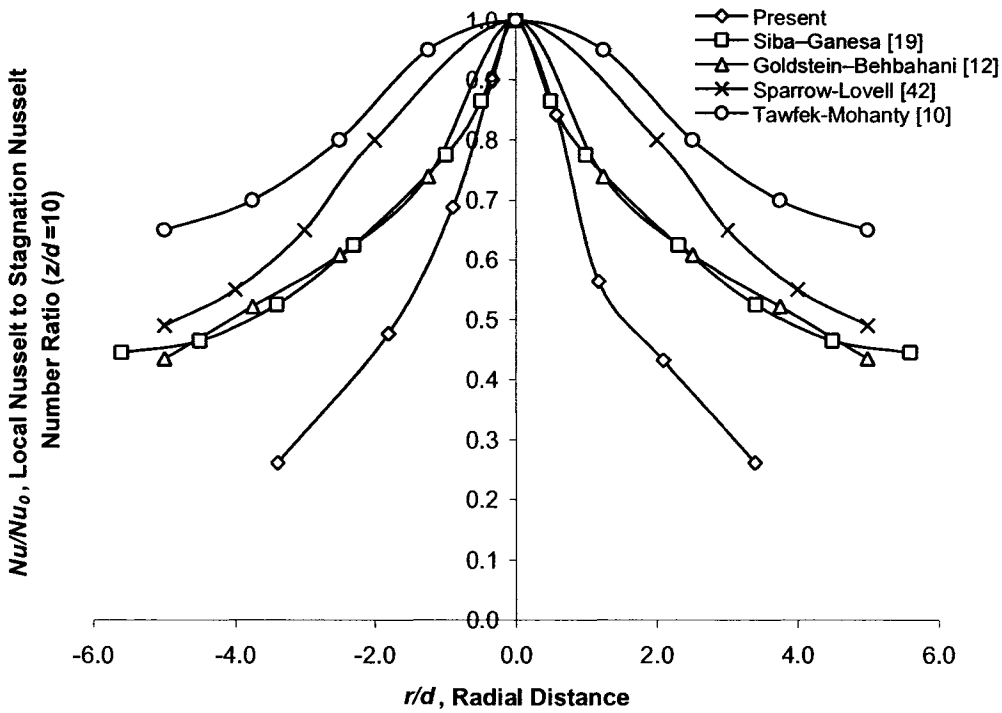

Figure 4.34 Comparison of Nu/Nu_0 ratio for various authors and the present work at $z/d = 10$.

The discrepancy between results may be due to at least 2 significant causes: the jet temperature and the separation distance, z. Nusselt number is a strong function of heat flux, q'', which depends on temperature difference (between the moving air and the surface of the plate). As can be seen from the temperature distribution of the air jet, as z increases, the distribution becomes parabolic. This is due to mixing with cool surrounding air. At large z the horizontal temperature difference between the centre line and the outer edge of the free jet becomes more. This is reflected in a higher rate of heat transfer near the impingement point and a much lower one as r/d increases. All of the published data dealt with heated plates and room temperature air,

so mixing with surrounding air did not affect the temperature of the jet. This was reflected in less steep Nu/Nu_0 ratios.

It is important to note that although z/d may be the similar for all published data presented in this thesis, the separation distance z is different in all cases – as the nozzle diameter, d, is not the same (see Table 4.2). For a nozzle diameter of 32 mm (present study), the distance z becomes more significant than that of Siba-Ganesa, Sparrow-Lovell, Tawfek-Mohanty and Goldstein-Behbahani.

4.3 Repeatability

A repeatability analysis was performed for the $z/d = 6$ case. The plots may be seen in Appendix H. It was found that the test was repeatable within ± 9%.

CHAPTER 5: CONCLUSIONS AND RECOMMENDATIONS

In this thesis an experimental study of the heat transfer through thin fibrous layers has been performed. The experimentation mimicked some of the standard bench top tests used today as outlined in Chapter 2. Substitution of a flame by a warm air jet allowed this project to centre on heat transfer by convection and conduction only – avoiding radiation. All the objectives presented in Chapter 1 were met satisfactorily. In this chapter conclusions are presented along with several technical recommendations aimed to improve the current research.

5.1 Conclusions

Objective 1: *To study heat transfer from a vertical warm jet of air impinging on a horizontal surface - rates of heat transfer will be obtained as a function of time and location.*

- Heat transfer profiles were obtained for 10 nozzle-to-plate separations with the flat plate alone. It was found that the shape depends on nozzle-to-plate distance, which results in distinctive heat transfer profiles. For small separations ($z/d < 3$), secondary peaks appeared off the stagnation point due to the disappearance of the stabilizing streamwise pressure gradient, producing turbulence along the free wall jet. For large separations ($z/d \geq 3$), heat transfer monotonically decays from the stagnation point as a result of turbulent flow near the centre of the plate.

- As time increased, the rates of heat transfer between the air jet and the plate decreased. This was reflected in the surface heat flux history by a drastic jump at the beginning of the tests, which decreased as time increased.

- The heat transfer profile was compared to that of other authors. The results showed a sharper decrease of heat transfer as (*r/d* increase) compared to that of the other authors. The discrepancy between results may be due to at least 2 significant causes: the jet temperature and the separation distance. At large separations the temperature difference between the centre line and the outer edge of the free jet becomes more significant, caused by mixing with cool surrounding air. This was reflected in steep Nu/Nu_0 ratios not observed in other tests.

Objective 2: *To study the performance of thin fibrous materials located in two positions relative to the horizontal surface – in contact and a space away.*

- Three types of fabric: Nomex® IIIA, Indura® and Kevlar®/PBI were tested.
- Fabric was tested in 2 positions relative to the flat plate: in contact and 6 mm away from the plate. Fabric samples placed in contact were tested at 10 different nozzle-to-plate separations. Fabric samples located 6 mm away were tested only at the first 3 nozzle-to-plate separations. Increasing the separation beyond 3 nozzle diameters resulted in unacceptable results.
- In all cases – contact and non-contact tests –, Nomex® IIIA consistently allowed higher rates of heat transfer. Indura® and Kevlar®/PBI performed

comparably during the contact tests, but varied significantly during non-contact testing.

- It was found that adding a 6 mm gap space contributed to a significant reduction in heat transfer. The largest difference was found with Indura®, were heat transfer decreased to about 1/3 of its original.
- As time increased, the rates of heat transfer between the air jet and the plate/fabric system decrease. This is reflected in the surface heat flux history. The jump at the beginning of the tests was found to be less drastic than that of the flat plate alone.

Objective 3: *To compare the energy transfer across the air gap with a solid bottom boundary to that across an air gap with a porous bottom boundary.*

- A steel shim stock sheet was placed 6 mm away from the plate and tested under the same conditions as the FR fabric. It was painted with matte black paint to increase its absorptivity.
- The tests produced results that were unacceptable, as heat transfer data seemed to be scattered. These tests showed that the experimental set up was not appropriate to obtain reliable results.

5.2 Technical Recommendations

Although the majority of the objectives seemed to have been met satisfactorily, a few changes in the procedure/experimental set up may help improve the accuracy and the range of validity for the results. Changing the jet temperature,

for example, may have helped testing beyond z/d > 3 for non-contact testing as well as obtaining reliable results for the shim stock testing. Replacing the electric heaters or adding more to the existing experimental set up could achieve this. Increasing the jet Reynolds number may also allow increasing the separation testing range. This could be achieved by decreasing the nozzle's exit diameter (and or the nozzle's contraction), increasing the air pressure supply or a combination of all.

5.3 Future Work

As mentioned in previously, the present work is part of a larger series of projects aimed to further knowledge in the area of protective clothing and test protocols used in the evaluation of materials, clothing and protective equipment. Future research in this area is very broad, in particular for the evaluation of protective clothing. The present work could be complemented by replacing the air jet with an impinging flame. This would allow present results to be compared against work that includes radiation effects. The effects of dried, oven-dried and wet fabric samples could also be analysed using the present experimental set up.

REFERENCES

[1] CMA Managers Guide "Assessing Flame Resistant Clothing Use", Arlington, VA, 1997, pp 8-9.

[2] Standard Guide for Heated System Surface Conditions That Produce Contact Burn Injuries (ASTM C1055), American Society for Testing Materials, 1992.

[3] Edwards, J.S., "Development of an Instrumented Dynamic Mannequin Test to Rate the Thermal Protection Provided by Protective Clothing", MSc Thesis in Fire Protection Engineering. Worcester Polytechnic Institute, 2004, pp 2-32.

[4] Cavanagh, J.M., "Clothing Flammability and Skin Burn Injury in Normal and Micro-Gravity", MSc Thesis in Mechanical Engineering. University of Saskatchewan, 2004, pp 10-16.

[5] Diller, K., "Analysis of Skin Burns" in Heat Transfer in Medicine and Biology, Shitzer, A. and Eberhart, R.C., Eds., Plenum Press, New York, 1985, pp. 85-134.

[6] Stoll, A.M. and Greene, L.C., "Relationship Between Pain and Tissue Damage due to Thermal Radiation", Journal of Applied Physiology, Vol.14, 1959, pp. 373-382.

[7] Stoll, A.M. and Chianta, M.A., "Heat Transfer Through Fabrics as Related to Thermal Injury", Transactions of the New York Academy of Science, Vol.33, 1971, pp.649-669.

[8] Dale, J.D., Ackerman, M.Y., Crown, B.M., Hess, D., Tucker, R. and Bitner, E., "A Study of Geometry Effects on Testing Single Layer Fabrics for Thermal Protection", *Performance of Protective Clothing: Issues and Priorities for the 21st Century: Seventh Volume, ASTM STP 1386*, C.N. Nelson and N.W. Henrry, Eds., American Society for Testing Materials, West Conshohocken, PA, 2000.

[9] Torvi, D.A., "Heat Transfer in Thin Fibrous Materials Under High Heat Flux Conditions", Thesis for Doctor of Philosophy Department of Mechanical Engineering, Edmonton, AB. University of Alberta, 1997, pp 1-222.

[10] Mohanty, A.K. and Tawfek, A.A., "Heat Transfer due to a Round Jet Impinging Normal to a Flat Surface", International Journal of Heat and Mass Transfer, Vol.36, 1993, pp. 1639-1647

[11] Huang, L. and El-Genk, M., "Heat Transfer of an Impinging Jet on a Flat Surface", International Journal of Heat and Mass Transfer, Vol.37, 1994, pp. 1915-1923.

[12] Goldstein, R.J., Behbahani, A.I. and Heppelmann, K., "Streamwise Distribution of the Recovery Factor and the Local Heat Transfer Coefficient to an Impinging Circular Air Jet", International Journal of Heat and Mass Transfer, Vol.29, 1986, pp. 1227-1235.

[13] Perry, K.P., "Heat Transfer by Convection from a Hot Gas Jet to a Plane Surface", Proc. Mech. Engng. Inst, Vol.168, 1954, pp.775-784.

[14] Popiel, C.O., van Der Meer, T.H., Hoogendoorn, C.J., "Convective Heat Transfer on a Plate in an Impinging Round Hot Gas Jet of Low Reynolds Number", International Journal of Heat and Mass Transfer, Vol.23, 1980, pp. 1055-1068.

[15] Vander, D.T., Incropera, F.P. and Viskanta, R., "Local Convective Heat Transfer from a Heated Surface to an Impinging, Planar Jet of Water", International Journal of Heat and Mass Transfer, Vol.34, 1991, pp. 611-623.

[16] Tawfek, A.A., "Heat Transfer and Pressure Distributions of an Impinging Jet on a Flat Surface", International Journal of Heat and Mass Transfer, Vol.32, 1996, pp. 49-54.

[17] Gardon, R. and Akfirat, J.C. "The Role of Turbulence in Determining the Heat Transfer Characteristics of Impinging Jets", International Journal of Heat and Mass Transfer, Vol.8, 1965, pp. 1261-1272.

[18] Meola, C., De Renzis, M. and Carlomagno, G.M., "Experimental Investigation of an Air Jet Impinging to a Flat Plate", University of South Naples, Department of Power and Applied Thermodynamics, Naples, 2004, pp.1-2.

[19] Siba, E.A., Ganesa-Pillai, M., Harris, K.T. and Haji-Sheikh, A., "Heat Transfer in High Turbulence Air Jet Impinging Over a Flat Circular Disk", Journal of Heat Transfer, Vol.125, 2003, pp.257-265.

[20] Goldstein, R.J. and Seol, W.S., "Heat Transfer to a Row of Impinging Circular Air Jets Including the Effect of Entrainment", International Journal of Heat and Mass Transfer, Vol.34, 1991, pp. 2133-2147.

[21] Hansen, L.G. and Webb, B.W., "Air Jet Impingement Heat Transfer from Modified Surfaces", International Journal of Heat and Mass Transfer, Vol.36, 1993, pp. 989-997.

[22] Beitelmal, A.H., Saad, M.A. and Patel, C.D., "Effects of Surface Roughness on the Average Heat Transfer of an Impinging Air Jet", Int. Comm. Heat Mass Transfer, Vol.27, 2000, pp.1-12.

[23] Tawfek, A.A., "Heat Transfer Studies of the Oblique Impingement of Round Jets Upon a Curved Surface", Heat and Mass Transfer, Vol.38, 2002, pp.467-475.

[24] Martin, H. "Heat and Mass Transfer between Impinging Gas Jets and Solid Surfaces", Advances in Heat Transfer, Vol. 13, 1977, pp.1-60.

[25] Viskanta, R. "Heat Transfer to Impinging Isothermal Gas and Flame Jets", Exp. Thermal Fluid Sci., Vol.6, 1993, pp.111-134.

[26] Dong, L.L., Cheung, C.S. and Leung, C.W., "Heat Transfer Characteristics of an Impinging Butane/Air Flame Jet of Low Reynolds Number", Experimental Heat Transfer, Vol.14, 2001, pp.265-282.

[27] Kremer, H., Buhr, E. and Haupt, R., "Heat Transfer from Turbulent Free-Jet Flames to Plane Surfaces", N.H. Afgan et al. (eds), Heat Transfer in Flames, Scripta, Washington, DC, 1973, pp.463-472.

[28] Torvi, D.A. and Sawcyn, C.M.J., "Flow Visualizations in Air Spaces Between Protective Fabrics and Sensors in Protective Clothing Tests", Department of Mechanical Engineering, University of Saskatchewan, Saskatoon, AB. 2004, pp.1-6

[29] Cornwell, K., "The Flow of Heat", Van Nostrand Reinhold Company, New York, 1977, pp.56-59

[30] Crown, E.M., Rigakis, K.B., Dale, J.D., "Systematic Assessment of Protective Clothing for Alberta Workers", Final Research Project Report prepared for Alberta Occupational Health and Safety, Edmonton, AB., 1989, pp Appendix 19.

[31] Lawton, B and Klingenberg, G., "Transient Temperature in Engineering and Science", Oxford University Press, New York, 1996, pp45-99

[32] Vosen, S.R., "Unsteady Heat Transfer During the Interaction of a Laminar Flame with a cold Wall", Thesis for Doctor of Philosophy Department of Mechanical Engineering, University of California, Berkeley, 1983, pp 87-88.

[33] Woodard, J.B., "An Experimental and Theoretical Study of Heat Transfer in Constant Volume and Compression-Expansion Systems Including the effects of Flame Propagation", Thesis for Doctor of Philosophy Department of Mechanical Engineering, University of California, Berkeley, 1982, pp.100-104.

[34] Diller, T.E. and Kidd, C.T., "Evaluation of Numerical Methods for Determining Heat Flux with a Null Point Calorimeter", Proc. of the 43rd International Instrumentation Symposium, ISA, Research Triangle Park, NC, 1997, pp.357-369.

[35] Diller, T.E., "Methods for Determining Heat Flux from Temperature Measurements", Proc. of the 42nd International Instrumentation Symposium, ISA, Research Triangle Park, NC, 1996, pp. 251-260.

[36] Cook, W.J., and Felderman, E.J., "Reduction of Data from Thin-Film Heat Transfer Gauges: A Concise Numerical Technique", AIAA Journal, Vol. 4, 1966, pp.561-562.

[37] Martin, H. "Heat and Mass Transfer between Impinging Gas Jets and Solid Surfaces", Advances in Heat Transfer, Vol. 13, 1977, pp.1-60.

[38] Incropera, F.P., DeWitt, D.P., "Introduction to Heat Transfer", Third Edition, John Wiley & Sons, New York, 1996, pp.362-364.

[39] Torvi, D.A., "Heat Transfer in Thin Fibrous Materials Under High Heat Flux Conditions", Thesis for Doctor of Philosophy Department of Mechanical Engineering, Edmonton, AB. University of Alberta, 1997, pp 155-156.

[40] Lee, Y.M. and Barker, R.L., "Effect of Moisture on the Thermal Protective Performance of Heat-Resistance Fabrics", Journal of Fire Sciences, Vol. 4, 1986, pp.315-331

[41] Morel, T., "Comprehensive Design of Axisymmetric Wind Tunnel Contractions", Journal of Fluids Engineering, Vol. 97, 1975, pp.225-233

[42] Sparrow, E.M. and Lovell, B.J., "Heat Transfer Characteristics of an Oblique impinging Circular Jet", Journal of Heat Transfer, Vol. 102, 1980, pp.202-209

[43] Lawson, L.K., "Moisture and Fabric Effects on Heat Transfer", Thesis for Master of Science in Textiles and Clothing, Department Human Ecology, Edmonton, AB. University of Alberta, 2002, pp 1-107.

APPENDIX A: Semi-Infinite Solid Calculation

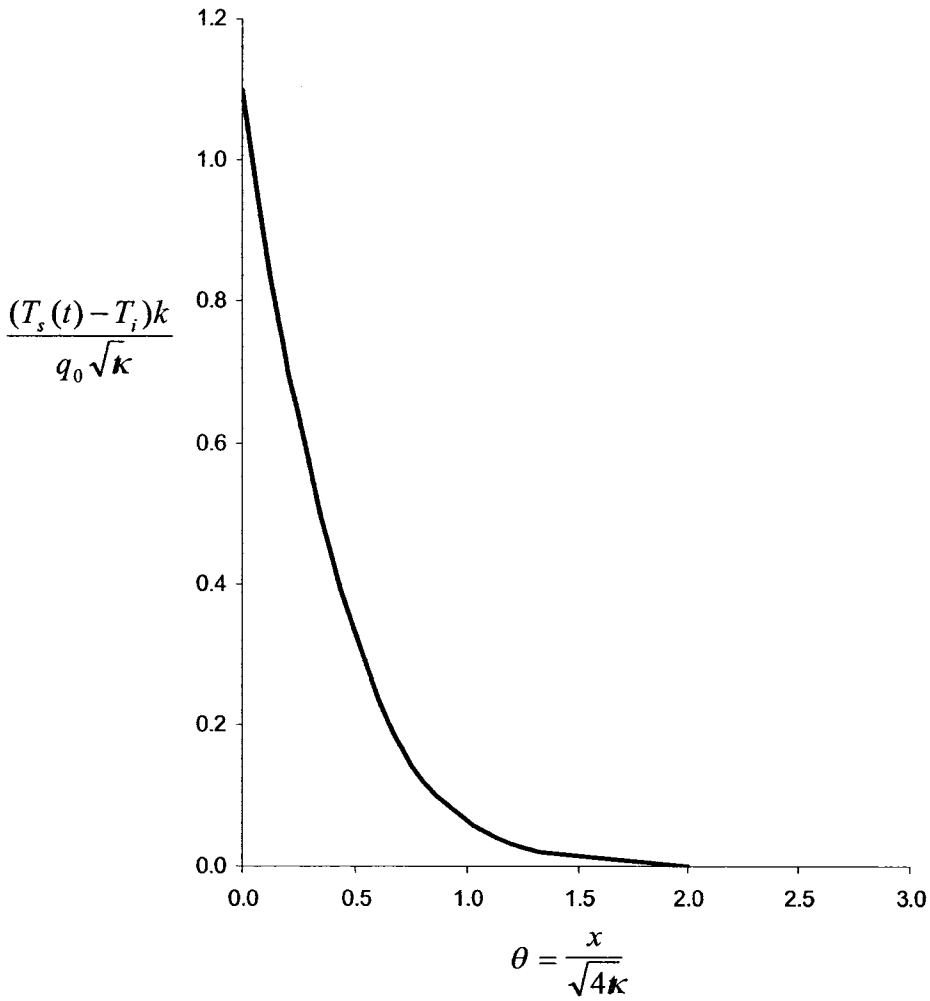

Figure A1 Dimensionless response of a semi-infinite solid to a step change of surface heat flux (source [31])

Definitions:

x : Flat plate thickness (21 mm)
k : Flat plate thermal conductivity (0.97 W/m•K)
ρ : Flat plate density (1877 kg/m^3)
c_p: Flat plate specific heat (1205 J/kg•K)
κ : Flat plate thermal diffusivity ($k / \rho c_p = 4.3 \cdot 10^{-7}$ m^2/s)
t : Time for which plate behaves like a semi-infinite solid (s)

From Figure A1, for semi-infinite behaviour $\theta \leq 2$, therefore

$$\theta = \frac{x}{\sqrt{4\kappa}} = 2 \tag{A1}$$

Solving for time, t

$$t = \frac{x^2}{4\theta^2 \kappa} \tag{A2}$$

$$t = \frac{(0.021)^2}{4(2)^2(4.3 \cdot 10^{-7})}$$

$$\underline{t = 64.8 \text{ s} \approx 65 \text{ s}}$$

After the plate has been exposed to a sudden change in surface hat flux, it will behave like a semi-infinite solid for 65 seconds. This means that the temperature rise at the surface does not affect the back temperature of the plate until 65 seconds have passed.

APPENDIX B: One Dimensional Heat Flux Approximations From Various Authors

Surface heat flux history can be obtained if the surface temperature history is known. Six approximations from 4 different authors were tested: Cook-Felderman [36], Vosen [32], Woodard [33] and Diller [34 and 35]. They all seemed to provide comparable results, except for Diller's approximations. Computer code was build for all 6 approximations but only the Cook-Felderman was used to ensure consistency. This appendix is meant to show the general equations implemented in the computer code. Theoretical details regarding their origin, assumptions and more can be found in their respective references indicated in square brackets []. The computer code can be found in Appendix E. Results from all approximations were compared using the same data file. Table B1 shows a sample file with results from all authors.

Definitions:

k : Flat plate thermal conductivity (0.97 W/m•K)

ρ : Flat plate density (1877 kg/m^3)

c_p: Flat plate specific heat (1205 J/kg•K)

B : Thermocouple calibration factor (see Appendix K for details)

t_n: Time in seconds at which a temperature is measured

Δt: Temperature difference (t_n-t_{n-1})

i, τ : Dummy variable of summation and time constant for thermocouple, respectively

T_s: Surface temperature at a particular time (temperature difference from temperature at time "0")

Note:

It is important to note that all data files must be initialised to 0 for both time and temperature change.

Cook-Felderman [36]

$$q_n''(t) = B\sqrt{\frac{k\rho_p}{\pi}} \bullet \left[\frac{T_s(t_n)}{t_n^{1/2}} + \sum_{i=1}^{n-1} \left(\begin{array}{l} \dfrac{T_s(t_n) - T_s(t_i)}{(t_n - t_i)^{1/2}} - \dfrac{T_s(t_n) - T_s(t_{i-1})}{(t_n - t_{i-1})^{1/2}} \\ + 2\dfrac{T_s(t_i) - T_s(t_{i-1})}{(t_n - t_i)^{1/2} + (t_n - t_{i-1})^{1/2}} \end{array} \right) + \frac{T_s(t_n) - T_s(t_{n-1})}{(\Delta t)^{1/2}} \right] \quad \textbf{(A)}$$

Vosen [32]

$$q_n''(t) = 2B\sqrt{\frac{k\rho_p}{\Delta t \pi}} \bullet \sum_{i=0}^{n-1} \left(T_s(t_{i+1}) - T_s(t_i)\right)\left(\sqrt{n-1} - \sqrt{n-i-1}\right) \quad \textbf{(B)}$$

Woodard [33]

$$q_n''(t) = B\sqrt{\frac{k\rho_p}{\pi}} \bullet \left[\frac{T_s(t_n)}{t_n^{1/2}} + \sum_{i=1}^{n-2} \left(\begin{array}{l} \dfrac{T_s(t_n) - A_{i+1} - B_{i+1}(2t_n - t_{i+1})}{(t_n - t_{i+1})^{1/2}} \\ - \dfrac{T_s(t_n) - A_{i+1} - B_{i+1}(2t_n - t_i)}{(t_n - t_i)^{1/2}} \end{array} \right) + B_n\sqrt{t_n - t_{n-1}} \right] \quad \textbf{(C)}$$

Where,

$$A_{i+1} = T_s(t_i) - t_i\left(\frac{T_s(t_{i+1}) - T_s(t_i)}{t_{i+1} - t_i}\right)$$

$$B_{i+1} = \left(\frac{T_s(t_{i+1}) - T_s(t_i)}{t_{i+1} - t_i}\right)$$

$$B_n = \left(\frac{T_s(t_n) - T_s(t_{n-1})}{t_n - t_{n-1}}\right)$$

Diller [34 and 35]

$$q_n^{\cdot}(t) = 2B\sqrt{\frac{k\varphi_p}{\Delta t\pi}} \bullet \sum_{i=1}^{n} \frac{T_s(t_i) - T_s(t_{i-1})}{\sqrt{n-i} + \sqrt{n+1-i}} \qquad \text{(D1)}$$

$$q_n^{\cdot}(t) = 2B\sqrt{\frac{k\varphi_p}{\Delta t\pi}} \bullet \sum_{i=1}^{n} \left(T_s(t_i) - T_s(t_{i-1})\right)\left(\sqrt{n+1-i} - \sqrt{n-i}\right) \qquad \text{(D2)}$$

$$q_n^{"}(t) = B\sqrt{\frac{k\varphi_p}{\Delta t\pi}} \bullet \sum_{i=1}^{n} \frac{T_s(t_i) - T_s(t_{i-1})}{\sqrt{n+1-i}} \qquad \text{(D3)}$$

Table B1. Sample file showing time, temperature and heat flux obtained with the different approximations.

Time	Temperature Difference	Surface Heat Flux, q_n" (kW/m^2)					
t_n (s)	T_s (°C)	A	B	C	D1	D2	D3
0.00	0.000	0.000	0.000	0.000	0.000	0.000	0.000
0.21	0.695	2.565	2.594	2.535	0.000	0.000	0.000
0.41	4.911	16.815	16.813	16.824	1.075	1.075	0.917
0.61	7.941	18.666	18.655	18.672	7.344	7.344	6.313
0.81	10.373	19.476	19.461	19.481	10.383	10.383	9.191
1.01	12.200	19.021	19.005	19.025	12.185	12.185	10.990
1.21	13.740	18.776	18.759	18.779	13.010	13.010	11.909
1.41	14.940	18.016	17.999	18.019	13.520	13.520	12.503
1.61	16.433	19.221	19.204	19.225	13.630	13.630	12.720
1.81	17.232	17.361	17.343	17.362	14.360	14.360	13.431
2.01	18.039	17.019	17.002	17.021	13.989	13.989	13.210
2.21	19.000	17.471	17.453	17.473	13.866	13.866	13.153
2.41	19.846	17.269	17.252	17.271	14.094	14.094	13.385
2.61	20.745	17.529	17.512	17.531	14.156	14.156	13.482
2.81	21.445	16.987	16.970	16.989	14.357	14.357	13.690
3.01	22.159	16.947	16.930	16.949	14.264	14.264	13.649
3.21	22.968	17.315	17.298	17.317	14.278	14.278	13.686
3.41	23.779	17.524	17.506	17.526	14.478	14.478	13.881
3.61	24.615	17.815	17.797	17.817	14.676	14.676	14.078
3.81	25.239	17.261	17.243	17.262	14.914	14.914	14.311
4.01	25.753	17.754	16.736	16.755	14.817	14.817	14.262
4.21	26.429	17.166	17.178	17.168	14.625	14.625	14.117
4.41	27.128	17.389	17.371	17.390	14.761	14.761	14.243

APPENDIX C: Conditioning Fabrics

Effects of Oven-Dry and Conditioned Fabric

Many tests have been performed regarding conditioning fabrics. The following information was obtained from Torvi [9]. "There were minimal differences in the temperature histories and the time to the Stoll criterion for the fabrics in their conditioned and oven-dried states. The backside temperatures were slightly higher in the oven-dried case, as there was no ablative effect of moisture. This in turned caused the slight decreases in the times required to exceed Stoll criterion." (Torvi, 1997, Pp155) More information can be obtained in Reference [9].

Table C1 Average times required to exceed Stoll Criterion for Conditioned and Oven-Dried fabric specimens – Source [9] Bench top type experiments

	Time to Exceed Stoll Criterion (s)	
Preparation of Sample	**Kevlar®/PBI**	**Nomex® IIIA**
Conditioned	6.4	7.0
Oven-Dried	6.1	6.6

Effects of Moisture

Lawson [43] studied the effects of dry, conditioned and wet fabric in clothing systems (cotton undergarments + protective fabric) worn by wildland firefighters. Testing was performed using a combined radiative and convective heat flux flame (83 kW/m^2). Table C2 shows the results obtained using dry, conditioned and wet fabric samples. Further information can be found in Reference [43].

Table C2 The effects of moisture on heat transfer and transferred energy through different fabrics under an incident heat flux of 10 kW/m^2 – Source [43]

Fabric	Moisture Condition	Mean Peak Heat Flux (kW/m^2)	Mean Time at Peak Heat Flux (s)	Mean Total Energy (kJ)
Indura®	Dry	3.34	61.08	0.356
	Conditioned	3.13	83.64	0.313
	Wet	3.23	28.30	0.263
Nomex IIIA®	Dry	3.70	55.55	0.411
	Conditioned	3.38	67.80	0.354
	Wet	3.18	26.11	0.266

APPENDIX D: Procedure for Embedding Thermocouples

Thermocouple installation system with M-Bond 43-B, 600 and 6109 Adhesive Systems

Manufacturer: Measurements Group, Inc.
Micro-Measurements Division
P.O. Box 27777
Raleigh, NC 27611, USA

Instruction Bulletin: M-Line Accessories B-130-14

Products:
CSM-1A Degreaser
M-Prep Conditioner A
M-Prep Neutralizer 5A
Silicon-Carbide Paper
CSP-1 Cotton Applicators
MJG-2 Mylar Tape
TFE-1 Teflon Film
HSC-1 Spring Clamp
GT-14 Pressure Pad

Installation techniques are described in the instruction bulletin quoted as well as professionally prepared videotapes available for the Measurements Group. Request Bulletin 318 for details.

APPENDIX E: Computer Code

Q-Basic Routine for all tests:

```
'PROGRAM TO OBTAIN TEMPERATURE OF 16 THERMOCUPLES MOUNTED ON A FLAT
'SQUARE PLATE and IMPINGED WITH HOT AIR JET
'RAUL MUNOZ 2003/2004

DECLARE SUB readchan (DASCHAN%, chan%, COUNT%, R%)
DECLARE SUB DAS8 (MD AS INTEGER, BASADR AS ANY, FLAG AS INTEGER)
DECLARE SUB TYPET (adCOUNT, gain, rtemp, temp!)
DECLARE SUB REFTEMP (rtemp)
DEFINT I-N
DIM t(16)
TYPE twowords
        a AS INTEGER
        b AS INTEGER
END TYPE
CLS

'Initialize Dash 8 Mode 0
        BASADR% = 768: FLAG% = 0: MD% = 0
        CALL DAS8(MD%, BASADR%, FLAG%):


temp = 0
FOR i = 1 TO 100
CALL REFTEMP(rtemp)
temp = temp + rtemp
NEXT i
LOCATE 2, 50: PRINT "REF TEMP:"
LOCATE 2, 60: PRINT USING " ####.##"; temp / 100


'--------------------------TAKE DATA--------------------------------

        CALL readchan(chan%, range%, COUNT%, FLAG%)
        testtime! = 70! 'time in seconds
        STARTTIME! = TIMER
        DIM tcdata!(testtime! + 1, 17)

FOR n = 1 TO 10000

nsample = 500
gain = 200
DASCHAN% = 1
FOR chan% = 0 TO 15
```

```
adCOUNT = 0

                FOR i = 1 TO nsample  'NUMBER OF SAMPLES
                        CALL readchan(DASCHAN%, chan%, COUNT%, FLAG%)
                        adCOUNT = adCOUNT + COUNT%
                NEXT i
                adCOUNT = adCOUNT / nsample
                CALL TYPET(adCOUNT, gain, rtemp, temp!)
                t(chan% + 1) = temp!
                LOCATE (chan% + 1), 1
                PRINT USING "CHAN ## #####.####"; chan% + 1; temp!
                LOCATE 4, 50: PRINT USING "TIMER:  ######.##"; TIMER - STARTTIME!
                tcdata!(n, 1) = TIMER - STARTTIME!
                tcdata!(n, chan% + 2) = temp!
                LOCATE 5, 50: PRINT "Check Up # "; n

                NEXT chan%

dtime! = TIMER - STARTTIME!
IF dtime! > testtime! THEN n = 10000 + 1

NEXT n

'LOCATE 6, 50: PRINT USING "TIME:  ####.##"; dtime!;
'  END


'GET TEMPERATURE DIFFERENCE

DIM subdata!(1, 16)
FOR s = 1 TO 16
subdata!(1, s) = tcdata!(1, s + 1)
NEXT s
FOR col = 1 TO 16
        FOR row = 1 TO testtime! + 1
        tcdata!(row, col + 1) = tcdata!(row, col + 1) - subdata!(1, col)
        NEXT row
NEXT col



STORE:
'Find out next test number
 OPEN "A:\TESTS\Test.NO" FOR INPUT AS #1
 INPUT #1, TESTNUMBER
 CLOSE #1
'Open file with current test number
          IF TESTNUMBER < 1000 THEN
                  OPEN "A:\TESTS\TEST." + RIGHT$(STR$(TESTNUMBER + 10000), 3) FOR
OUTPUT AS #2
          ELSE
           OPEN "A:\TESTS2\TEST." + RIGHT$(STR$(TESTNUMBER + 10000), 3) FOR OUTPUT
AS #2
 END IF

'Write data set
```

```
        PRINT #2, DATE$; "  "; TIME$: PRINT #2, n

        PRINT #2, "Time:    ";
FOR t = 1 TO 17

        FOR c = 1 TO testtime!
        PRINT #2, USING "#####.##"; tcdata!(c, t);
                NEXT c
                PRINT #2, ""
                PRINT #2, USING "Chan: ###"; t;
        NEXT t

CLOSE #2

'Increment test number and write to file
        TESTNUMBER = TESTNUMBER + 1
        OPEN "A:\TESTS\TEST.NO" FOR OUTPUT AS #1
        PRINT #1, TESTNUMBER
 CLOSE #1

END



DEFSNG I-N
'Subroutine that returns a digital count from a single channel
'of and EXP-16 attached to a DASH-8
SUB readchan (DASCHAN%, chan%, COUNT%, R%) STATIC
DEFINT I-N
DIM LT AS twowords
'Lock DASH-8 on the one channel that EXP-16 is connected to.
                        LT.a = DASCHAN%: LT.b = DASCHAN%: MD% = 1
                        CALL DAS8(MD%, LT, FLAG%)
                        IF FLAG% <> 0 THEN PRINT "ERROR IN MODE 1"; FLAG%
                        IF FLAG% <> 0 THEN GOTO 2
'set EXP-16 channel address.
                        MD% = 14
                        CALL DAS8(MD%, chan%, FLAG%)
                        IF FLAG% <> 0 THEN PRINT "ERROR IN MODE 14"; FLAG%
                        IF FLAG% <> 0 THEN GOTO 2:
'A/D conversion using mode 4.
                        MD% = 4
                        CALL DAS8(MD%, COUNT%, FLAG%)
                        IF FLAG% <> 0 THEN PRINT "ERROR IN MODE 4"; FLAG%
2 :  R% = FLAG%
END SUB

DEFSNG I-N
SUB REFTEMP (rtemp) STATIC
 DEFINT I-N
DIM LT AS twowords
'Lock DAS8 on channel 7
                DASCHAN% = 7
                LT.a = DASCHAN%: LT.b = DASCHAN%: MD% = 1
                CALL DAS8(MD%, LT, FLAG%)
                IF FLAG% <> 0 THEN
```

```
            PRINT "ERROR IN MODE 1"; FLAG%
                END IF
'A/D conversion using mode 4.
                IF FLAG% = 0 THEN
                MD% = 4
            CALL DAS8(MD%, COUNT%, FLAG%)
             END IF
             IF FLAG% <> 0 THEN PRINT "ERROR IN MODE 4"; FLAG%
'Calculate reference temperature
 rtemp = 5 * (COUNT% / 2047) / .0244


          END SUB

DEFSNG I-N
'Subroutine takes an A/D count from a Dash8/Exp16
'combination and returns a temperature using a Type T thermocouple polynomial
'(Type T is Copper - Constantan) Polynomial Range -30 to 150C
'
SUB TYPET (COUNT, gain, rtemp, temp!) STATIC
DEFINT I-N
'Calculate voltage in millivolts
            v! = ((COUNT / 2047) * 5 / gain) * 1000!

          ' Coefficients from Sciemetric Canada - Source ANSI
' Degrees C to mV
A1 = -.0012
A2 = .038619
A3 = 4.3656E-05
A4 = -2.0671E-08
V1 = A1 + rtemp * (A2 + rtemp * (A3 + rtemp * A4))
V2 = v! + V1
'Millivolts to temperature
B1 = -.0099
B2 = 25.883
B3 = -.6964
B4 = .02613
temp! = B1 + V2! * (B2 + V2! * (B3 + V2! * B4))

' V! = (count% * gain) / (2047 * 5 * 1000!)
' V! = count%
' temp! = V!  ' + rtemp

END SUB
```

Matlab routine for heat flux approximations:

Cook-Felderman

```
function [q]=torvi(Dat,cal)
%Function that gives local heat flux given surface temperature as a function of time
%Input Matrix size (n by 2) where the first column is the time (in seconds) and the
%second the delta T in Celsius
%Created by Raul Munoz using Cook-Felderman's Approximation
%University of Alberta, August 2004

%Define constants
Cp=1205;   %Ws/kg-C
rho=1877;  %kg/m3
k=0.97;    %W/m-C

%Multiply Factors
z=sqrt(cal*Cp*rho*k/pi);
%get n, number data points
r=size(Dat);
m= r(1,1);
%From Data, obtain the time step
t=Dat(m,1);
Deltat= t/(m-1);
%initialize variables
n=1;
i=1;
semitotal=0; %Initialize sum of factors
q(n,1)=0; %Heat flux at t=0 s is assumed to be 0

%Procedure - Torvi's Approximation of Duhame's Theroem
  for n=1:(m-1)
    n=n+1;
    for i=1:(n-1)
    a=Dat(n,2);
    b=Dat(i,2);
    c=Dat(n,1);
    d=Dat(i,1);
    y=i-1;
      if y<1,
        e=0;
        f=0;
        else
        e=Dat(y,2); f=Dat(y,1);
      end

    suma(i)=((a-b)/sqrt(c-d))-((a-e)/sqrt(c-f))+2*((b-e)/(sqrt(c-d)+sqrt(c-f)));
    semitotal=sum(suma);
```

```
    i=i+1;
    end
    %Heat flux in kW/m2 as a function of time
    q(n,1)=z*(semitotal+ Dat(n,2)/sqrt(Dat(n,1))+ (Dat(n,2)-Dat(n-1,2))/sqrt(Deltat))/1000;
  end
 %Plot heat flux versus time
 plot(Dat(:,1), q, '-b'); xlabel('t, time(s)'); ylabel('q", Heat Flux (kW/m2)');
```

Vosen

```
function [q]=vosen(Dat,cal)
%Function that gives local heat flux given surface temperature as a function of time
%Input Matrix size (n by 2) where the first column is the time (in seconds) and the
%second the delta T in Celsius
%Created by Raul Munoz using Steven Vosen PhD Degree Approximation
%University of Alberta, August 2004

%Define constants

Cp=1205;   %Ws/kg-C
rho=1877;  %kg/m3
k=0.97;    %W/m-C

%cal=1;  %1.2574; %Calibration Factor, still under investigation

%get n, number data points
r=size(Dat);
m= r(1,1);

%From Data, obtain the time step
t=Dat(m,1);
Deltat= t/(m-1);

%Multiply Factors
z=2*sqrt(cal*Cp*rho*k/(pi*Deltat));
%initialize variables

n=1;
i=0;
semitotal=0; %Initialize sum of factors
q(n,1)=0; %Heat flux at t=0 s is assumed to be 0

%Procedure - Vosen's Approximation of Duhame's theorem

   for n=2:(m)
      for i=0:(n-1)
          if i<1,
          a=0;
          b=0;
          else
          a=Dat(i+1,2);
          b=Dat(i,2);
          end
      suma(i+1)=(a-b)*(sqrt(n-i)-sqrt(n-i-1));
      semitotal=sum(suma);
      i=i+1;
      end
```

```
    %Heat flux in kW/m2 as a function of time
    q(n,1)=z*semitotal/1000;
    n=n+1;
  end
%Plot heat flux versus time
plot(Dat(:,1), q, '-.r'); xlabel('t, time(s)'); ylabel('q", Heat Flux (kW/m2)');
```

Woodard

```
function [q]=woodard(Dat,cal)
%Function that gives local heat flux given surface temperature as a function of time
%Input Matrix size (n by 2) where the first column is the time (in seconds) and the
%second the delta T in Celsius
%Created by Raul Munoz using Joan Woodard PhD Degree Approximation
%University of Alberta, August 2004
%Define constants
Cp=1205;   %Ws/kg-C
rho=1877;  %kg/m3
k=0.97;    %W/m-C
%cal=1;  %1.2574; %Calibration Factor, still under investigation
%get n, number data points
r=size(Dat);
m= r(1,1);
%From Data, obtain the time step
t=Dat(m,1);
Deltat= t/(m-1);
%Multiply Factors
z=sqrt(cal*Cp*rho*k/pi);
%initialize variables
n=1;
i=1;
semitotal=0; %Initialize sum of factors
q(n,1)=0; %Heat flux at t=0 s is assumed to be 0

%Procedure - Woodard's Approximation of Duhame's Theorem

  for n=2:(m)
    for i=1:(n-2)
    a=Dat(i,2);
    c=Dat(i,1);
    b=Dat(i+1,2);
    d=Dat(i+1,1);
    f=Dat(n,2);
    g=Dat(n,1);
    An=a-c*((b-a)/(d-c));
    Bn=((b-a)/(d-c));
    %Sum part of approximation
    suma(i)=((f-An-Bn*(2*g-d))/sqrt(g-d)-(f-An-Bn*(2*g-c))/(sqrt(g-c)));
    semitotal=sum(suma);
    i=i+1;
    end
    %Heat flux in kW/m2 as a function of time
        h=Dat(n-1,2);
    j=Dat(n-1,1);
    k=Dat(n,2);
    l=Dat(n,1);
```

```
    Bnn=((k-h)/(l-j));
    q(n,1)=z*((k/sqrt(l)+semitotal)+Bnn*sqrt(l-j))/1000;
    n=n+1;
  end
%Plot heat flux versus time
plot(Dat(:,1), q, ':g'); xlabel('t, time(s)'); ylabel('q", Heat Flux (kW/m2)');
```

Diller (D1)

```
function [q]=diller6(Dat,cal)
%Function that gives local heat flux given surface temperature as a function of time
%Input Matrix size (n by 2) where the first column is the time (in seconds) and the
%second the delta T in Celsius
%Created by Raul Munoz using Cook's approximation on page 254 of diller paper. Eq.6
%University of Alberta, August 2004

%Define constants

Cp=1205;   %Ws/kg-C
rho=1877;  %kg/m3
k=0.97;    %W/m-C

%get n, number data points
r=size(Dat);
m= r(1,1);
%From Data, obtain the time step
t=Dat(m,1);
Deltat= t/(m);
%cal=1;  %1.2574; %Calibration Factor, still under investigation
%Multiply Factors
z=2*sqrt(cal*Cp*rho*k/(pi*Deltat));
%initialize variables
semitotal=0; %Initialize sum of factors

%Procedure
  for n=1:m
    for i=1:(n-1)
    a=Dat(i,2);
    y=i-1;
      if y<1,
        b=0;
      else
        b=Dat(y,2);
      end

    suma(i)=(a-b)/(sqrt(n+1-i)+sqrt(n-i));
    semitotal=sum(suma);
    i=i+1;
    end
    %Heat flux in kW/m2 as a function of time
    q(n,1)=z*semitotal/1000;
    n=n+1;
  end
 %Plot heat flux versus time
 plot(Dat(:,1), q, '-.b'); xlabel('t, time(s)'); ylabel('q", Heat Flux (kW/m2)');
```

Diller (D2)

```
function [q]=diller8(Dat,cal)
%Function that gives local heat flux given surface temperature as a function of time
%Input Matrix size (n by 2) where the first column is the time (in seconds) and the
%second the delta T in Celsius
%Created by Raul Munoz using Cook's approximation on page 254 of diller paper. Eq.8
%University of Alberta, August 2004

%Define constants

Cp=1205;   %Ws/kg-C
rho=1877;  %kg/m3
k=0.97;    %W/m-C


%get n, number data points
r=size(Dat);
m= r(1,1);

%From Data, obtain the time step
t=Dat(m,1);
Deltat= t/(m-1);
%cal=1;  %1.2574; %Calibration Factor, still under investigation
%Multiply Factors
z=2*sqrt(cal*Cp*rho*k/(pi*Deltat));
%initialize variables
semitotal=0; %Initialize sum of factors
%Procedure
  for n=1:(m)

    for i=1:(n-1)
    a=Dat(i,2);
    y=i-1;
      if y<1,
        b=0;
      else
        b=Dat(y,2);
      end
        suma(i)=(a-b)*(sqrt(n+1-i)-sqrt(n-i));
    semitotal=sum(suma);
    i=i+1;
    end
    %Heat flux in kW/m2 as a function of time
    q(n,1)=z*semitotal/1000;
    n=n+1;
  end
 %Plot heat flux versus time
 plot(Dat(:,1), q, '-.g'); xlabel('t, time(s)'); ylabel('q", Heat Flux (kW/m2)');
```

Diller (D3)

```
function [q]=diller9(Dat,cal)
%Function that gives local heat flux given surface temperature as a function of time
%Input Matrix size (n by 2) where the first column is the time (in seconds) and the
%second the delta T in Celsius
%Created by Raul Munoz using Diller/Kidd's Approximation
%University of Alberta, August 2004

%Define constants
Cp=1205;   %Ws/kg-C
rho=1877;  %kg/m3
k=0.97;    %W/m-C
%get n, number data points
r=size(Dat);
m= r(1,1);

%From Data, obtain the time step
t=Dat(m,1);
Deltat= t/(m-1);
%cal=1;  %1.2574; %Calibration Factor, still under investigation
%Multiply Factors
z=sqrt(cal*Cp*rho*k/(pi*Deltat));
%initialize variables

n=1;
i=1;
semitotal=0; %Initialize sum of factors
q(n,1)=0; %Heat flux at t=0 s is assumed to be 0

%Procedure
  for n=1:(m-1)
    n=n+1;
    for i=1:(n-1)
    a=Dat(i,2);
    y=i-1;
      if y<1,
        b=0;
      else
        b=Dat(y,2);
      end

    suma(i)=(a-b)/sqrt(n+1-i);
    semitotal=sum(suma);
    i=i+1;
    end
    %Heat flux in kW/m2 as a function of time
    q(n,1)=z*semitotal/1000;

  end
```

```
%Plot heat flux versus time
plot(Dat(:,1), q, '-.y'); xlabel('t, time(s)'); ylabel('q", Heat Flux (kW/m2)');
```

Processing of Results using a Matlab program:

```
%Program to obtain HF Approximations using Duhamel's theorem based on Cook-Felderman
%for calculating surface heat flux history as a function of surface temperature and time
%Input: a (n X m) Matrix (time and delta Temperature for all thermocouples)
%for accurate results, remember to verify that initial time and initial temperature
%MUST be initialized at 0
%Raul Munoz, August 2004

disp ('*******************************************************')
disp ('          HEAT FLUX APPROXIMATIONS                 ')
disp ('*******************************************************')

disp (")
% Time-Temperature Matrix MUST have time as its first column
D= input('Enter Time-Temperature Matrix - Verify that Matrix is Initialized at 0:  ');
% Calibration Factor Matrix is a Column Matrix with the calibration factor SQUARED of
% each thermocouple used. If Unknown, type "0" and the program will assume a calibration
% factor of 1 for all thermocouples used.
c= input('Enter Calibration Factor Matrix SQUARED - Type "0" if Unknown:          ');

% Initialization routine
s=size(D);
row=s(1,1);
column=s(1,2);
q=zeros(row,column);
q(:,1)=D(:,1);

% If you don't have the calibration factor for the thermocouples type "0" for this
% Matrix

if c<1,
   c=ones(column,1);
else
   c=c;
end

% Routine to obtain heat flux coefficient "h" in kW/m2 using Cook-Felderman's Approximation

for w=1:(column-1)

cal=c(w,1); %Calibration Factor
Dat=zeros(row,2);
Dat(:,1)=D(:,1);
Dat(:,2)=D(:,w+1);

% Torvi Approximation with NO time history plots
```

```
q(:,w+1)=torvi(Dat,cal);

end

%q



% ------------------------------
% Save the theoretical data to a file

cd('C:\WINNT\Profiles\rmunoz\Desktop\Rohit')
[fname,newpath] = uiputfile('C:\WINNT\Profiles\rmunoz\Desktop\Results\*.csv','Choose Output File
Name');
file = fopen(fname,'w');  % creat a new file
%Write the data to the file
[n,m] = size(q);
for i = 1:n
   for j = 1:m
      if j == m
         fprintf(file,'%5.7f,\n',q(i,j));
         else
         fprintf(file,'%5.7f,',q(i,j));
      end
   end
end
fclose(file);     % close the file
cd('C:\WINNT\Profiles\rmunoz\Desktop\Results')

%-----------------------------------
% End of the program.
```

APPENDIX F: Semi-log of Nusselt Number Distribution as a Function of Radial Distance

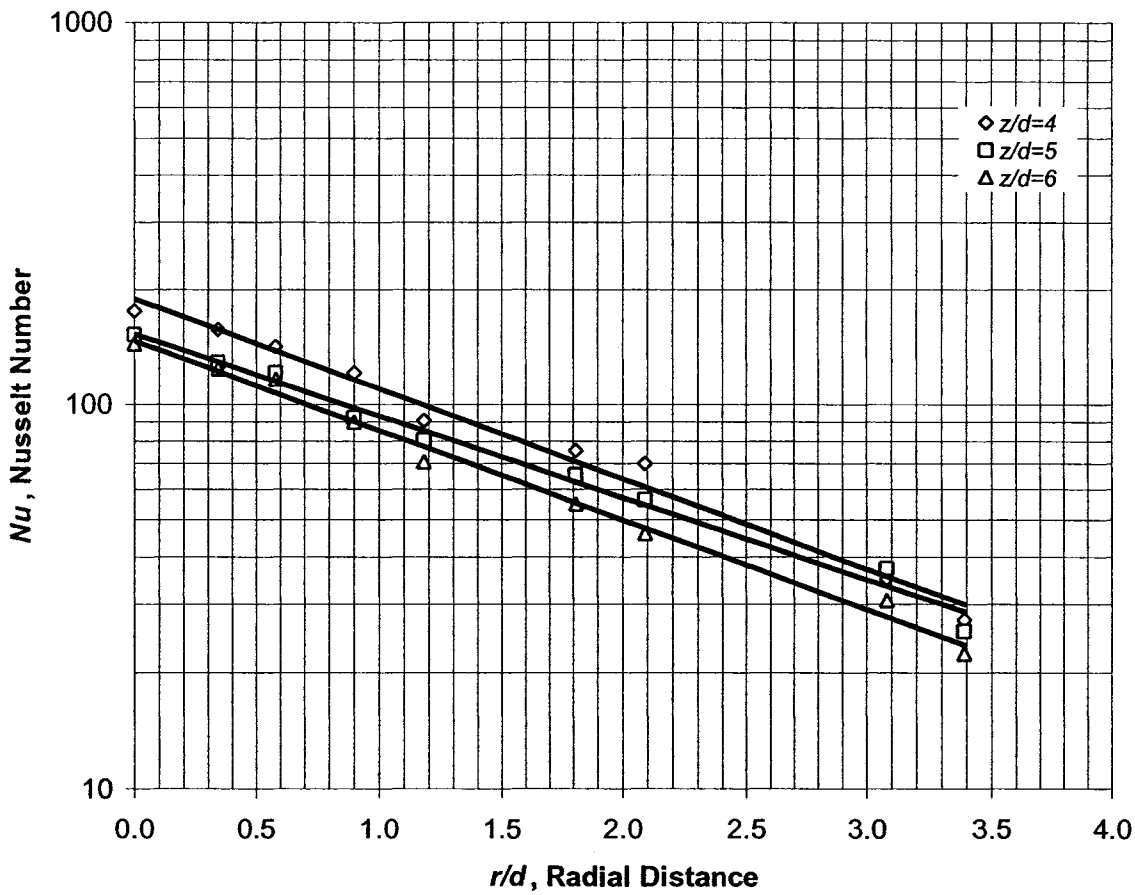

Figure F1 Semi-log plot of Nusselt Number versus radial distance for z/d=4, 5 and 6.

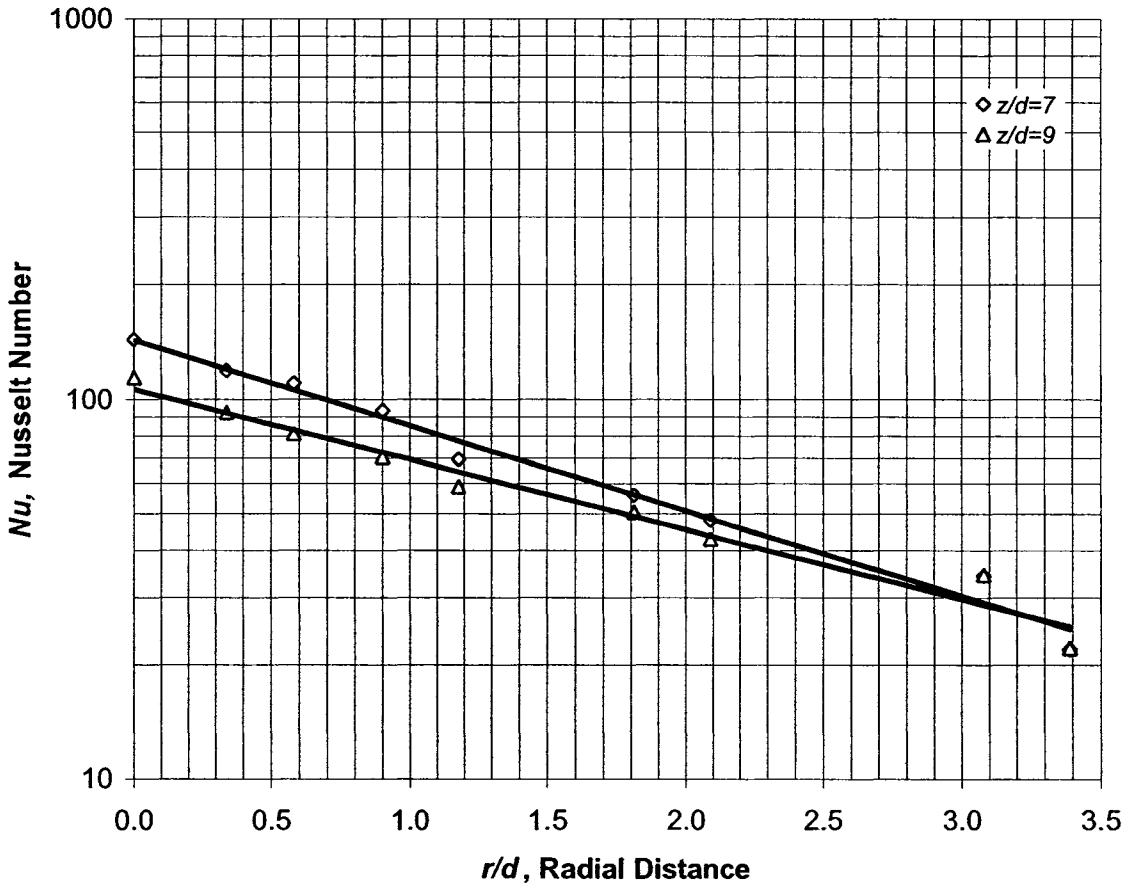

Figure F2 Semi-log plot of Nusselt Number versus radial distance for z/d=7 and 9.

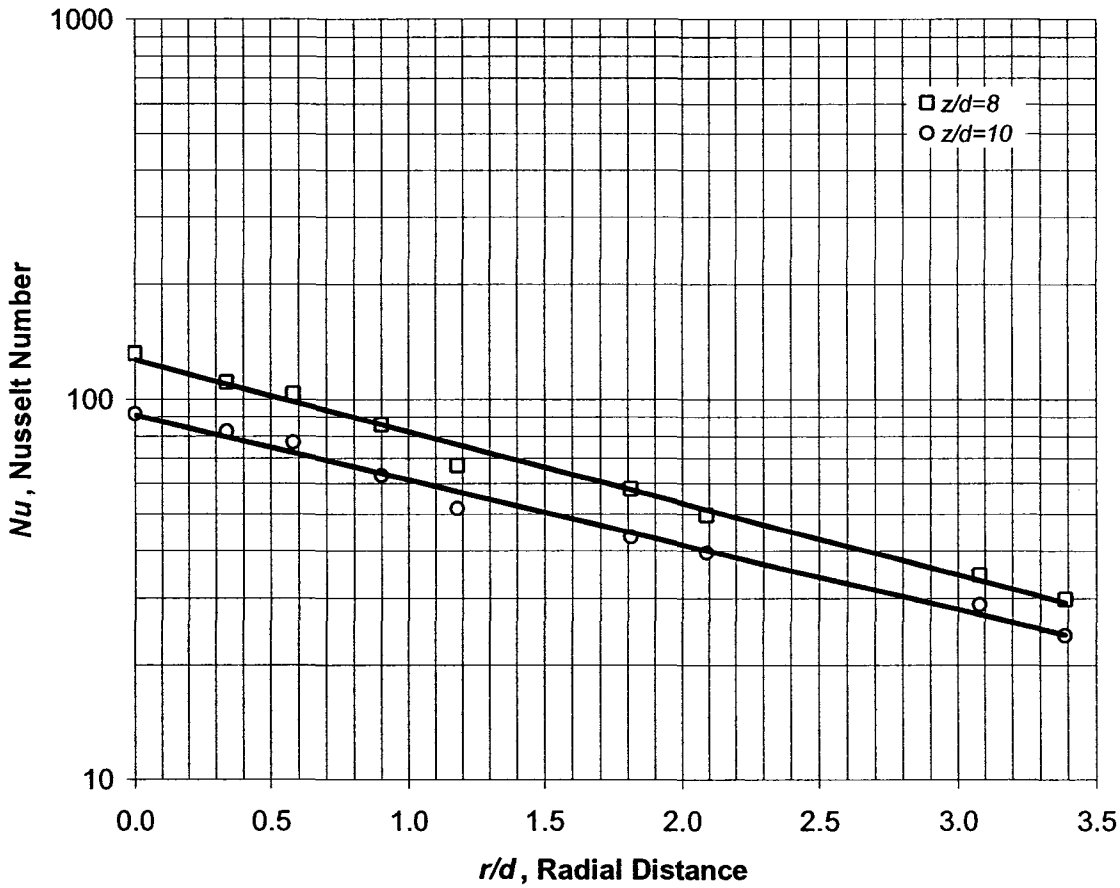

Figure F3 Semi-log plot of Nusselt Number versus radial distance for z/d=8 and 10.

APPENDIX G: Results of Shim Stock located 6 mm Away from Flat Plate

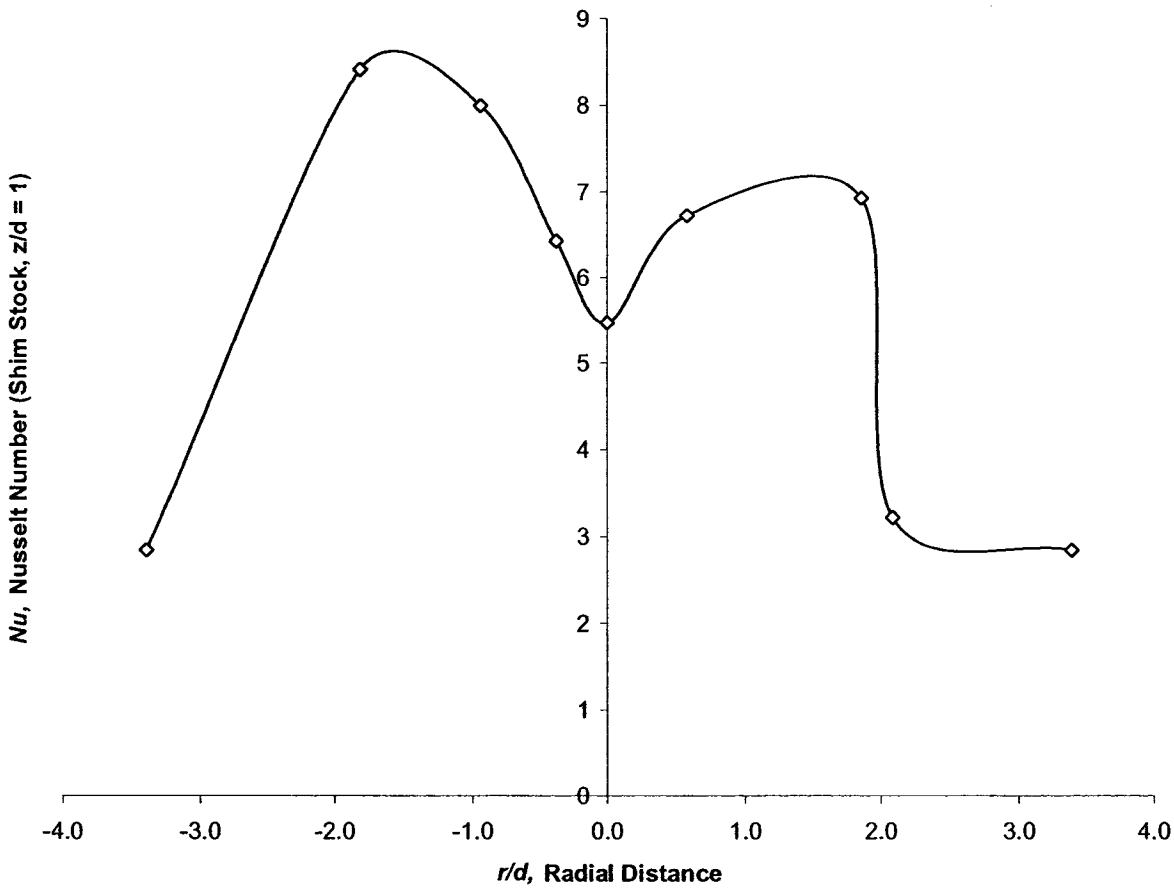

Figure G1 Nusselt number distribution for shim stock placed 6 mm away from flat plate. Plot at time = 65 seconds and $z/d = 1$.

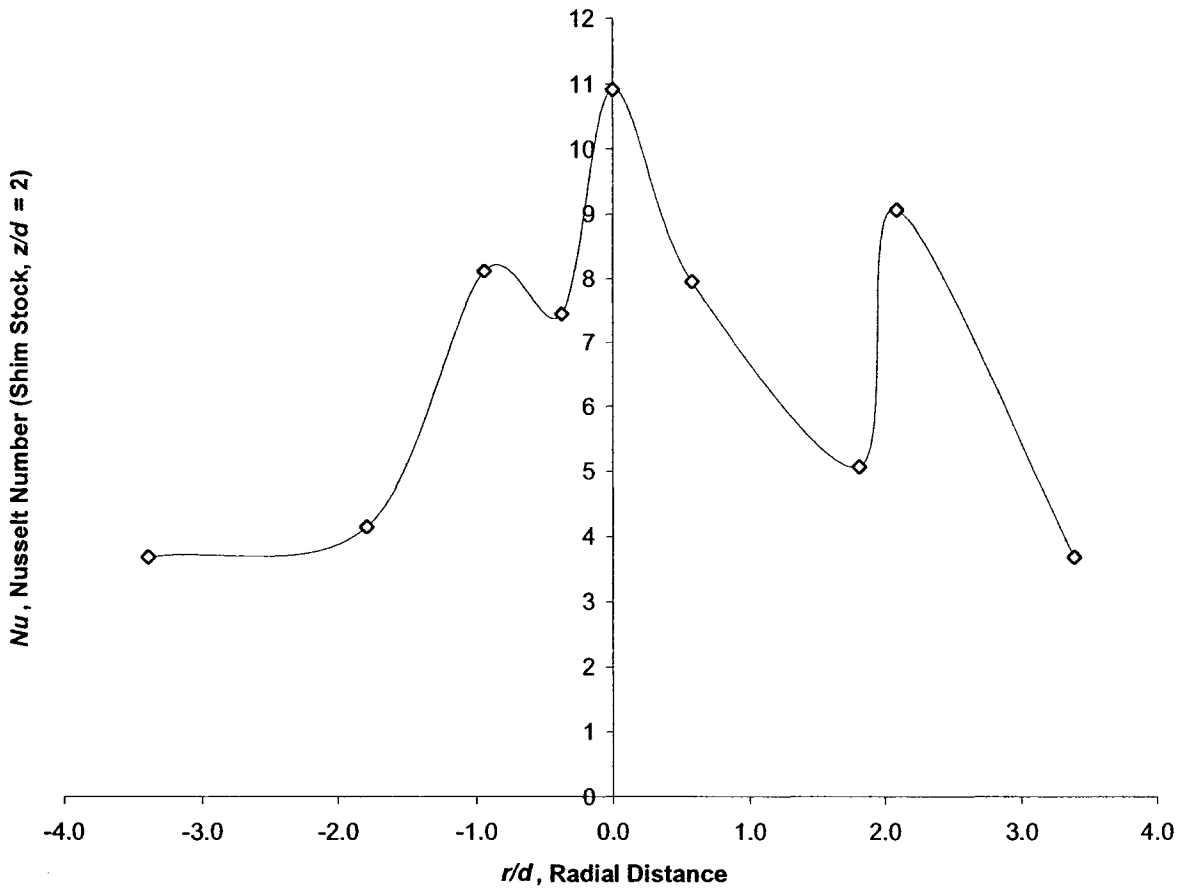

Figure G2 Nusselt number distribution for shim stock placed 6 mm away from flat plate. Plot at time = 65 seconds and $z/d = 2$.

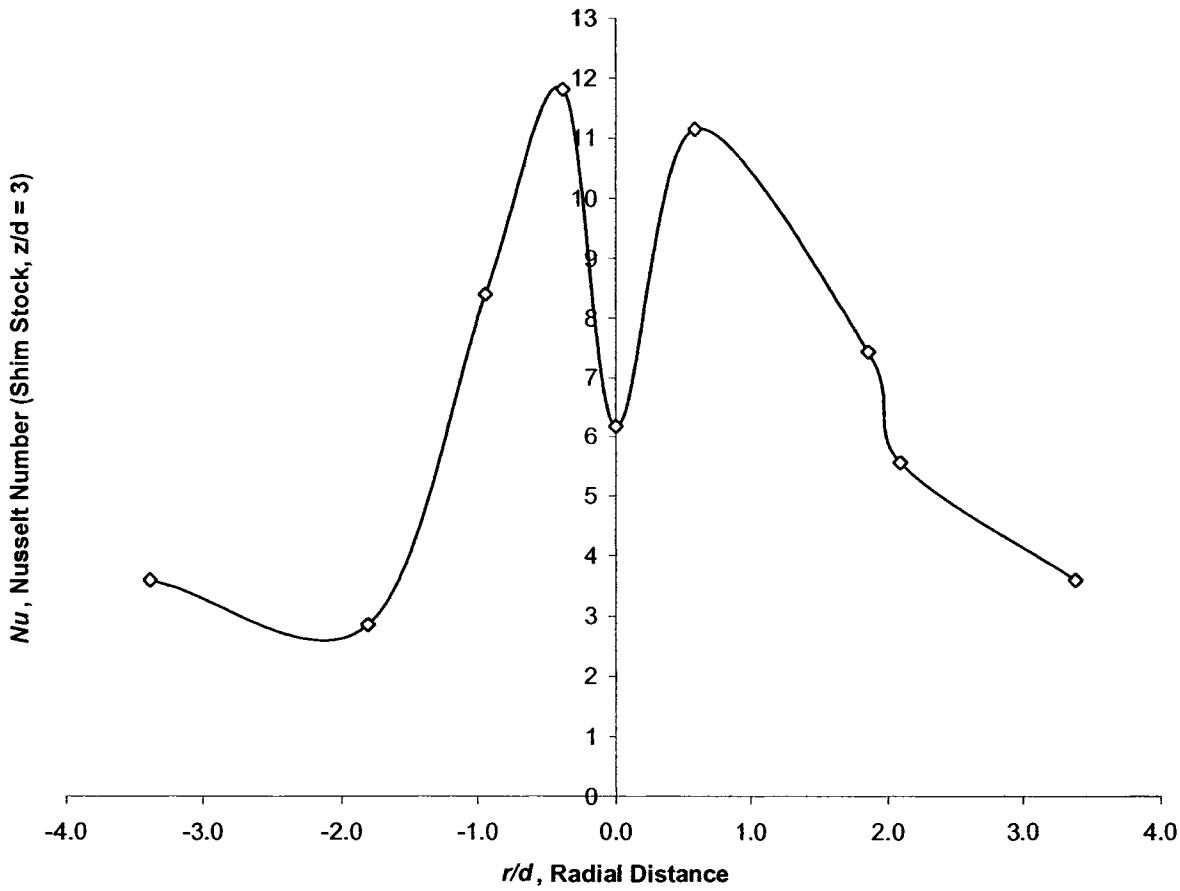

Figure G3 Nusselt number distribution for shim stock placed 6 mm away from flat plate. Plot at time = 65 seconds and $z/d = 3$.

APPENDIX H: Repeatability Tests

Table H1 Repeatability results for all thermocouples in plate for $z/d = 6$ at 65 seconds.

Trial Number	*Thermocouple*															
	a	***b***	***c***	***d***	***e***	***f***	***g***	***h***	***i***	***j***	***k***	***l***	***m***	***n***	***o***	***p***
1	28.87	62.46	82.75	120.90	145.87	117.72	68.23	48.22	18.10	33.08	57.76	86.99	127.32	125.15	96.90	50.51
2	31.62	62.32	81.68	122.45	144.00	123.06	70.55	43.91	22.93	26.35	56.75	84.10	128.51	135.24	90.67	52.23
3	29.15	67.32	81.41	115.51	143.22	113.65	69.04	47.14	22.87	27.27	55.74	86.00	127.62	133.91	93.94	53.22
4	30.73	66.33	85.62	118.31	144.01	116.41	70.73	46.08	22.40	30.73	54.96	90.21	124.12	131.40	94.21	52.92
5	28.44	65.70	89.42	115.32	148.56	113.68	70.02	45.30	27.03	33.36	55.65	90.78	122.70	130.05	90.68	53.20
6	27.41	69.24	83.72	114.31	146.60	113.82	72.02	47.67	20.93	33.50	52.80	83.60	124.88	134.56	96.03	50.38
Average	*29.37*	*65.56*	*82.88*	*117.80*	*145.40*	*116.39*	*70.35*	*46.39*	*22.37*	*30.72*	*55.61*	*86.95*	*125.86*	*131.72*	*93.74*	*52.08*
Error % (2XSTD)	*10.5*	*8.3*	*3.8*	*5.6*	*3.7*	*6.3*	*3.1*	*7.0*	*26.1*	*20.8*	*6.1*	*6.9*	*3.7*	*5.7*	*5.6*	*5.0*

Average Error in Profile: **8.91%**

APPENDIX I: Calibration Factors

Table I1 List of calibration factors for each of thermocouples in flat plate

Thermocouple Radial Distance, *r/d*	Calibration Factor, *B*
0.00	1.083
0.33	1.331
0.34	1.217
0.38	1.260
0.58	1.030
0.90	1.312
0.90	1.022
0.94	1.143
1.18	1.249
1.79	1.040
1.81	1.131
1.86	1.090
2.09	1.346
3.08	1.025
3.13	1.034
3.39	1.329

APPENDIX J: Thermocouple Rake

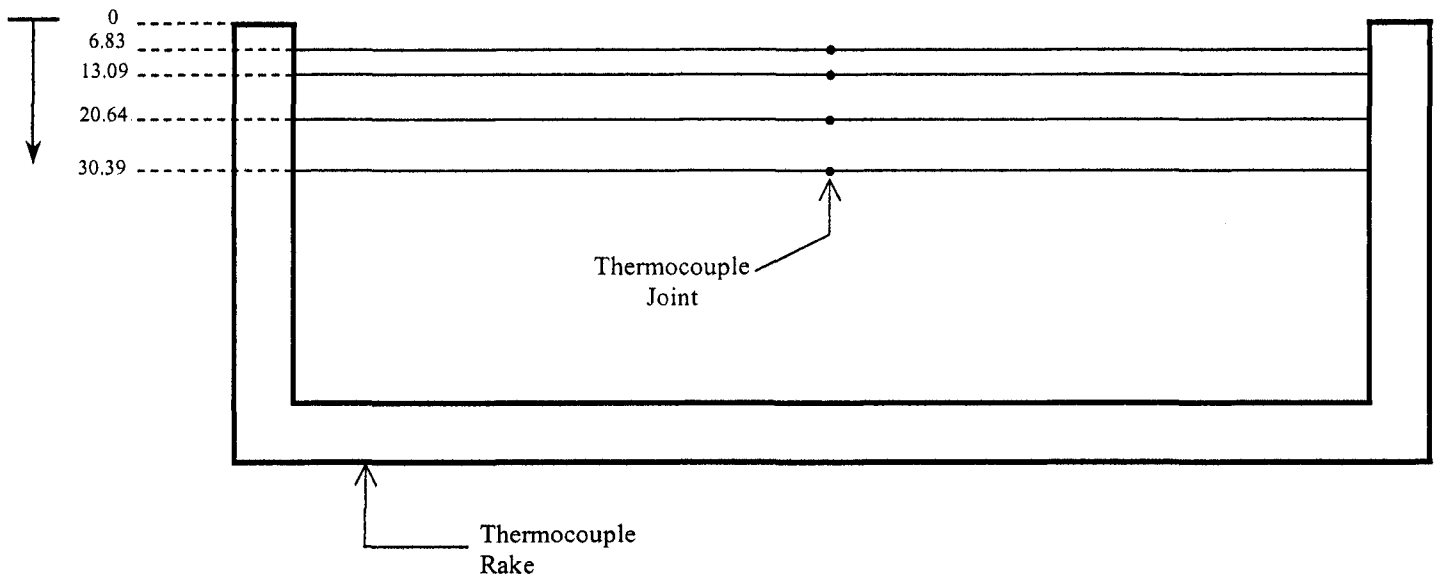

Figure J1 Profile of Thermocouple rake and plate

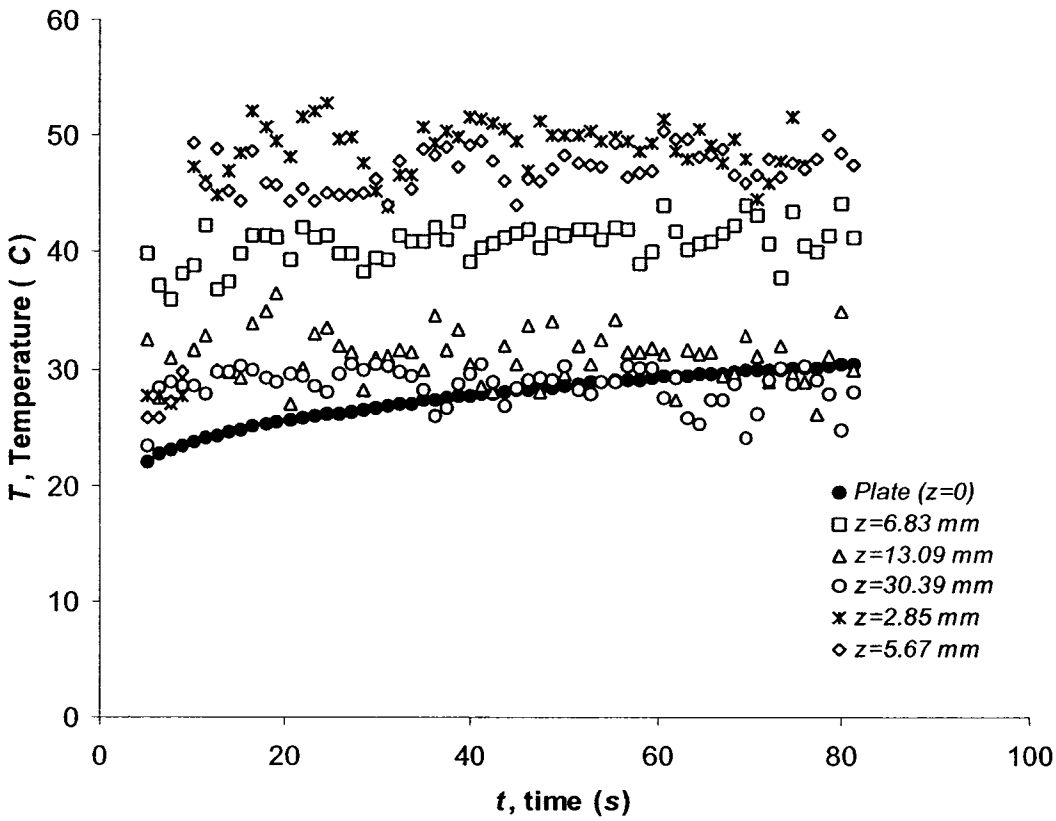

Figure J1 Temperature measured at various distances from plate for r/d = 3.31

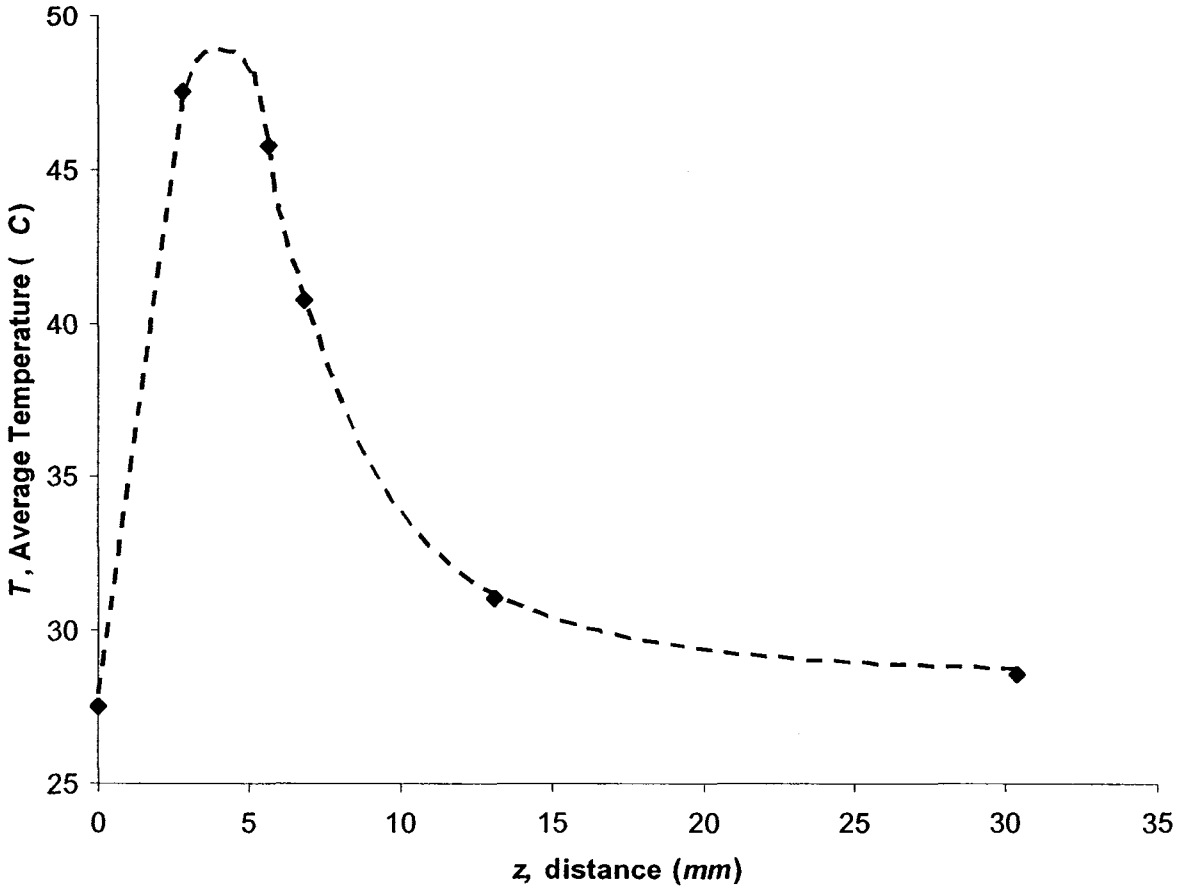

Figure J2 Average Temperature measured at various z's